Experimental Techniques to Determine the Young's Modulus of the Trachea

Vera Hermawan

**Thesis submitted in partial fulfilment
of the degree of
the Master of Engineering**

**Auckland University of Technology
Auckland
New Zealand**

September 2004

Acknowledgement

I wish to express my profound gratitude to my supervisor, Professor Ahmed Al-Jumaily, Director, Diagnostics and Control Research Centre (DCRC) at the Auckland University of Technology, for his patience, support, guidance and advice throughout this research.

I would like to give special thanks to my husband, Jeff, my son, Max and my parents for their support, patience and love in the process of completing this work.

Sincere thanks are also extended to helpful friends at DCRC; all staff of Faculty of Science & Engineering for their kindness and encouragement during my studying period at the Auckland University of Technology and friendly staff at the Auckland Meat Processors.

Abstract

In addition to its usefulness in modeling and simulation processes, the modulus of elasticity is an index which is highly used in biomedical identifications and tissue characterizations. For many composite and viscoelastic materials an "accurate modulus" is an idealistic hypothesis and an "equivalent modulus" is normally of a high biomechanical significance. The composite shape of the trachea, which consists of the smooth muscles and cartilage rings, renders the fact that an equivalent modulus is in place for many applications. In this paper three in-vitro nondestructive testing techniques are presented to determine the Young modulus of elasticity of the trachea and the results are compared with the standard uniaxial state of stress method. These techniques are based on: (1) simulating the trachea as a pressurized vessel and deducing a special relationship between the pressure and the radial strain; (2) using two hydrophones and studying the variation in acoustic transmittance caused by the presence of the trachea in a water-bath; (3) considering the trachea as a thin cylindrical shell and determining the resonance vibration response. Elaborate discussion is presented to identify the "pros" and "cons" of each technique and final practical recommendations are made.

Table of Contents

List of Figures

List of Tables

Statement of Originality

‘I hereby declare that this submission is my own work and that, to the best of my knowledge and belief, it contains no material previously published or written by another person nor material which to a substantial extent has been accepted for qualification of any other degree or diploma of a university or other institution of higher learning, except where due acknowledgement is made in the acknowledgements.’

Vera Hermawan

2 September 2004

Nomenclature

A	Cross-sectional area [m^2]
A_i	Arbitrary coefficient of axial displacement
B_i	Arbitrary coefficient of circumferential displacement
C_i	Arbitrary coefficient constant of radial displacement
c	Speed of sound [ms^{-1}]
c_1	Speed of sound in medium 1 [ms^{-1}]
c_2	Speed of sound in medium 2 [ms^{-1}]
d	Inner diameter [m]
E	Young's modulus of elasticity [Pa]
E_1	First Young's modulus of elasticity [Pa]
E_2	Second Young's modulus of elasticity [Pa]
E_3	Third Young's modulus of elasticity [Pa]
F	Force applied [N]
g	Acceleration due to gravity [9.8 ms^{-2}]
h	Thickness of a cylinder [m]
h_w	Height water level from the opening of the clamped trachea [m]
k	Constant assigned in displacement function of vibration equations $k = \dfrac{sin(\mu l/2r)}{sinh(\mu l/2r)}$
k_1	Wave number in medium 1
k_2	Wave number in medium 2
L	Instantaneous length [m]
L_0	Initial length [m]
ΔL	Length of deformation [m]
l	Cylindrical length [m]
l_h	Distance between transmitter and receiver hydrophones [cm]
l_w	Cut-length [m]
dl	Unit length of section element [m]
M	Mass of loads [kg]
M_B	Bulk modulus of a medium [Pa]
m	Number of nodal axial half waves

n	Number nodal waves in circumferential vibration forms
n_t	Number of trachea tested
$\mathbf{P}_i$	Complex pressure amplitude of incident wave [Pa]
$\mathbf{P}_r$	Complex pressure amplitude of reflected wave [Pa]
$\mathbf{P}_{r1}$	Complex pressure amplitude of reflected wave from the in-interface between water and trachea [Pa]
$\mathbf{P}_{r2}$	Complex pressure amplitude of reflected wave from the out-interface between trachea and water [Pa]
$\mathbf{P}_t$	Complex pressure amplitude of transmitted wave [Pa]
$\mathbf{P}_{t1}$	Complex pressure amplitude of transmitted wave from the in-interface between water and trachea [Pa]
$\mathbf{P}_{t2}$	Complex pressure amplitude of transmitted wave from the out-interface [Pa]
$\mathbf{p}$	Pressure wave [Pa]
$\mathbf{p}_i$	Incident pressure wave equation [Pa]
$\mathbf{p}_r$	Reflected pressure wave equation [Pa]
$\mathbf{p}_t$	Transmitted pressure wave equation [Pa]
q	Fluid pressure [Pa]
$\mathbf{R}$	Pressure reflection coefficient
R	Inner radius of cylindrical vessel [m]
R_{arc}	Large arc radius of maximum deformation [m]
R_i	Instantaneous outer radius of cylindrical vessel [m]
R_{out}	Outer radius of cylindrical vessel [m]
R_2	Arbritrary constant coefficient in cubic equation for the non-dimensional frequency
R_1	Arbritrary constant coefficient in cubic equation for the non-dimensional frequency
R_0	Arbritrary constant coefficient in cubic equation for the non-dimensional frequency
ΔR	Inner radial deformation of cylindrical vessel [m]
ΔR_m	Mean radial deformation [m]
ΔR_{max}	Maximum radial deformation [m]
ΔR_{out}	Outer radial deformation [m]

r	Mean radius [m]
s	Arc length of section element [m]
$\mathbf{T}$	Pressure transmission coefficient
$\mathbf{T}_1$	Pressure transmission coefficient of the in-interface between water and trachea
$\mathbf{T}_2$	Pressure transmission coefficient of the in and out-interface between three medium, water, trachea and water
$\mathbf{T'}_2$	Pressure transmission coefficient of the out-interface between trachea and water
t	Time [s]
t_0	Initial time [s]
t_1	End time [s]
$\mathbf{u}$	Normal particle velocity of pressure wave [m/s]
$\mathbf{u}_i$	Normal particle velocity of incident pressure wave [m/s]
$\mathbf{u}_r$	Normal particle velocity of reflected pressure wave [m/s]
$\mathbf{u}_t$	Normal particle velocity of transmitted pressure wave [m/s]
u_x	Axial displacement [m]
u_θ	Circumferential displacement [m]
δu_x	Differentiation of axial displacement [rad.m/s]
δu_θ	Differentiation of circumferential displacement [rad.m/s]
v	Poisson's ratio
w	Radial displacement [m]
δw	Differentiation of radial displacement [rad.m/s]
x	Spatial distance in vibration forms [m]
x_t	Direction or thickness (spatial distance) of a planar interface between two media [m]
z	Characteristic impedance of a medium [Pa s/m]
z_t	Characteristic impedance of trachea [Pa s/m]
z_w	Characteristic impedance of water [Pa s/m]
z_1	Characteristic impedance of medium 1 [Pa s/m]
z_2	Characteristic impedance of medium 2 [Pa s/m]

α	Constant coefficients assigned in roots of non-dimensional natural frequencies $\alpha = \left[-\frac{1}{27}\left(R_1 - \frac{R_2^2}{3} \right)^3 \right]^{\frac{1}{2}}$
β	Angle of arc [rad]
Δ	Non-dimensional natural frequency
Δ_1	Non-dimensional natural frequency from root 1
Δ_2	Non-dimensional natural frequency from root 2
Δ_3	Non-dimensional natural frequency from root 3
δ	Differentiation or variations
ε	Strain
μ	Part of roots quantity that ensures to meet the end condition of displacement function $\frac{\mu l}{r} = 1.506\pi, 3.5\pi, 5.5\pi, 7.5\pi, ...$
θ	Spatial angle in vibration forms [rad]
θ_1	Constant assigned in vibration equation $\theta_1 = 1 + k^2$
θ_2	Constant assigned in vibration equation $\theta_2 = 1 - k^2 + \frac{2r}{\mu l} sin \frac{\mu l}{r}$
$d\theta$	Angle of section element [rad]
ρ	Density [kgm^{-3}]
ρ_1	Density of medium 1 [kgm^{-3}]
ρ_2	Density of medium 2 [kgm^{-3}]
σ	Stress [N/m^2]
σ_1	Axial stress [N/m^2]
σ_2	Circumferential or hoop stress [N/m^2]
$(\sigma_2)_{max}$	Maximum hoop stress [N/m^2]
σ_3	Radial stress [N/m^2]
$(\sigma_3)_{max}$	Maximum radial stress [N/m^2]
τ_{max}	Maximum axial shear stress [N/m^2]
ω	Angular frequency [rads^{-1}]

ξ	Constant coefficient in assumed displacement function of vibration equation assigned as $\frac{1}{\xi} = \frac{h^2}{12r^2}$
∇	*i*th root of the auxiliary equation where $\nabla^4 = \nabla^2\left(\nabla^2\right) = \frac{\partial^2}{\partial x^2} + \frac{1}{r^2}\frac{\partial^2}{\partial \theta^2}\ \frac{\partial}{\partial t}$

Chapter 1
Introduction

1.1 Background

In addition to its usefulness in modelling and simulation processes, the modulus of elasticity is an index which is highly used in biomedical identifications and tissue characterisations. One of the main abnormalities of tissue and organs is associated with the increase of their stiffness. For example, any lump which builds up within an organ changes the texture of the tissue and makes it harder or stiffer. Other stiffness variation is associated with muscle inflammation and swelling, which results in pain and restricted activities.

An example of respiratory ailments such as asthma is a breathing disorder that originates from conditions where the airway passages are constricted by either inflammation or allergy, which results in smooth muscle shortenings and swelling of the of inner lining of the airway walls. These create airway contraction and narrowing, which results in mucus build up, airflow restriction and breathing difficulties. In many cases, an increase in a tissue's stiffness is associated with airway wall muscle contractions. Normally the stiffness is assessed by the mechanical property Young's modulus of elasticity. This is an index parameter that can be used to compare normal and abnormal tissues.

For many composite viscoelastic materials an "accurate modulus" is an idealistic hypothesis, which is normally replaced by an average or "equivalent modulus". The latter is normally of a high biomechanical significance. This research focuses on the trachea which is the main breathing inlet passage to the respiratory system. It consists of smooth muscles, cartilage rings and connective tissues. Due to the nature of these various components, the tracheal structure is nonhomogeneous and non-isotropic, which leads to complexity in determining an appropriate modulus of elasticity. Thus an 'equivalent' modulus is in place for many of its applications. Values reported in the literature are within the range of 0.2 to 5.8 MPa [1, 2] and no absolute value is available. Furthermore, a standard non-destructive technique of measurement has been adopted to determine such a parameter.

This research focuses on developing appropriate measuring techniques to determine the modulus of elasticity and to compare those techniques and make appropriate recommendations. Three *in vitro* non-destructive techniques are developed and compared with a conventional destructive method, normally referred to as standard uniaxial state of stress. This method determines stiffness of an object by applying loads and measuring deformation. Although this method is a destructive approach, it is still commonly used for the study of stress and strain relationships in biological tissues such as lung tissues [3], smooth muscles [4], bones, cartilages [1] and others [5]. To avoid changes in the mechanical properties of the biological tissues, they are usually tested in fresh conditions using some preservative chemicals and are used for short term periods [6]. In this chapter, literature review of relevant research will be discussed.

1.2 Literature Survey

There are no specific techniques stated to be the most suitable for measuring the Young's modulus of nonhomogeneous viscoelastic tissues such as the trachea. In the biomechanical area, many modellings, simulations and experimental investigations have been carried out to determine the mechanical property of the respiratory organs and tissue. An example of the numerous simulation study is the work by Tomlinson et al [7, 8] who used a computer software Bath*fp* to model the whole respiratory system from a tracheobronchial tree, which includes the trachea and respiratory passageways, to the lung system. The gas flow, lung motion and their interconnection are observed and studied. By this simulated model of the tracheobronchial tree, the effects of tracheobronchial wall stiffness are assessed. Another study is by Wada and Tanaka [9] which included computational simulation of the gas exchange, tissue deformation, and pulmonary circulation models of the respiratory systems. Al-Jumaily and Du [10-12] have modelled and simulated the airways for identifying and detecting obstruction. The results demonstrated that the input impedance resonant frequencies can locate the obstruction with its degree of severity in any of the airway branches. Reisch et al [13] evaluated through mathematical modeling whether forced oscillation technique could provide an early detection for airway obstruction. The results of this technique suggested that it is a valuable tool for assessing the degree of upper airway obstruction in patients with obstructive sleep apnea syndrome.

Numerous experimental investigations of the respiratory mechanics, have focused on the respiratory flow and airway impedance. Forced oscillation technique is a common non-invasive method to determine the degree of airway impedance [14, 15]. With this technique, Fredberg et al [15] measured input impedance by generating pressure waveforms from a transient acoustic pulse generator to propagate along the wavetube to the airways inside a dog's lung. A microphone was installed in the airway opening to detect the incident waves and the reflected pressure waves from the lung response. The microphone output signals were then amplified, low-pass filtered and digitised. The signal's ratio by the discrete Fourier transforms was the complex reflection coefficient related to the input impedance of the airway termination. The results showed lung responses depended on the volume of the lungs, airway branching structures and airway walls responses. Lung responses exhibited numerous resonances and antiresonances below 10,000 Hz [15].

Another established non-invasive approach is commonly known as the acoustic reflection method using two-microphones strategy. This method is based on the principle of acoustic wave propagation and reflection in a duct which involves sound waves, the use of microphones and wave tubes [16-18]. This acoustic reflection method gives the longitudinal cross-sectional area profile along the airway, a useful method in understanding the structure and function of the airways. The lumped model approach of this method also describes the frequency dependent behaviour of the respiratory system.

Al-Jumaily and Al-Fakhiri [19] have developed a mathematical model to study the influence of elastance variation on the respiratory system dynamics. They used the acoustical approach to determine the impedance at the throat using impedance recursion formulas for both symmetric and asymmetric structures to consider. "The response of the lung structure indicates that when the airway wall varies, as the case during an asthma attack, the overall normalised input impedance frequency spectrum could be used to give a reasonable signature for identifying such abnormality"[19].

The above literature shows the significance of using the acoustic approach for respiratory system measurements and diagnosis. However, in terms of determining a mechanical property such as the elastance and the stress and strain relationship, many of the studies tend to focus on a specific element rather than the whole structure. In other words, those investigations focus on a smooth muscle, a cartilage or a lung tissue rather than the trachea as a whole. This literature review presents various experimental techniques carried out by other researchers to determine the Young's modulus for smooth muscles, lung tissues, cartilages and other tissues.

Sarma et al [4] developed a material model of a tracheal smooth muscle tissue from experimental data by simulating the mechanical response through a three-dimensional non-linear finite element analysis. The model was validated against experimental data. A canine tracheal smooth muscle was bisected and isolated from the rest of the tissue. Then it was subjected to electrical stimulation between platinum electrodes. The stimulation caused contraction or shortening of the muscle. The ends of the muscle were held fixed at its length in the beginning of each contraction. The results showed that the stiffness increased as the muscle shortened and thus the degree of stiffness is shortening-dependent. The preliminary results indicated that the experimental and material modelling approach adequately describe the smooth muscle length-dependent characteristics. This paper mostly presents the relationship between the stress and strain and no specific values are disclosed for the stiffness of smooth muscle.

Tai and Lee [20] used triaxial force, also an extension test was used by Hoppin et al [3] to examine relative directional dependent deformation behaviour of dogs lung tissues. The tissues were initially ventilated with air and saline solution for a leak test and pressure-volume measurements. The triaxial test used stretching apparatus of loads placed to stretch the mounted specimen in three orthogonal directions. The tests were conducted inside up to 10 cmH_2O saline solution and also in the atmospheric air of up to 30 cmH_2O. The experiment for each tissue consists of triaxial and uniaxial loading cycles. The results show mild (less than 10% of the mean deformation) anisotropic deformation exists in the younger lung tissues and no locational dependence of deformation in the lower and upper lobes of the lung. This experiment did not directly measure any elasticity parameter, but only observed the three-dimensional deformations. As a conclusion, they validated the homogenous and isotropic assumptions for the structure.

Likhitpanichkul et al [1] used a standard uniaxial loading to measure the mechanical properties of articular cartilages. This method has been widely used in tissue engineering to study explants and gel-cell-complexes. This study also assumed the cartilage tissue to be of an isotropic and linearly elastic material. The Young's modulus of cartilage measured was 0.36 MPa and Poisson's ratio of 0.2. The electrical response was then obtained and results showed that the response and material properties are closely related to the fixed charged density of the tissue.

Sera et al [2] studied the inspiratory and expiratory flow in a tracheostenosis model. They used pig's trachea and measured the Young's modulus of elasticity of its smooth muscle and cartilage. The trachea was placed in the saline bath and was pressurised internally and externally. The applied pressure was varied between 0 and 15 cmH_2O. A laser displacement meter was used to measure the maximum deformation in the radial direction for the smooth muscles and cartilage rings. The Young's modulus obtained was 5.8 ± 2.9 MPa for the cartilage rings and 0.65 ± 0.32 MPa for the smooth muscle. These values together with a realistic stenosis model, were then used to fabricate a three-dimensional tracheal model for measuring flow or velocity field.

Wiebe [5] developed an instrument to measure the tensile property of a very small biological tissue. The device worked to determine the uniaxial stress-strain characteristics of a monolayer embryonic epithelia tissue, a specimen from an amphibian. The stress and strain relationship was produced but no specific stiffness values were disclosed in this paper.

Suki et al [21] used excised calf trachea and wave propagation to measure the phase velocity and input impedance with open and closed end for frequencies between 16 and 1600 Hz at two axial tensions. The results demonstrated the relationship between the volumetric wall parameters and the tracheal geometry which enabled the material properties of viscosity and Young's modulus to be estimated. The latter gives a value of 0.26×10^4 cmH_2O for the soft tissue and 2×10^4 cmH_2O for the cartilage.

Holzhäuser and Lambert [22] developed a mathematical model for the tracheal structures which included the cartilage rings and the smooth muscles membrane. The changes of cross-sectional area was investigated when the trachea was subjected to the transmural pressure difference, a method to relieve breathing difficulties by affecting the width of tracheal cross-sectional area. The main aspects that are influential to the change in the cross-sectional area are the tensile force of the membrane and the elasticity and shape of cartilage rings. The results have been compared with the previous study on rabbits' tracheal deformation for validation. The Young's modulus of rabbits' tracheal cartilage was 10 MPa which is similar to the calculations in the modelling using human data [23].

1.3 Biomaterials and Viscoelasticity

This section describes the properties of viscoelasticity and biomaterial tissues with elaboration on the techniques in preparing and treating *in vitro* composites for practical purposes. In general, soft biological tissues have the following characters which are important factors to consider when designing an experiment [6]:

(a) Soft biomaterial tissues are usually composites and will almost certainly exhibit non-linear elasticity. This means that the mechanical response will depend on the level of strain imposed.

(b) These materials will probably be anisotropic, which means the mechanical properties will depend on the direction of loading.

(c) Biological tissues are viscoelastic, which means the mechanical response will vary with rate or duration of loading. Viscoelastic materials have the features of *relaxation*, *creep* and *hysteresis*. Relaxation or *stress relaxation* refers to a condition when sudden strain is applied and held constant causing its induced corresponding stress to decrease in time. Creep, on the other hand, occurs when sudden stress is applied and maintained constant causing the body to continually deform. When the body is subjected to cyclic loading, the stress and strain relationship creates hysteresis which usually differs to the process of unloading.

(d) Large deformations of up to or greater than 100% are likely and must be accommodated for by the test instruments and the methods used to calculate stress and strain. Anything above 1% or so is beyond the strict limits of linear elasticity theory.

(e) At high strains there is great deal of re-orientation of the components leading to very strange Poisson's ratios

Ideally, in all *in vitro* experiments tissues should be treated and maintained in a biologically stable state to mimic *in vivo* characteristics as much as possible. For short term tests, a buffered saline solution is sufficient to be used as a bathing medium.

The uniaxial tensile test is the simplest test of material's elasticity, measuring the deformation produced by applied loads [6]. An important factor to consider in carrying out this experiment is the ability to control the degree or rate of deformation. The specimen is to be gripped in an appropriate clamp at both ends. Usually a tensile testing machines serves this purpose; however, depending on the specimen's structure, a tension system may need to be custom built. The deformation is often measured in the central portion of the specimen, away from the influence of the clamps, by using displacement type transducer [6, 24].

Biaxial testing is a desirable tensile test for studying biomaterial properties in two orthogonal directions. This method has been developed to characterise skin [6], lung parenchyma [3, 20] and pericardium [6]. A rectangular tissue is held horizontally in a temperature-controlled saline chamber by a set of silk threads attached to metal hooks along its four edges. Each thread connects to a binder post on one of four force-distributing platforms. The threads can be tensioned independently to ensure uniform distribution of force to the four edges of the sample. The specimen is extended biaxially by moving all four force platforms at uniform rates, so that the specimen stays in the same location and suffers no shear distortion [6].

A non-contact measurement method is described by Fung [24] for analysing *in vitro* three-dimensional blood vessels. The vessel is immersed in a saline bath at 37°C, clamped and stretched or shortened at a specific rate of force. The displacement measurements are conducted and recorded using two closed-circuit television cameras focused on the specimen and two video dimension analysers. Although this non-contact method enables measurements for an isolated specimen, the mechanical properties are influenced by the mounting of the specimen. The middle portion, however, is less affected by stress due to the clamped ends and is more suitable to be selected for measurement [24].

The behaviour of viscoelastic biomaterials is normally described by three mechanical models, namely the *Maxwell model*, the *Voigt model* and the *Kelvin model* [24]. All of these models are composed of a combination of linear springs with spring constant and dashpot with coefficients of viscosity. A linear spring is an element to produce instantaneous deformation proportional to the load and a dashpot is to produce a velocity proportional to the load at any instant. In the *Maxwell model*, the same force is transmitted from the spring to the dashpot. For the *Voigt model*, the spring and the dashpot have the same displacement and *the Kelvin model* is the sum of the force from the spring and the force from the *Maxwell* element.

1.4 Objectives and Methodology

The aim of this research is to develop non-invasive and non-destructive experimental techniques to determine the trachea wall's Young's modulus of elasticity. The main objectives of this research are:

1. To develop the following measuring techniques:

(a) *The pressure difference method*, which is based on simulating the trachea as a pressurised vessel and deducing a special relationship between the pressure and the radial strain

(b) *The two-hydrophones method*, which is based on using two hydrophones and studying the variation in acoustic transmittance caused by the presence of the trachea in a water-bath

(c) *The vibration method*, which considers the trachea as a cylindrical shell and determines the resonance vibration response.

2. To conduct uniaxial state of stress tests on the trachea in order to determine reference values for comparisons. This method is referred to as the *conventional tension method*. Due to the structural complexity of the trachea, Young's modulus will be determined in:

(a) circumferential direction with the connective tissue and muscle

(b) circumferential direction without the connective tissue and muscle

(c) axial direction

3. Compare and analyse the results from the above tests. The results of the three proposed methods are compared against those obtained from the conventional uniaxial state of

stress method. Elaborate and discuss the results to identify the “pros” and “cons” of each technique.

4. Recommend appropriate methods for future use.

Chapter 2
Theoretical Principle

2.1 Introduction

There is no unique theory or method suited for determining the Young's modulus of elasticity of viscoelastic tissues as in this particular case of the trachea. The tracheal tissue mainly consists of smooth muscles and cartilage rings layered together with other connective tissues which shape a non-uniform geometrical structure. It is thereof a form of non-homogeneous and non-isotropic material which renders the fact that using an average or an 'equivalent modulus' is normally of a higher biomechanical significance than an 'accurate modulus'. The latter is an idealistic hypothesis and less in place with many applications.

This research investigates four different experimental approaches to obtain comparative values of the Young's modulus of elasticity where at the end, recommendations for a suitable method are made. This chapter describes the theoretical principles that support the experimental part developed in chapter 3.

2.2 Conventional Tension Method

This is a standard uniaxial state of stress testing method which is normally used for uniform and homogeneous materials. Applying tension loads introduces stress in the object, thus increasing its initial length. The rate of this increase determines the Young's modulus of elasticity E. This relationship is Hooke's Law for uniaxial state of stress which can be expressed as

$$\frac{F}{A} = E\frac{\Delta L}{L_0} \tag{2.1}$$

where

F = the tensile force applied to the object with the unit Newton (N)

A = the cross sectional area being subjected to the tensile force (m^2)

E = Young's modulus of elasticity with the unit Pascal (Pa) or N/m^2

ΔL = the deformation length of the trachea
L_0 = the original clamped length without loads

$\frac{F}{A}$ is the stress and $\frac{\Delta L}{L_0}$ is the engineering strain which is usually simplified to

$$\sigma = E\varepsilon \tag{2.2}$$

For viscoelastic materials a true strain is normally defined as $\frac{\Delta L}{L}$ where L is the instantaneous length. For comparative purposes, both the engineering and the true strain are taken into consideration to calculate the Young's modulus.

In common homogeneous materials such as metal rods, the elastic relationship of stress with strain shows a constant rate or linearity of its deformation. However, for a viscoelastic material the result is expected to be non-linear [2]. This shows that there is a change of the modulus of elasticity when stress or loads are increased. Linearisation is carried out by considering the first linear elastic deformation slope over smaller range of loads as the initial value of the Young's modulus. The second linear slope and so on are to be recorded accordingly.

This is to be taken as a 'standard' method where the test results from the other techniques are to be compared with. The drawback of this method is a direct contact with the destructive effect of loads and tissue dehydration. Although these may change the tissue's mechanical properties, provided sufficient care is taken for the setup (such as not applying loads more than 150 grams), this destructive effect can be minimised. Results should present a general trend and common range of values for the Young's modulus of elasticity.

2.3 Pressure Difference Method

This method is based on simulating the trachea as a pressurised vessel and deducing a special relationship between the pressure and the radial deformation [2]. This approach is carried out by placing the tissue under fluid pressure and changing the pressure by adjusting the height of the fluid. Through the radial deformation detected, the Young's Modulus of elasticity can then be determined.

The trachea is mounted by clamping both of its ends to tubes which are connected to two pressure reservoirs filled with water as shown in Figure 2.1. The pressure difference across the trachea is achieved by changing the heights of the reservoirs.

The principle that supports this approach is derived by assuming the basic structure of the trachea as a cylindrical vessel with uniform internal pressure. The formula available in the literature [25] assumes uniform radial deformation. However, this is not replicated in reality as the trachea will most likely bulge when pressure is applied. This creates complexity in obtaining uniform radial deformations and an appropriate geometrical averaging has to be achieved. Using the maximum measured deformation located in the middle part of the trachea [24], a formula is developed to determine a mean radial deformation.

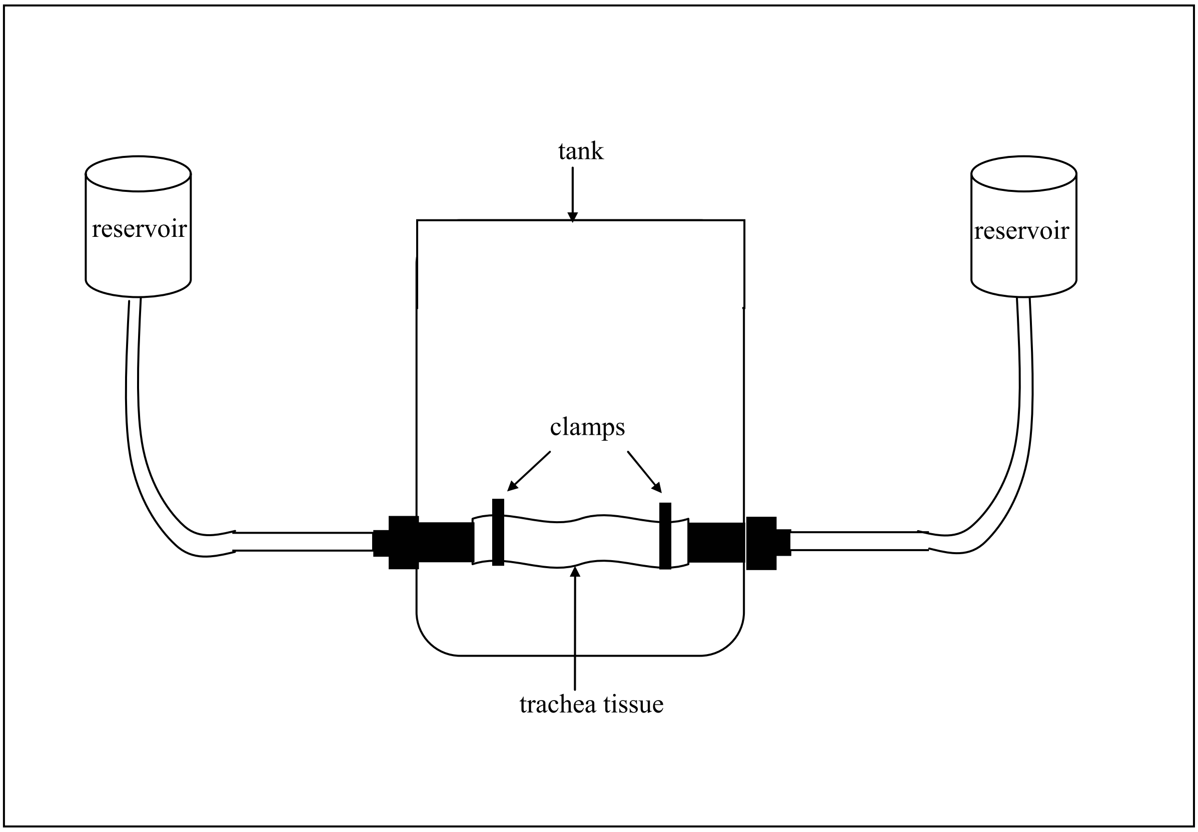

Figure 2.1 Diagram of the clamping system of the trachea tissue

The fluid pressure is varied and controlled by changing the heights of the reservoirs vertically in order to achieve different water levels from the point where water enters the trachea. Hence the pressure applied q with the unit of Pascal (Pa) is expressed as

$$q = \rho g h_w \tag{2.3}$$

where

ρ = density of water, 998 kg/m^3.

g = acceleration due to gravity 9.8 m/s^2

h_w = height of water level from the opening of the clamped trachea.

With this particular setup, it is essential to obtain a suitable physical and mathematical expression for the relationship between the radial deformation of the trachea and the applied internal pressure. Hence, the function of radial deformation formula is to be determined in terms of the applied pressure.

As the size of the trachea varies for different species, in the present application the trachea is considered either as a thin shell or a thick shell based on the thickness and radius or h/R ratio. For the former normally $h/R < 1/10$ while for the latter $h/R > 1/10$.

2.3.1 Thin-walled Cylindrical Vessel

To define the symbolic configuration in Figure 2.2:

q = unit pressure(force per unit area) which in this case is water pressure level

R = inner radius of cylinder

h = wall thickness

l = length of cylinder

To determine the circumferential or hoop stress σ_2, consider an axial section element of unit length dl as shown in Figure 2.3, the force balance yield

$$2\sigma_2 h\, dl\, sin\frac{d\theta}{2} = qRdld\theta \tag{2.4}$$

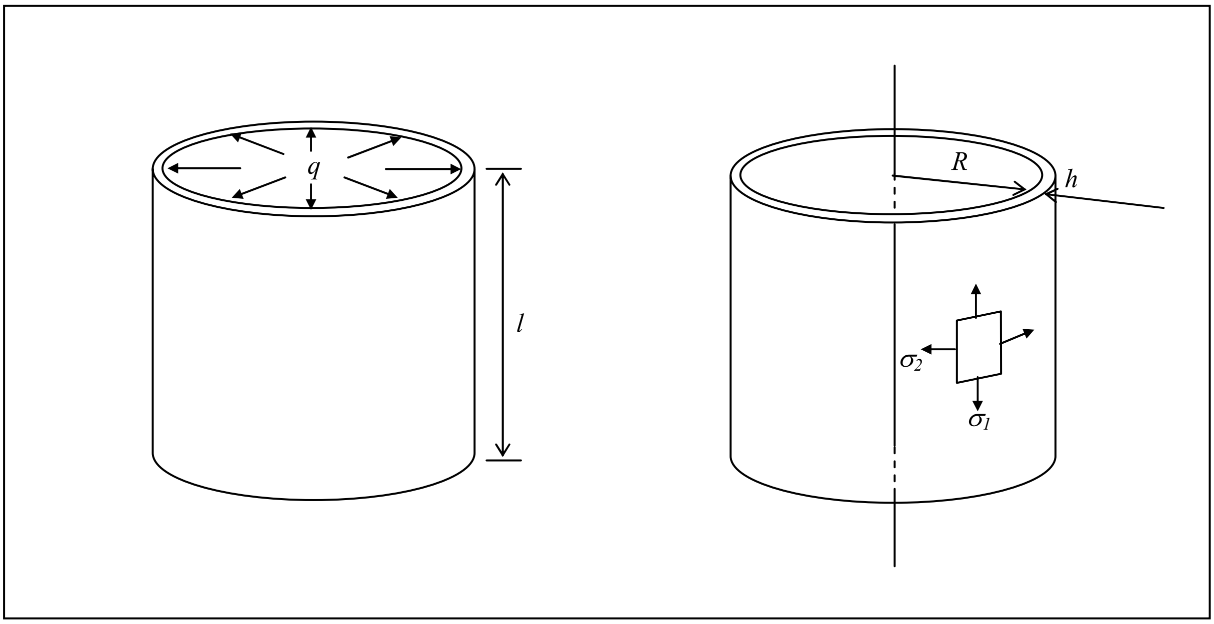

Figure 2.2 Configurations of thin-walled cylindrical pressure vessel with uniform radial pressure

However, for small $d\theta$, $\sin\frac{d\theta}{2}$ approximately is equal to $\frac{d\theta}{2}$. This reduces equation (2.4) to

$$\sigma_2 = \frac{qR}{h} \tag{2.5}$$

This can be written in terms of strain $\frac{\Delta R}{R}$ as

$$\sigma_2 = E\frac{\Delta R}{R} \tag{2.6}$$

where E is the Young's modulus of elasticity, ΔR is the radial deformation. Substituting equation (2.5) into equation (2.6) and rearranging to obtain

$$\Delta R = \frac{qR^2}{Eh} \tag{2.7}$$

This can be written as

$$q\frac{R}{h} = E\frac{\Delta R}{R} \tag{2.8}$$

where a plot of $q\frac{R}{h}$ versus $\frac{\Delta R}{R}$ results in E.

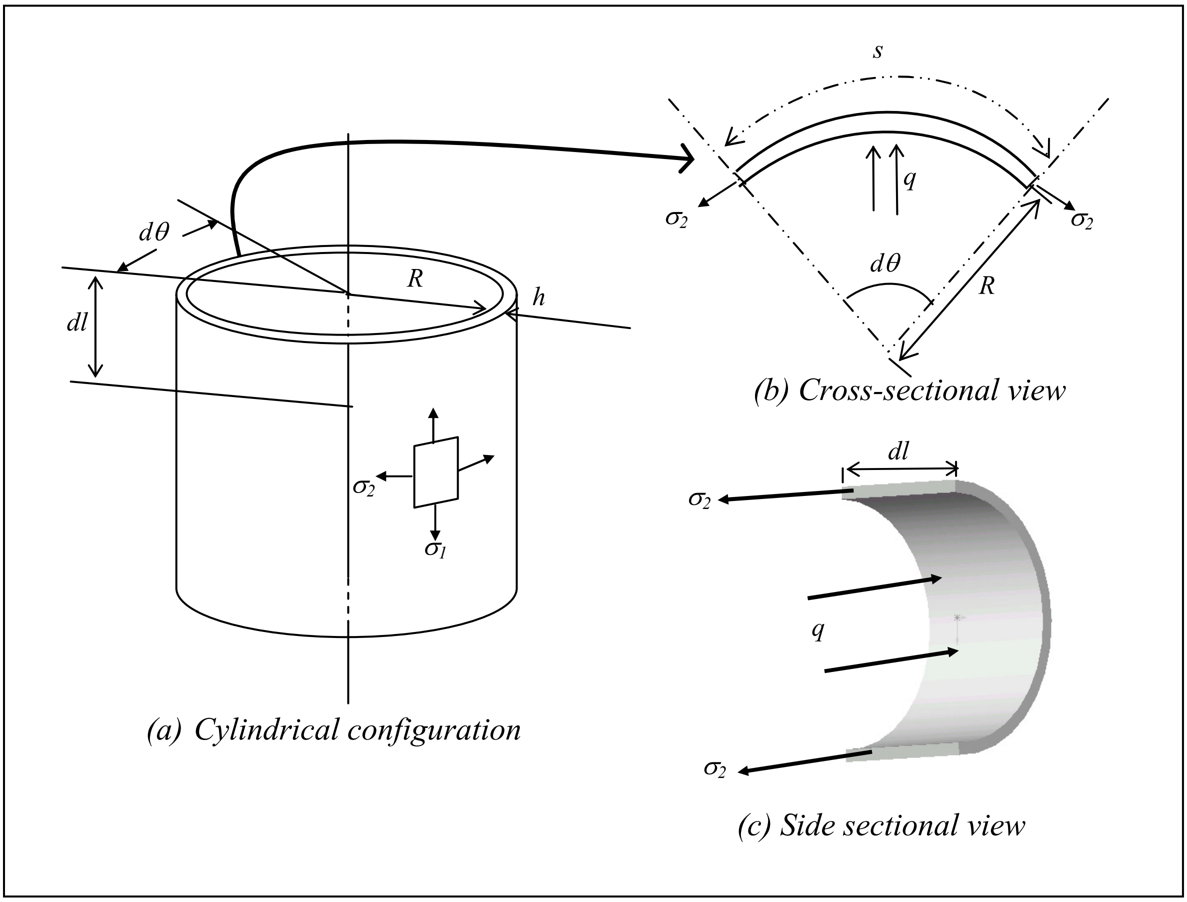

Figure 2.3 Section of thin cylindrical shell

2.3.2 Thick-walled Cylindrical Vessel

The configuration of a thick-walled cylindrical vessel is shown in Figure 2.4.

To define the symbolic configuration in Figure 2.4:

R_{out} = outer radius

R = inner radius

r = mean radius

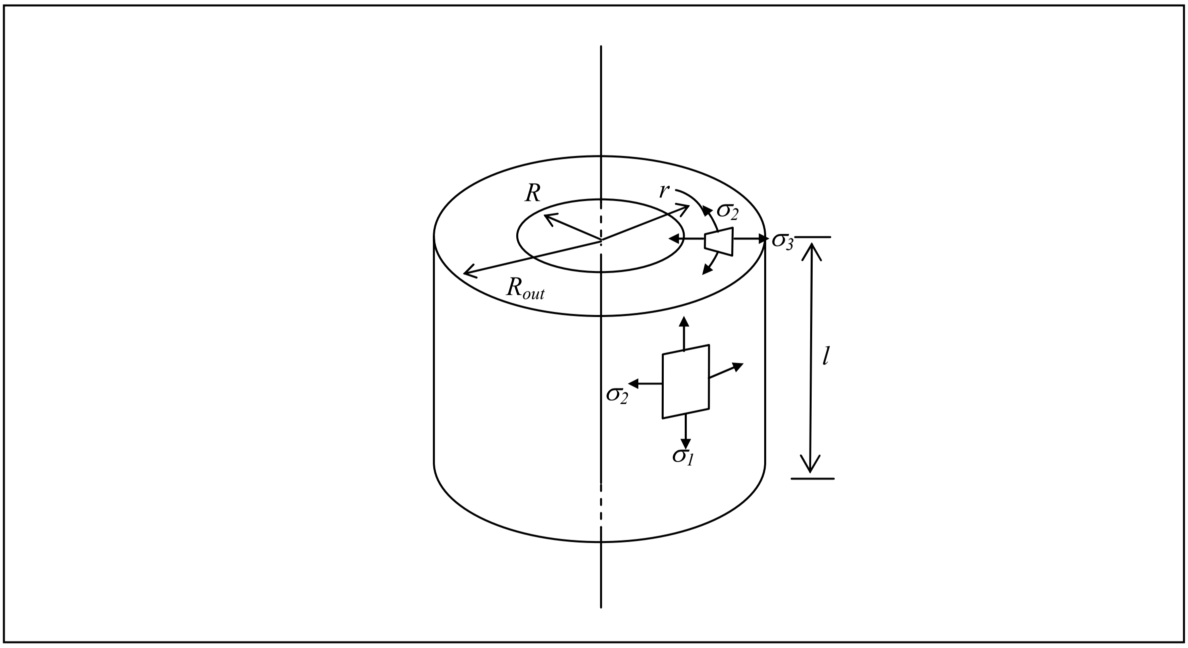

Figure 2.4 Configurations of thick-walled cylindrical pressure vessel with uniform radial pressure

σ_1, σ_2, σ_3 are normal stresses in the longitudinal, circumferential and radial directions respectively. Again with a uniform internal radial pressure q and free-ends at $r = R$, the hoop stress σ_2 and radial stress σ_3 may be written as [25]

$$\sigma_2 = \frac{qR^2(R_{out}^2 + R^2)}{r^2(R_{out}^2 - R^2)},\ (\sigma_2)_{max} = q\frac{R_{out}^2 + R^2}{R_{out}^2 - R^2} \tag{2.9}$$

$$\sigma_3 = \frac{-qR^2(R_{out}^2 - r^2)}{r^2(R_{out}^2 - R^2)},(\sigma_3)_{max} = -q \tag{2.10}$$

and the longitudinal shear stress is given by

$$\tau_{max} = \frac{\sigma_2 - \sigma_3}{2} = q\frac{R_{out}^2}{R_{out}^2 - R^2} \tag{2.11}$$

The outer and inner radial deformation formulas are, respectively, expressed as

$$\Delta R_{out} = \frac{q}{E}\frac{2R_{out}R^2}{R_{out}^2 - R^2} \tag{2.12}$$

$$\Delta R = \frac{qR}{E}\left(\frac{R_{out}^2 + R^2}{R_{out}^2 - R^2} + v\right) \tag{2.13}$$

where v is the Poisson's ratio. Experimentally, the detection of the changes in radial direction is made on the outer radius ΔR_{out}. Hence calculations are done only based on equation (2.12).

Again to compare with the stress and strain from the conventional tension method, equation (2.12) is rearranged to take the form

$$q\frac{2R^2}{R_{out}^2 - R^2} = E\frac{\Delta R_{out}}{R} \tag{2.14}$$

2.3.3 Application to Present Work

The main formula used for the calculations of the experimental results are equations (2.8) and (2.14). Both of them will be used for comparison purposes.

As previously mentioned, the viscoelastic complexity and non-uniformity of the trachea is also to be considered. Unlike the smooth structured cylinder, the grooves and joints of the tracheal cartilage and its surrounding connective muscle cause uneven changes in the radius when pressure increases. One side of the trachea wall can bulge more than its opposite side. The trachea also tends to bulge with maximum deformation in the middle between the clamped ends. Since the above formulas are based on disregarding the axial stresses, further geometrical adjustment is necessary to obtain the radial deformation. Figure 2.5 illustrates the condition when a large pressure is being applied to the trachea.

The formulas from equations (2.8) and (2.14) are suitable for a free-ends pressure vessel with uniform radial deformation, however, the experimental vessel is clamped at the two ends, which generates a bulge shape. To accommodate for this problem, it is appropriate to consider the geometrical 'mean' radial deformation ΔR_m instead of using the measured maximum deformation at the centre. Figure 2.6 illustrates the radial deformation of the trachea during experimental testing. The two ends have zero deformation, while the centre has maximum deformation. This may be considered as an arc of a circle with very large radius R_{arc}, a length l and a maximum deformation ΔR_{max}.

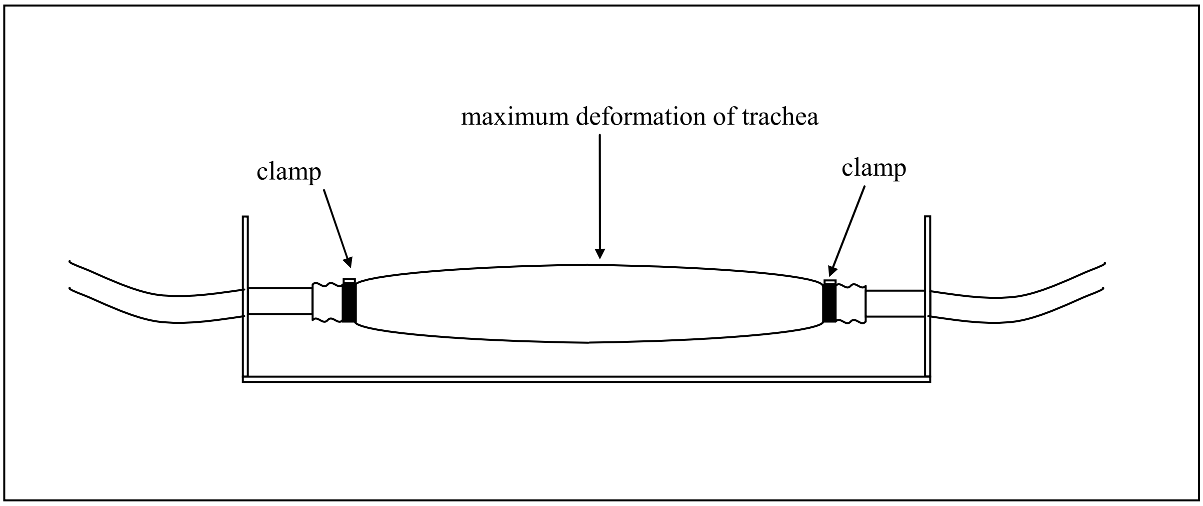

Figure 2.5 Trachea clamped at both ends inside the tank with maximum radial deformation in the middle.

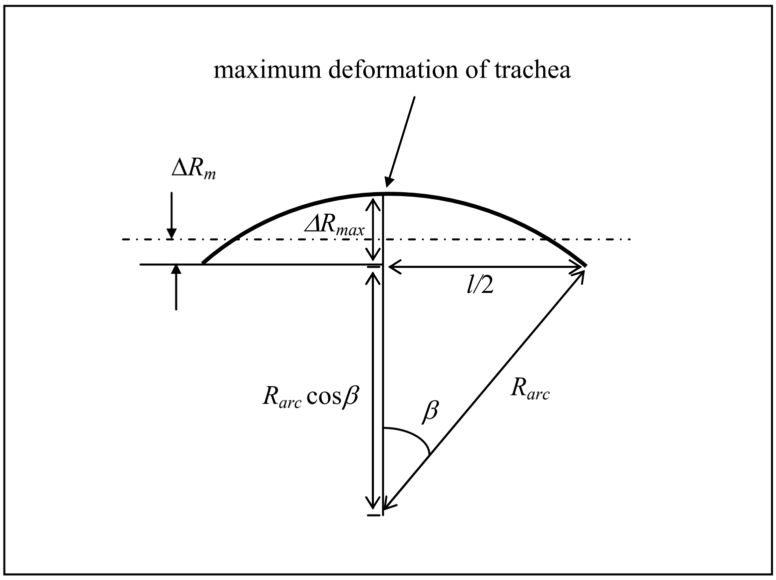

Figure 2.6 Deformation of trachea treated as an arc form

The mean radial deformation can be found by applying the following geometrical formula of a common sector with the condition $\beta \le \pi/4$ [25]

$$\Delta R_m = 0.3 R_{arc} \beta^2 \left(1 - 0.0976\beta^2 + 0.0028\beta^4\right) \tag{2.15}$$

From Figure 2.6 the following related trigonometric equations are applied to find an expression for R_{arc} and the angle β

$$\Delta R_{max} = R_{arc} - R_{arc} \cos\beta \tag{2.16}$$

which may be written as

$$R_{arc} \cos\beta = \sqrt{R_{arc}^2 - (l/2)^2} \tag{2.17}$$

Substituting equation (2.17) into equation (2.16) yields

$$\Delta R_{max} = R_{arc} - \sqrt{R_{arc}^2 - (l/2)^2} \tag{2.18}$$

Rearranging and squaring both sides to find an expression for R_{arc} as

$$R_{arc}^2 - 2R_{arc}\, \Delta R_{max} + \Delta R_{max}{}^2 = R_{arc}^2 - (l/2)^2 \tag{2.19}$$

and hence

$$R_{arc} = \frac{\Delta R_{max}^2 + (l/2)^2}{2\,\Delta R_{max}} \tag{2.20}$$

The angle β is

$$\beta = \sin^{-1} \frac{(l/2)}{R_{arc}} \tag{2.21}$$

Using equation (2.20) and (2.21), a value of mean deformation ΔR_m can be calculated by applying equation (2.15).

Experimentally ΔR_m is calculated for each step of increasing pressure q then a graph of q versus ΔR_m is drawn. The Young's modulus of elasticity E is obtained by calculating the slope of the graph with the related parameters in the formula for thin and thick-walled vessel. The value ΔR_m is to be substituted into ΔR in the equation (2.8) for the thin-walled vessel and into ΔR_{out} in the equation (2.14) for the thick-walled vessel.

Figure 2.7 shows a typical graph to find slope E.

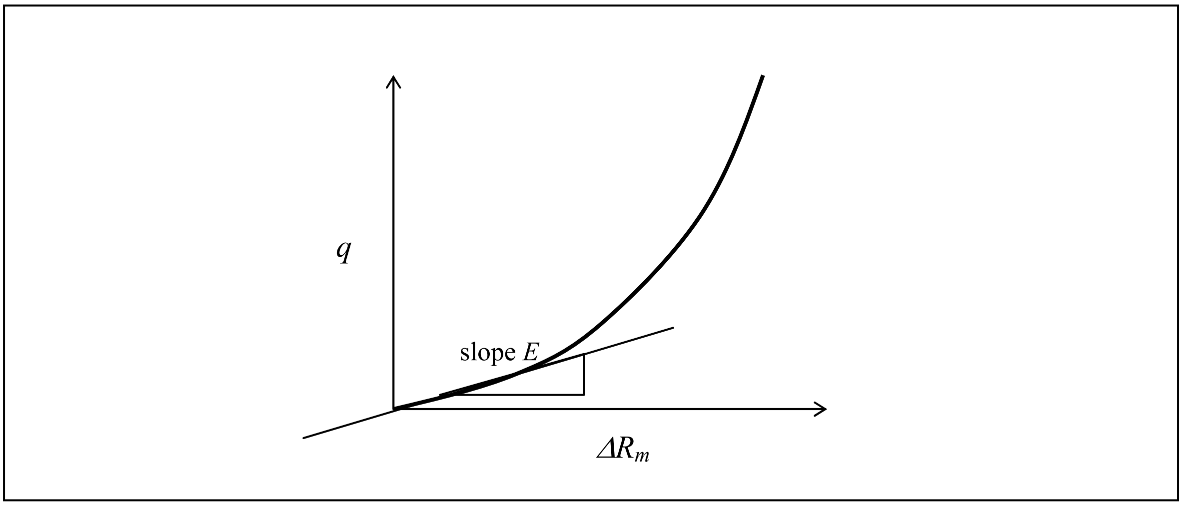

Figure 2.7 Typical graph of pressure applied versus radial deformation

2.4 Two-hydrophones Method

This particular method is proposed for the first time in this thesis and to the best of our knowledge it has not been used elsewhere for such an application. The method uses two hydrophones as the main apparatus for measuring comparative frequency responses in order to determine the Young's modulus of elasticity. The acoustic theory of transmission phenomena is applied to this methodology.

The theory of acoustic transmission considers that when an acoustic wave travels from one to another medium, at the interface two waves are generated, one reflects back and the other transmits through the second medium [26].

The assumptions made for this phenomenon are:

- the incident wave is planar
- the interface between the two mediums is planar.
- all mediums are fluids. Therefore any involvement of solid medium requires modification of the fact that the wave speed travels through the *bulk* modulus of the medium rather than Young's modulus. This assumption is justified as the density of the trachea is normally considered to equal the density of water.

The theory states that “the ratios of the pressure amplitudes and intensities of the reflected and transmitted waves to those of the incident wave depend both on the characteristic acoustic impedances and speeds of sound in the two media and on the angle of incidence with the normal to the interface” [26].

The characteristic impedance of a medium z is defined by

$$z = \rho c \tag{2.22}$$

where ρ is the equilibrium density of the fluid and c is the phase speed in the fluid.

The transmission from one fluid (I) to another (II) with the normal incidence is depicted in Figure 2.8. Assuming at the plane of interface $x_t = 0$ and $\mathbf{p}_i$, $\mathbf{p}_t$ and $\mathbf{p}_r$ are incident, transmitted and reflected pressure wave, respectively travelling in the positive x_t direction.

The pressure wave equations are [26]

$$\mathbf{p}_i = \mathbf{P}_i e^{j(\omega t - k_1 x_t)} \tag{2.23}$$

$$\mathbf{p}_r = \mathbf{P}_r e^{j(\omega t + k_1 x_t)} \tag{2.24}$$

$$\mathbf{p}_t = \mathbf{P}_t e^{j(\omega t - k_2 x_t)} \tag{2.25}$$

where

$\mathbf{P}_i$ = complex pressure amplitude of the incident wave

$\mathbf{P}_r$ = complex pressure amplitude of the reflected wave

$\mathbf{P}_t$ = complex pressure amplitude of the transmitted wave.

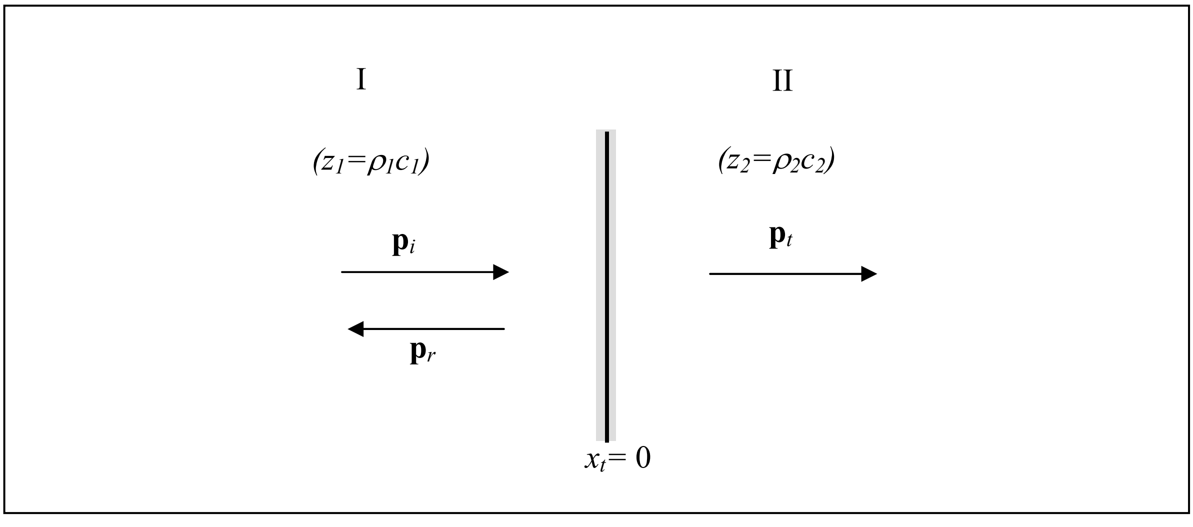

Figure 2.8. Reflection and transmission of plane waves normally incident on a boundary

$z_1=\rho_1 c_1$ is the characteristic impedance of fluid I and $z_2=\rho_2 c_2$ is the characteristic impedance of fluid II

The pressure transmission coefficient **T** is defined by

$$\mathbf{T} = \mathbf{P}_t / \mathbf{P}_i \tag{2.26}$$

and pressure reflection coefficient **R** is

$$\mathbf{R} = \mathbf{P}_r / \mathbf{P}_i \tag{2.37}$$

The theory also states that two boundary conditions must be satisfied for all times at all points on the interface [26] which are as follows

- The acoustic pressures on both sides of the interface are equal which means *continuity of pressure* – there is no net force on the plane separating the fluids.
- The particle velocities normal to the interface are equal which means *continuity of normal velocity* – the fluids remain in contact."

The pressure **p** and the normal particle velocity **u** in fluid I can be expressed as $\mathbf{p}_i + \mathbf{p}_r$ and $(\mathbf{u}_i + \mathbf{u}_r)x_t$ then the two boundary conditions are [26]

$$\mathbf{p}_i + \mathbf{p}_r = \mathbf{p}_t \qquad \text{at } x_t = 0 \tag{2.28}$$

$$\mathbf{u}_i + \mathbf{u}_r = \mathbf{u}_t \qquad \text{at } x_t = 0 \tag{2.29}$$

Division of **p/u** yields a statement of the continuity of *normal specific impedance* across the interface

$$\frac{\mathbf{p}_i + \mathbf{p}_r}{\mathbf{u}_i + \mathbf{u}_r} = \frac{\mathbf{p}_t}{\mathbf{u}_t} \qquad \text{at } x_t = 0 \tag{2.30}$$

Since a plane wave has $\mathbf{p/u}=\pm z$ depending on the direction of propagation becomes

$$z_1 \frac{\mathbf{p}_i + \mathbf{p}_r}{\mathbf{p}_i - \mathbf{p}_r} = z_2 \tag{2.31}$$

which leads to the reflection coefficient

$$\mathbf{R} = \frac{z_2 - z_1}{z_2 + z_1} = \frac{1 - z_1/z_2}{1 + z_1/z_2} \tag{2.32}$$

Since $1 + \mathbf{R} = \mathbf{T}$, the transmittance coefficient can be written as

$$\mathbf{T} = \frac{2z_2}{z_2 + z_1} = \frac{2}{1 + z_1/z_2} \tag{2.33}$$

Having known any of the characteristic impedance z, the value of bulk modulus M_B can be determined using the relationship

$$M_B = \frac{z^2}{\rho} \tag{2.34}$$

The Young's modulus E can then be determined through the relationship [25]

$$M_B = \frac{E}{3(1-2\nu)} \tag{2.35}$$

The formula in equation (2.35) is based on the consideration of strains caused by triaxial stresses.

2.4.1 Application to Present Work

For the main setup of the two-hydrophones method, one of the hydrophones is used as a transmitter and the other as a receiver.

The parameters obtained from the measurement devices are in the form of input and output pressure signals. These measurement devices are the receiver hydrophone and a digital oscilloscope. For this particular application, only the transmitted pressure waves are detected and hence the direct measurement of the reflected waves components are not of relevance to this work.

The simple setup of the two-hydrophones method is laid out in Figure 2.9. Setup 1 represents acoustic measurements in a single medium, basically water , and the second setup represents acoustic measurements in two mediums, water and trachea.

The basic principle of this method is to utilise the differences in the transmission coefficients resulting from the two setups. Setup 1 represents a complete transmission through a medium of water and Setup 2 represents a transmission via water and a trachea tissue. In this method z_w is the characteristic impedance of water and z_t is the characteristic impedance of trachea. The distance between the transmitter and receiver hydrophones are the same for the two setups.

In the two setups, transmission loss is normally associated with the use of the two hydrophones and the surrounding media. In this work, the acoustic losses are assumed to be the same in both setups based on the fact that the media (surrounding container) and two hydrophones are the same in the two setups.

The difference in magnitude of the transmission coefficients between Setup 1 and Setup 2 reflects the presence of the trachea tissue where its characteristic impedance z_t is to be determined. Knowing that the value of water and tracheal densities to be similar, the difference of the two coefficients is simply a function of tracheal bulk modulus which can be determined by the formula from equation (2.34).

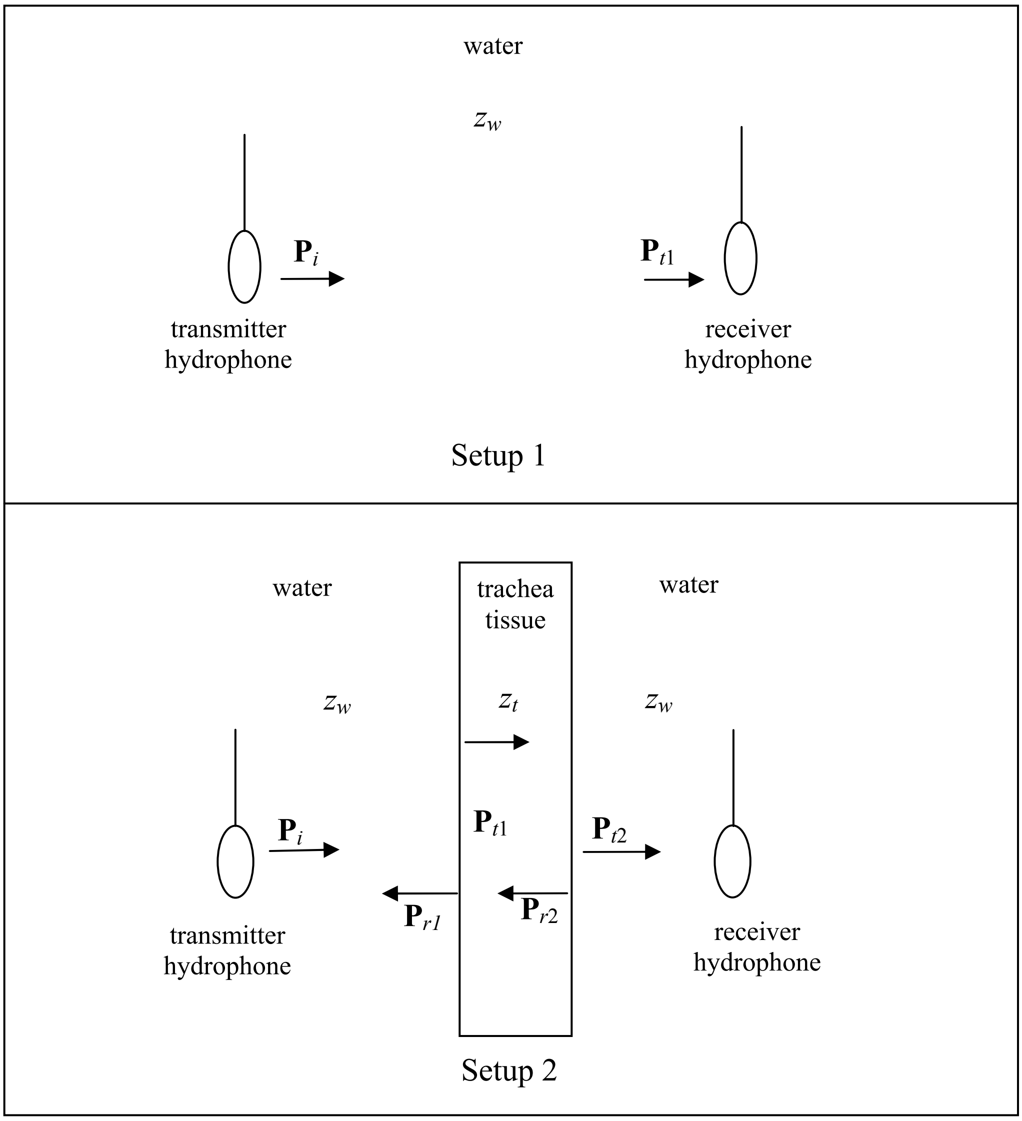

Figure 2.9 The two-hydrophones method

Figure 2.10 shows the following cases:

(a) Single medium water transmission with $\mathbf{P}_i$ as the pressure generates by the transmitter hydrophone and $\mathbf{P}_{t1}$ as the pressure measured by the receiver hydrophone.

(b) Transmission through three regions, water, trachea and then water again. with $\mathbf{P}_i$ as the pressure generates by the transmitter hydrophone; $\mathbf{P}_{r1}$ and $\mathbf{P}_{r2}$, pressure waves reflects at the in- and out-interface of the trachea, respectively; $\mathbf{P}_{t1}$ and $\mathbf{P}_{t2}$, are pressure signals transmitted in trachea and the second region of water, respectively. Also $\mathbf{P}_{t2}$ is the pressure measured by the receiver hydrophone.

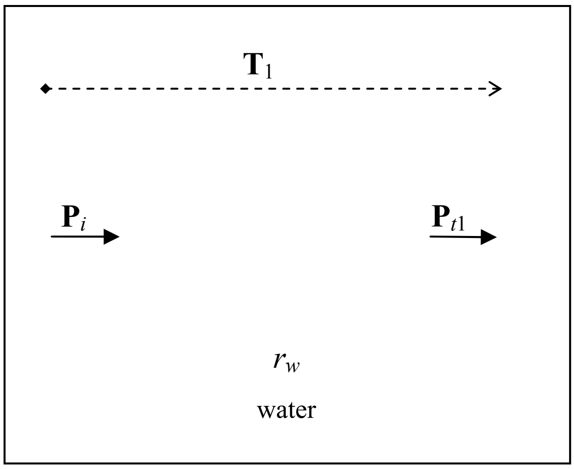

(a) Setup 1

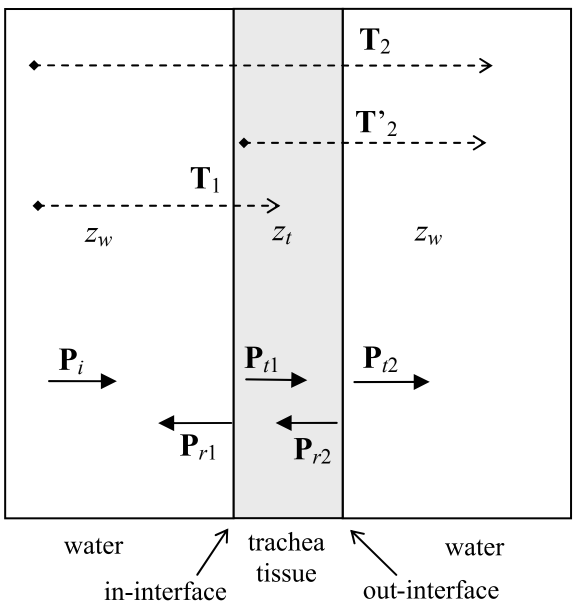

(b) Setup 2

Figure 2.10 Transmission of signal pressure

Steps of transmission expression of Setup 2 can be laid out as the scheme below

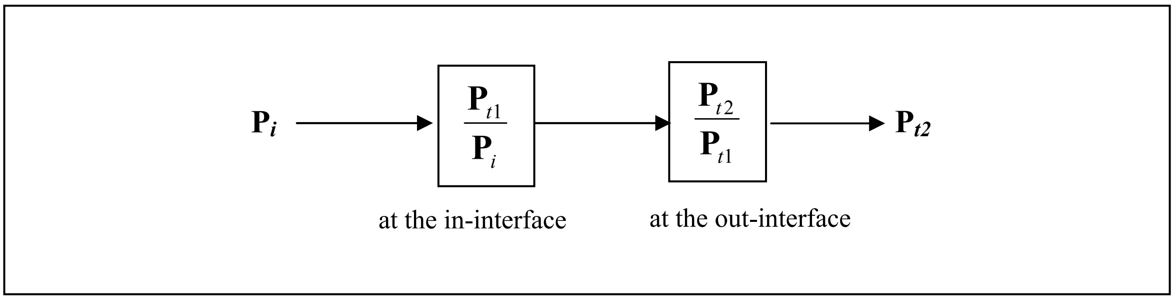

Figure 2.11 Transmission expression

The transmission coefficients of both setups can be expressed as:

Setup 1: $$\mathbf{T}_1 = \frac{\mathbf{P}_{t1}}{\mathbf{P}_i} \tag{2.36}$$

Setup 2: $$\mathbf{T}_2 = \frac{\mathbf{P}_{t2}}{\mathbf{P}_i} \tag{2.37}$$

An expression that represents the signal transmission of Setup 2 is thus

$$\frac{\mathbf{P}_{t2}}{\mathbf{P}_i} = \frac{\mathbf{P}_{t1}}{\mathbf{P}_i} \times \frac{\mathbf{P}_{t2}}{\mathbf{P}_{t1}} \tag{2.38}$$

Another simplified expression for this is:

$$\mathbf{T}_2 = \mathbf{T}_1 \times \frac{\mathbf{P}_{t2}}{\mathbf{P}_{t1}} \tag{2.39}$$

The coefficient $\frac{\mathbf{P}_{t2}}{\mathbf{P}_{t1}}$ stands for the transmission from the first tracheal boundary through to the water and receiver. It is assigned as

$$\mathbf{T}_2' = \frac{\mathbf{P}_{t2}}{\mathbf{P}_{t1}} \tag{2.40}$$

Equation (2.33) represents transmission in two regions of different medium only whereas in Setup 2, three regions are present. The first and third regions are of the same medium, water, and the second region is the trachea tissue. $\frac{\mathbf{P}_{t2}}{\mathbf{P}_i}$ needs to be derived for the three regions medium in terms of z_t, as follows.

At the first interface, equation (2.31) can be expressed as

$$z_w \frac{\mathbf{P}_i + \mathbf{P}_{r1}}{\mathbf{P}_i - \mathbf{P}_{r1}} = z_t \tag{2.41}$$

This can be written as

$$\mathbf{P}_{r1} = \frac{z_t - z_w}{z_w + z_t} \mathbf{P}_i \tag{2.42}$$

Also at the same interface, equation (2.28) can be written as

$$\mathbf{P}_i + \mathbf{P}_{r1} = \mathbf{P}_{t1} \tag{2.43}$$

This may be written as

$$\mathbf{P}_{r1} = \mathbf{P}_{t1} - \mathbf{P}_i \tag{2.44}$$

Substituting equation (2.44) into equation (2.42) gives

$$\boxed{\mathbf{P}_{t1} = \frac{2z_t}{z_w + z_t} \mathbf{P}_i} \tag{2.45}$$

At the second tracheal and water interface, equation (2.31) can be written as

$$z_t \frac{\mathbf{P}_{t1} + \mathbf{P}_{r2}}{\mathbf{P}_{t1} - \mathbf{P}_{r2}} = z_w \tag{2.46}$$

and equation (2.28) as

$$\mathbf{P}_{t1} + \mathbf{P}_{r2} = \mathbf{P}_{t2} \tag{2.47}$$

where rearrangement for $\mathbf{P}_{r2}$ becomes

$$\mathbf{P}_{r2} = \mathbf{P}_{t2} - \mathbf{P}_{t1} \tag{2.48}$$

Substituting equation (2.48) into equation (2.46) gives

$$\boxed{z_t \frac{\mathbf{P}_{t2}}{2\mathbf{P}_{t1} - \mathbf{P}_{t2}} = z_w} \tag{2.49}$$

Substituting equation (2.45) into (2.49) yields

$$z_t \frac{\mathbf{P}_{t2}}{\left[\dfrac{4z_t}{z_w + z_t}\mathbf{P}_i\right] - \mathbf{P}_{t2}} = z_w \tag{2.50}$$

Then the transmission coefficient can be expressed as

$$\frac{\mathbf{P}_{t2}}{\mathbf{P}_i} = \frac{4z_w z_t}{(z_w + z_t)^2} \tag{2.51}$$

As briefly explained before, although Setup 1 produces a complete transmission, its transmission coefficient does not add up to the ideal '1' due to the characteristic of the hydrophones. Since the same hydrophones are used in the two setups, one can assume that the losses between the hydrophones and water are the same in the two setups. Hence calculation straight from equation (2.51) does not give a correct value of z_t.

This approach of calculating z_t needs to consider the transmission loss. Since $\mathbf{P}_{t2}$ in equation (2.51) is the transmitted pressure after the loss, $\mathbf{P}_i$ needs to be normalised by a value that represents the pressure incident after this loss. The transmitted pressure $\mathbf{P}_{t1}$ from Setup 1 is a complete transmission value after the transmission loss by the hydrophones. Therefore, for equation (2.51), $\mathbf{P}_i$ of Setup 2 is assumed to be equal to $\mathbf{P}_{t1}$ from Setup 1

$$\mathbf{P}_i = \mathbf{P}_{t1} \tag{2.52}$$

which now yields

$$\boxed{\frac{\mathbf{P}_{t2}}{\mathbf{P}_{t1}} = \frac{4z_w z_t}{(z_w + z_t)^2}} \tag{2.53}$$

where the characteristic impedance of water is $z_w = 1.48 \times 10^6$ Pas/m.

This transmission equation (2.53) conforms with equation (2.40) $\mathbf{T}_2^{'} = \dfrac{\mathbf{P}_{t2}}{\mathbf{P}_{t1}}$ that stands for the transmission from the in-interface to the receiver hydrophone.

After solving for z_t, the rest of the values for the bulk modulus and Young's modulus can be determined by applying equation (2.34) and (2.35).

2.5 Vibration Method

In this part of the research, vibration is applied to the trachea in order to obtain the natural frequencies. In the experimental part of this research, the wall is excited as a simple diaphragm which validates the assumption of using thin wall theories. A derived formula of vibrated thin elastic cylindrical shell is used to determine the Young's modulus of elasticity of the tissue. This formula contains expressions of the relationship between the natural frequencies, the Young's modulus and other dimensional parameters. The Young's modulus can hence be found as a function of the natural frequency and other parameters that relates to the time dependent vibratory motions.

2.5.1 Free Vibration of Cylindrical Shells

The theory used for this experimental procedure is based on the formula for thin cylindrical shells after Donnell [27].

Vibrating a shell from a stationary or stable equilibrium position creates a scene that has a property of being time-dependent. When these vibratory motions occur in the absence of external loads, they are called as 'free' vibrations. On the other hand, whenever external loads are applied, they are referred to as 'forced' vibrations.

Donnell formulation is based upon the assumptions that the expressions for the changes in curvature and twist of the cylinder are the same as those of a flat plate [27]. He assumes that the effect of the transverse shearing-stress resultant on the equilibrium of forces in the circumferential direction is negligible. With these assumptions the equations shown in Appendix C are developed for axial, circumferential and radial equilibrium. For a clamped thin circular cylindrical shell, the non-dimensional natural frequency may be determined by solving the following characteristic equation for the non-dimensional natural frequency Δ

$$\Delta^3 - R_2\,\Delta^2 + R_1\,\Delta - R_0 = 0 \qquad (2.54)$$

where

$$\Delta = \rho r^2\left(1-v^2\right)\frac{\omega^2}{E} \tag{2.55}$$

$$\theta_1 = 1 + k^2 \tag{2.56}$$

$$\theta_2 = 1 - k^2 + \frac{2r}{\mu l} sin\frac{\mu l}{r} \tag{2.57}$$

$$\frac{1}{\xi} = \frac{h^2}{12r^2} \tag{2.58}$$

$$R_2 = \left(\frac{\theta_1}{\theta_2} + \frac{1-v}{2}\frac{\theta_2}{\theta_1}\right)\mu^2 + 1 + \frac{3-v}{2}n^2 + \frac{1}{\xi}\left(\mu^4 + n^4 + 2\mu^2 n^2 \frac{\theta_2}{\theta_1}\right) \tag{2.59}$$

$$R_1 = \frac{1-v}{2}\left(\mu^4 + n^4\right) + \left(\frac{\theta_1}{\theta_2} - \frac{v\theta_2}{\theta_1}\right)\mu^2 n^2 + \frac{1-v}{2}n^2 + \mu^2\left[\frac{\theta_1}{\theta_2} + \frac{\theta_2}{\theta_1}\frac{\left(1-v-2v^2\right)}{2}\right]$$
$$+\frac{1}{\xi}\left[\frac{1-v}{2}\left(n^2 + \mu^2\frac{\theta_2}{\theta_1}\right) + n^2 + \mu^2\frac{\theta_1}{\theta_2}\right] \times \left[\mu^4 + n^4 + 2\mu^2 n^2 \frac{\theta_2}{\theta_1}\right] \tag{2.60}$$

$$R_0 = \frac{1-v}{2}\left[1 - v\left(\frac{\theta_2}{\theta_1}\right)^2\right]\mu^4$$
$$+\frac{1}{\xi}\left\{\mu^2 n^2\left[\frac{1+v}{2}\frac{\theta_2}{\theta_1} - \frac{\theta_1}{\theta_2} - \left(\frac{1-v}{2}\right)^2\frac{\theta_2}{\theta_1}\right] - \frac{(1-v)}{2}\left(\mu^4 + n^4\right)\right\}\left[\mu^4 + n^4 + 2\mu^2 n^2\frac{\theta_2}{\theta_1}\right] \tag{2.61}$$

and

$$k = \frac{sin\left(\mu l/2r\right)}{sinh\left(\mu l/2r\right)} \tag{2.62}$$

The quantity μ insures that the end conditions will be met and satisfies the equation

$$tan\frac{\mu l}{2r} + tanh\frac{\mu l}{2r} = 0 \tag{2.63}$$

whose roots are

$$\frac{\mu l}{r} = 1.506\pi, 3.5\pi, 5.5\pi, 7.5\pi, \ldots \tag{2.64}$$

These values correspond to 1, 3, 5, 7, ...axial waves respectively. For an even number of half waves, a different but similar form of solution would have to be assumed.

It is required that the natural frequencies of free vibration must be real quantities, hence the cubic equation of (2.54) will have three real positive unequal roots expressed as

$$\Delta_1 = 2\alpha^{1/3} \cos\frac{\theta}{3} + \frac{R_2}{3} \tag{2.65}$$

$$\Delta_2 = 2\alpha^{1/3} \cos\frac{\theta + 2\pi}{3} + \frac{R_2}{3} \tag{2.66}$$

$$\Delta_3 = 2\alpha^{1/3} \cos\frac{\theta + 4\pi}{3} + \frac{R_2}{3} \tag{2.67}$$

where

$$\alpha = \left[-\frac{1}{27}\left(R_1 - \frac{R_2^2}{3} \right)^3 \right]^{1/2} \tag{2.68}$$

$$\theta = \cos^{-1}\left\{ \frac{1}{2\alpha}\left[R_0 - \frac{R_1 R_2}{3} + \frac{2R_2^3}{27} \right] \right\} \tag{2.69}$$

2.5.2 Application to Present Work

Up to this point, some of the important informations regarding the relationship between the natural frequencies and cylinder's dimensional parameter have been stated by the variational solution. Equation (2.55) in particular is the core equation that can be used to describe theoretical approximation of this method. The roots of the non-dimensional natural frequency Δ need to be determined through an extensive process of calculation involving various related coefficients such as R_2, R_1 and R_0.

This research selects the method of variational solution because it has direct representation to the experimental set up in terms of the parameters and their relationships. Both variational and exact methods give the same characteristics of the three natural frequencies obtained by the three roots which shows that one is always much lower than the other two. It is also noted that the variational solution method presents the closest agreement with the experimental data [27]. The 'exact' solution of Donnell's equation presents less direct practical relevance and thus is not elaborated in this section.

The experimental set up consists of a trachea tissue section being clamped at both ends. An electromagnetic shaker is positioned to excite the centre of the tissue as in Figure 2.12. A laser vibrometer is used to detect vibrations for different generated frequencies being displayed on the oscilloscope. At the peak growth of amplitude, the generated frequencies represent the resonance or natural frequencies of the trachea.

Equation (2.55) leads to an involved calculation process to find the non-dimensional natural frequencies Δ. Using the values of ω from the experimental results and the roots of Δ from equation (2.54) and implementing density ρ, Poisson's ratio v and radius r leads to the Young's modulus of elasticity E.

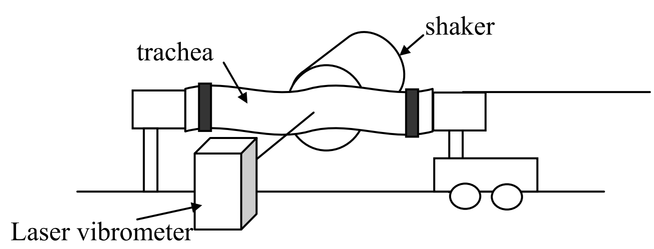

Figure 2.12 Layout of vibration method

Chapter 3
Experimental Investigation

3.1 Introduction

The experimental investigation includes a number of procedures to determine various mechanical properties of the airway wall, in particular the trachea. This chapter presents the details of the methodology used within this research describing the lists of equipment used, the design of the setup apparatus and the procedural approach to obtain measurements.

The four methods described in chapter 2 are converted to experimental setups in this chapter. The tissues used are excised pig tracheas as they are structurally the closest to humans [2]. Preparation of the tissues is also described in this chapter.

For comparison purpose, the first part of the experimentation is focused on the uniaxial state of stress in order to determine reference values. The other three methods are explained afterwards. These three techniques are referred to as:
(1) The pressure difference method
(2) The two-hydrophones method
(3) The vibration method

Analysis and discussion are given in chapter 5 along with conclusions and recommendations.

3.2 Pigs Trachea Preparation

Trachea tissues after being excised were brought to the Biology Laboratory to be prepared for experimentation. The outer connecting muscles, blood veins, and other attached arterial tissues were removed with scalpel on a dissecting board. The cleaned tissues were stored by immersing them in a container filled with 0.9 percent concentrated saline water. Figure 3.1 to 3.3 show the process of preparation.

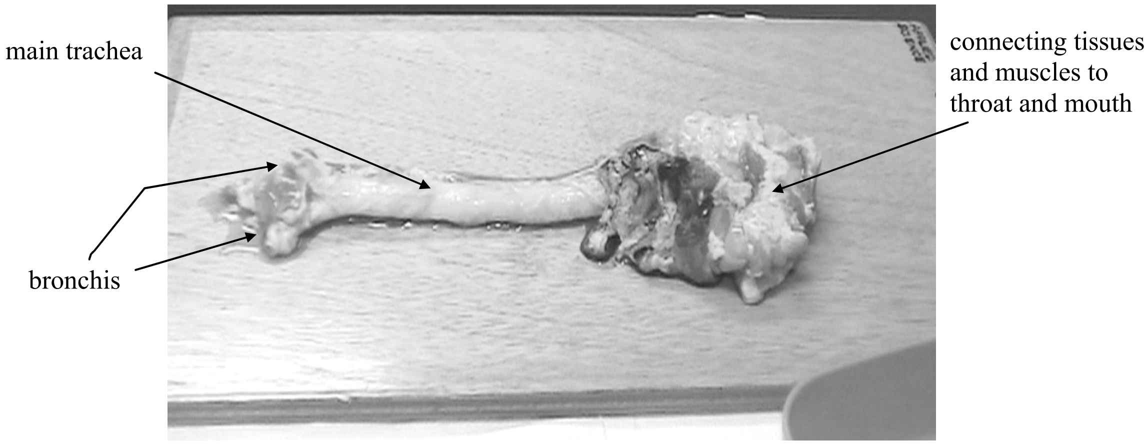

Figure 3.1 Uncleaned pigs trachea

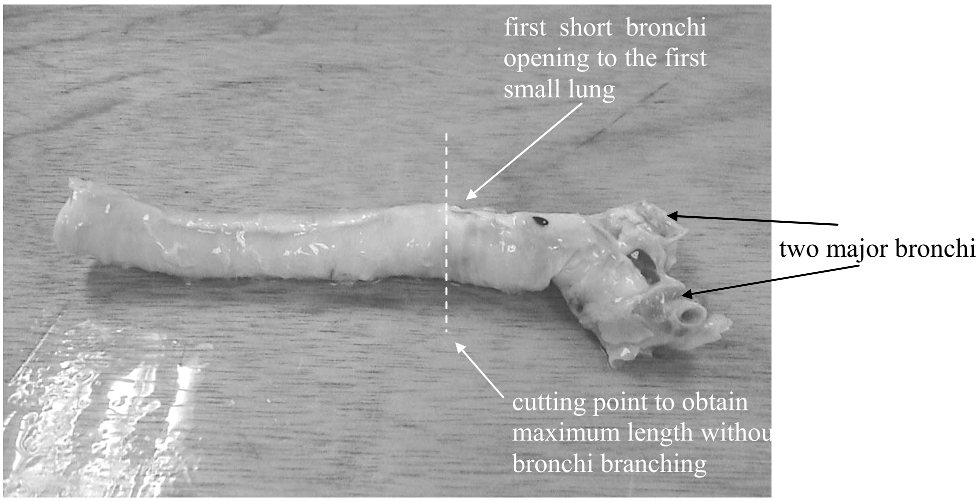

Figure 3.2 Cleaned pig's trachea tissue with two short-cut bronchis

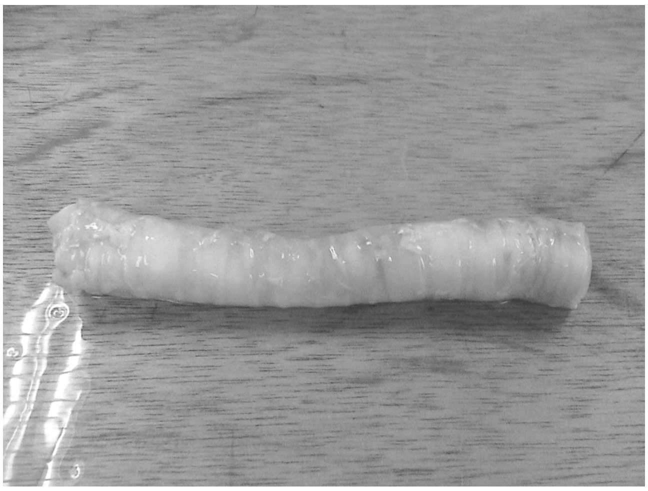

(a) length-wise view

Figure 3.3 Prepared pig's trachea tissue ready to be measured and mounted

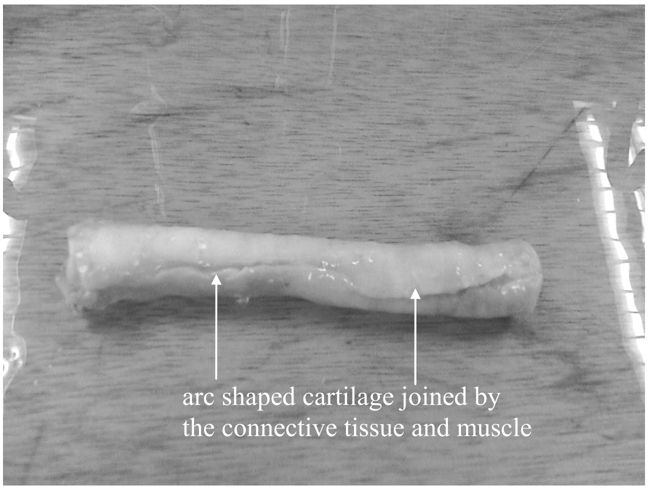

(b) length-wise view opposite from (a) where the arc shaped cartilage joins by connective tissue muscles to form circular cylindrical shell

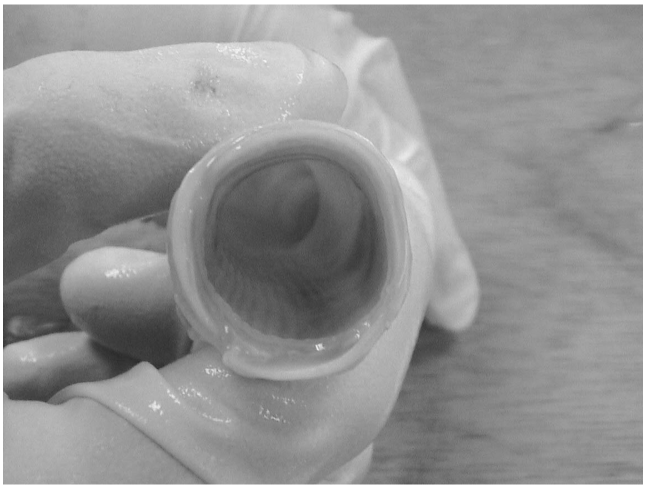

(c) cross-sectional view

Figure 3.3 Prepared pig's trachea tissue ready to be measured and mounted (continued)

Dimensional measurements were taken for the thickness, inner radius and density. A vernier calliper is used to measure the thickness and the inner diameter. Tracheal density is obtained by utilising a scale for weighing and a water-filled measuring cylinder to obtain the trachea's volume through the displaced water.

As the nature of this research involves an extensive setup, it is often unachievable to complete the four methods within one day. The trachea tissue needs to be preserved to retain its freshness for the experiment to be carried out on the next day or any day within a week. It is believed that immersing it in saline solution and storing it in a covered container is sufficient for the short term storage to be used within two to three days. For a longer term storage but not more than two weeks, Tyrode's solution [28] or freezing are used as preservative. The recipe ingredients to make 1000 ml Tyrode's solution is shown in Table 3.1

Table 3.1 Ingredients of Tyrode's solution

Ingredients	Quantity
NaCl	8 g
KCl	0.2 g
$CaCl_2$	0.2 g
$MgCl_2$	0.1 g
$NaHCO_3$	1 g
NaH_2PO_4	0.05 g
d-glucose	1 g
Distilled water	1000 ml

The Tyrode's solution is prepared immediately before use by pouring 1000 ml distilled water into a flask. Then the other ingredients listed in Table 3.1 are added, shaken and stirred well.

3.3 Conventional Tension Method

This is a standard uniaxial state of stress test carried out by applying loads to stretch the tissues. The Young's modulus is determined through the rate of tissues deformation in term of its instantaneous strain as explained in chapter 2. This approach is considered destructive due to the way the tissues are prepared in order to provide the stresses equivalent to the circumferential stress. The tissues also have direct contact with the applied loads and thus only a small range of mass loads can be applied to detect the linear behaviour of the tissue.

Since limited information is available on the modulus of elasticity of the trachea, three types of uniaxial tests are conducted. It is felt that these methods will give satisfactory ranges for comparison. Further, the trachea is nonhomogeneous material and more than one modulus can be defined. In this work, three moduli are determined, one to exclude the connective tissue of the cartilage, the second is to include it and the third to look at the axial elasticity. Figure 3.3(b) and 3.4(b) show the connective tissue and muscle of the trachea.

3.3.1 Apparatus

The measurement devices consists of Keyence laser displacement meter model LK-031 and a multimeter. The rig is a custom built tension test system which consists of a wooden base, end pulley, a pole with horizontal clamping tube and four-wheels mini trolley with a clamping tube and string attached to connect to loads as shown in Figure 3.5. The loads used are in 5 g and 10 g increments to the total of 120 g. The horizontal clamping tubes are in 13 mm and 18 mm diameter pairs. The clamps are plastic hose clamps with adjustable grids in 15 mm and 20 mm size diameters. The clamp and clamping tube size is selected to fit the tracheal diameter in order to achieve a firm mounting. When both sizes of clamps do not fit the trachea, either one is too loose and another too small, an adjustment is made to the clamp size by cutting a small length off both ends of the grips.

3.3.2 Procedure of Circumferential Testing – Cutting the Trachea Along the Connective Tissue and Muscle

A trachea tissue is cut across into a ring shape about 2 cm in length l_w as shown in Figure 3.4(a). The ring shape is then cut across along the connective tissue and muscle between the closing end of the cartilage as shown in Figure 3.4(b). By such cutting, this circumferential testing excludes the connective tissue and muscle. With care, the tissue is opened as a flat strip as shown in Figure 3.4(c) and mounted where the cartilage grooves line up in the horizontal direction so that the tension force pulls along the same axes as the cartilage rings shown in Figure 3.4(d).

The plastic hose clamps are used to hold both ends of the tissues to the clamping tubes. One of the clamps stays fixed and the other is part of a trolley that acts as a pulling device connected to loads by a piece of string.

The direction of the tissue mounted and the applied force are such that to produce stresses equivalent to the circumferential stresses in a ring, as if before cutting it. Figure 3.5 illustrates the set up of the tension test rig. The strain from the circumferential testing represents the radial strain since it gives a similar ratio between the deformation and the initial length.

Measurements taken for the purpose of calculating the strain and stress involved in this test are:

- the initial length L_0 , which is the clamped length of the trachea between the two clamps mounted without any loads applied
- the cross sectional area A, which is the thickness h times the cut-length of the trachea l_w and under tensile force $F=Mg$.

Figure 3.4(d) depicts the configurations and the mounted cartilage direction for this test.

The laser displacement meter is used to detect the tissues deformation by the movement of the stretched tissue towards the loads. Starting from 0 g, the loads are increased by increments of 5 g to the total loads of 120 g. The readings are recorded after 30 seconds for every change of load in order to take maximum deformation after the load is applied.

The graphs of tensile stress versus strain are then plotted and the slope of this plot indicates the circumferential Young's modulus.

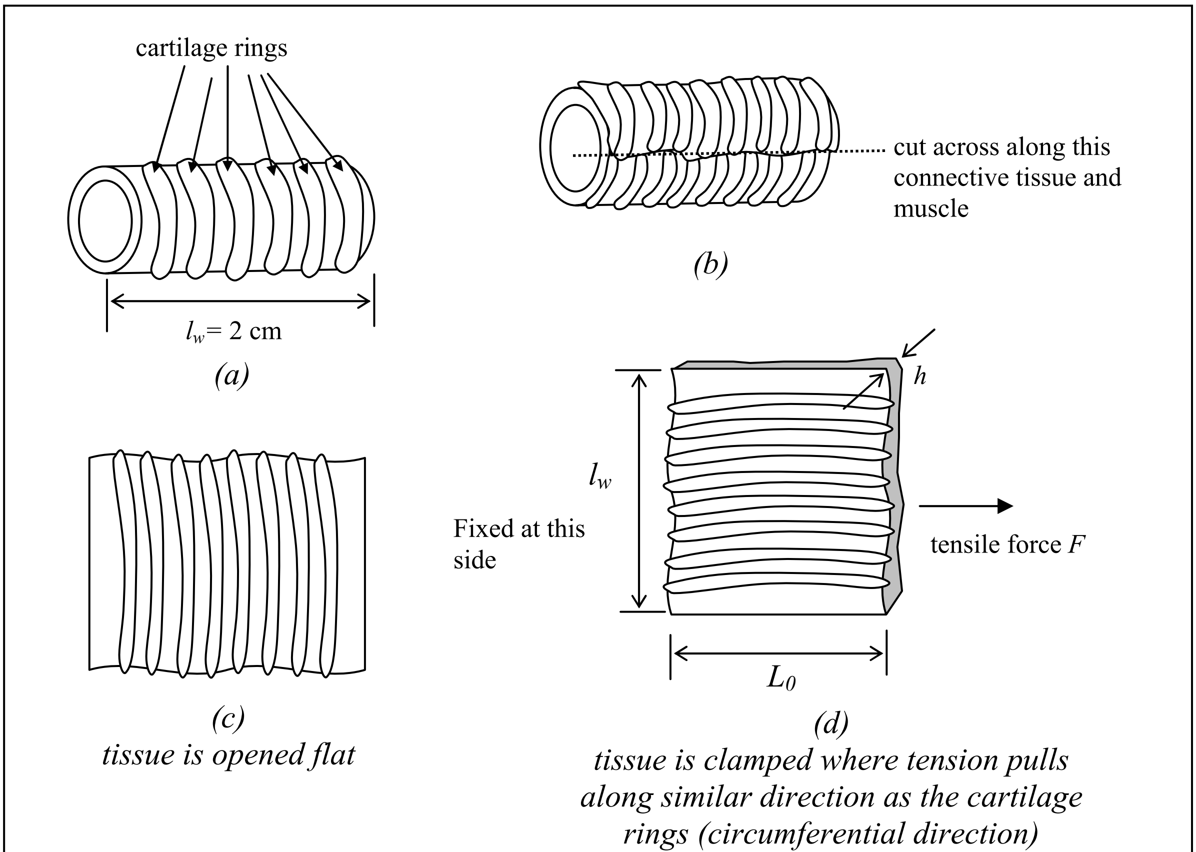

Figure 3.4 Cutting the trachea along the connective tissue and muscle

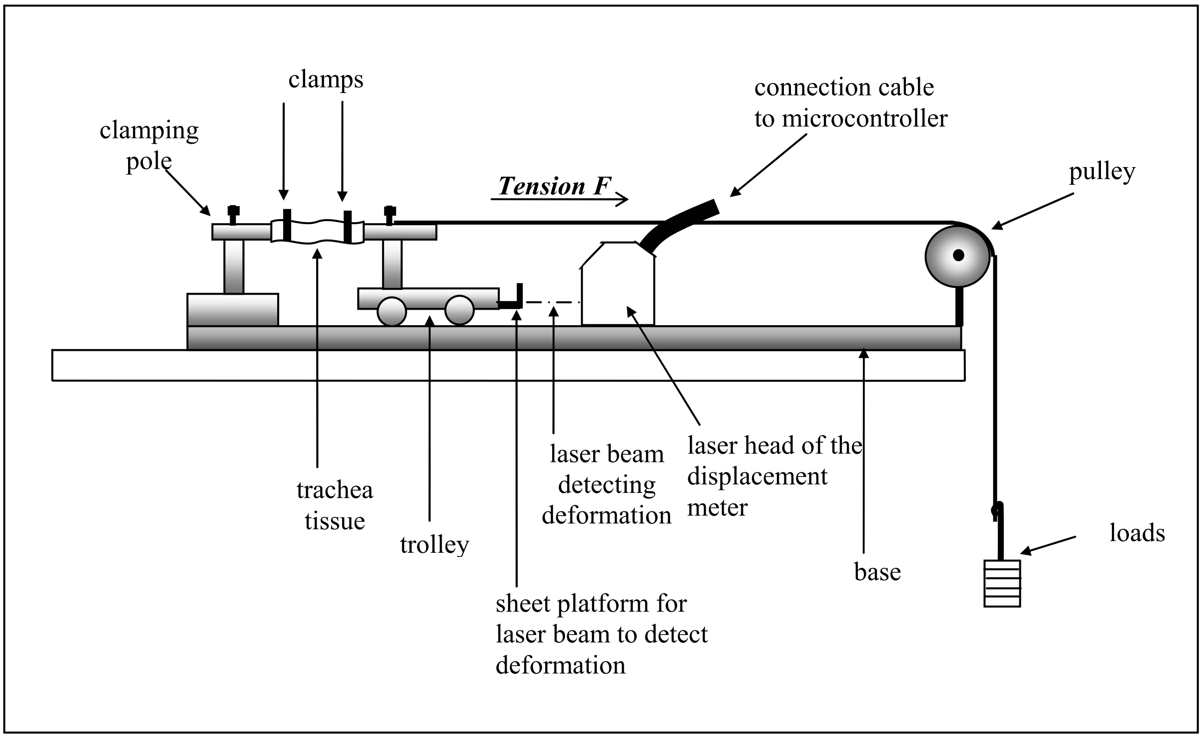

Figure 3.5 Conventional tension method system

3.3.3 Procedure of Circumferential Testing – Cutting the Trachea Along the Cartilage

Another section of trachea tissue is cut similarly across into a ring shape about 2 cm width. This time the ring shape is cut across horizontally along the cartilage part of the trachea, away from the connective tissue and muscle shown in Figure 3.6(a). By such cutting, this circumferential testing includes the connective tissue and muscle. Again the tissue is opened up as a flat strip and mounted where the cartilage grooves line up in the horizontal direction so tension force pulls in the same axes direction as the cartilage rings shown in Figure 3.6(b). Measurements are taken for the clamped length L_0 and the cross sectional area A. Similar procedure then follows as the previous test.

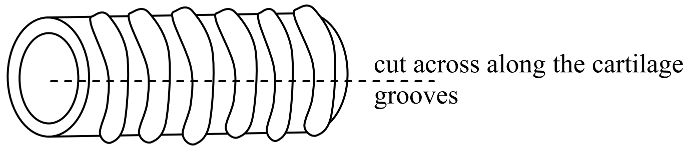

(a)

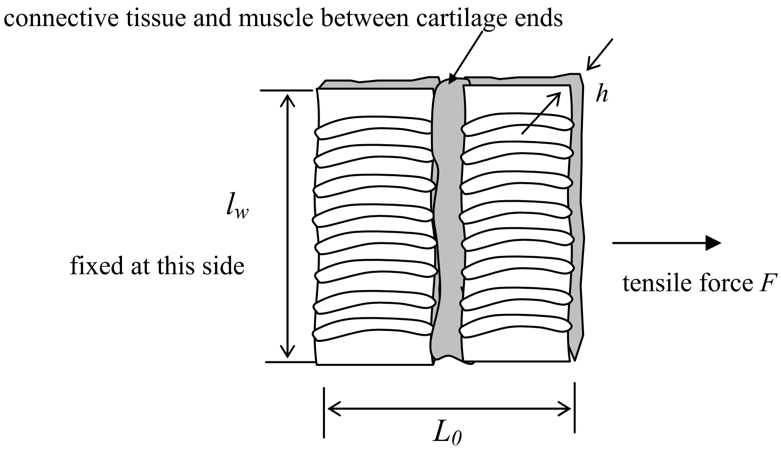

(b) tissue is clamped where tension pulls along similar direction as the cartilage rings (circumferential direction)

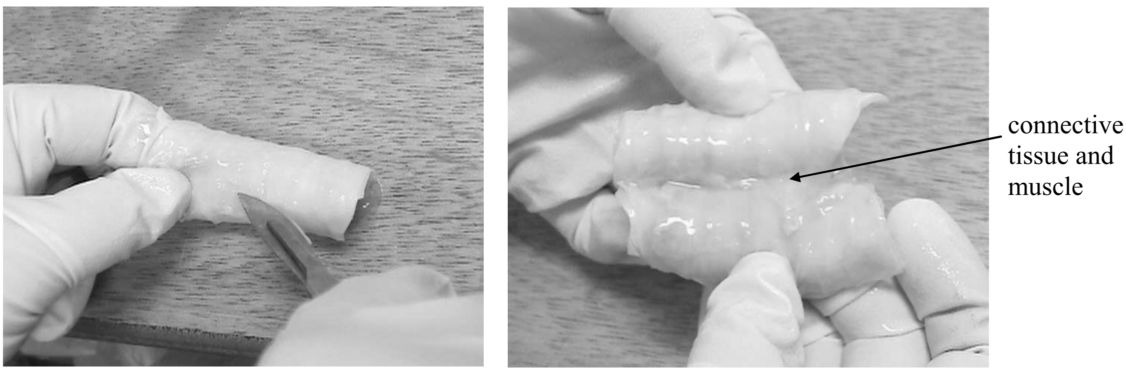

(c) Photographs of trachea cutting along the cartilage

Figure 3.6 Cutting the trachea along the cartilage

3.3.4 Procedure of Axial Testing

The remaining length of trachea tissue which has not been cut across and split-open is used for further tests to determine the axial Young's modulus. A similar setup is used for this experiment except that the tracheas are clamped directly to the axial tension as a cylinder-shaped element. The same procedure is repeated for this measurement. The graphs of tensile stress versus strain are also plotted and the slope of this curve indicates the axial Young's modulus. Diagrams from the experiments are shown in Figure 3.7 (a) and (b).

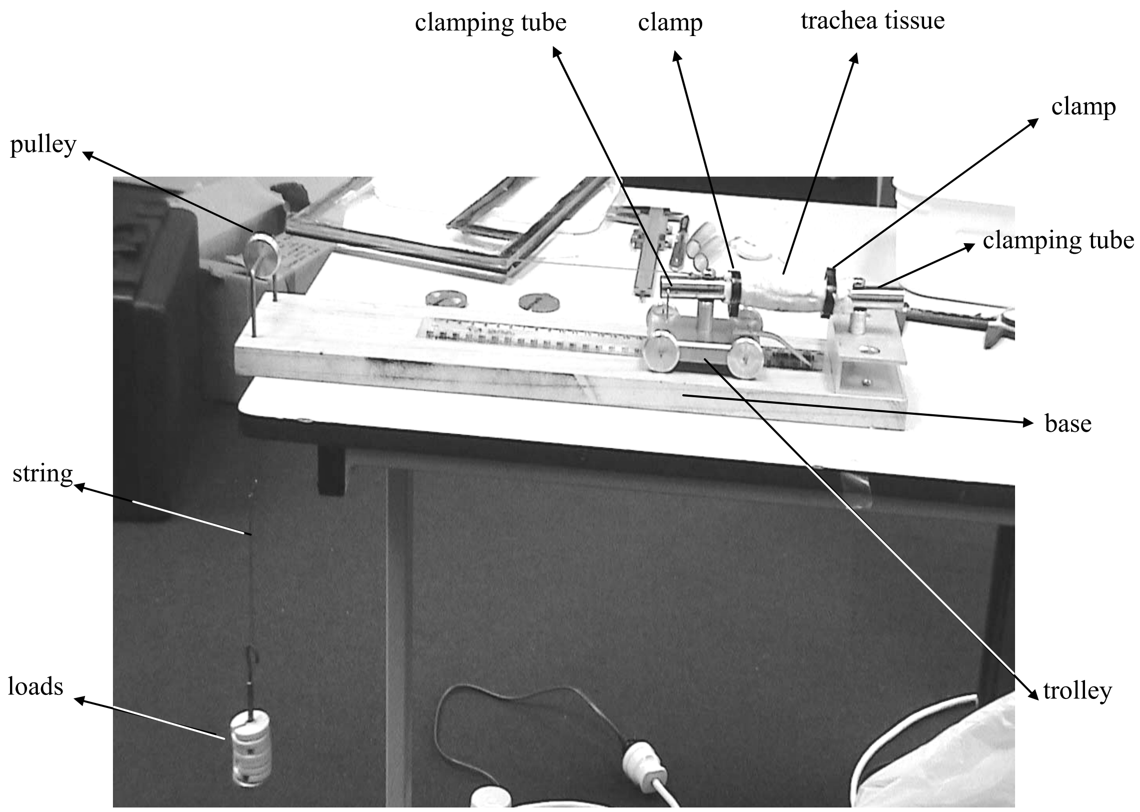

(a) Setup with hanging loads shown

Figure 3.7 Photographs of the conventional tension method setup for the axial deformation

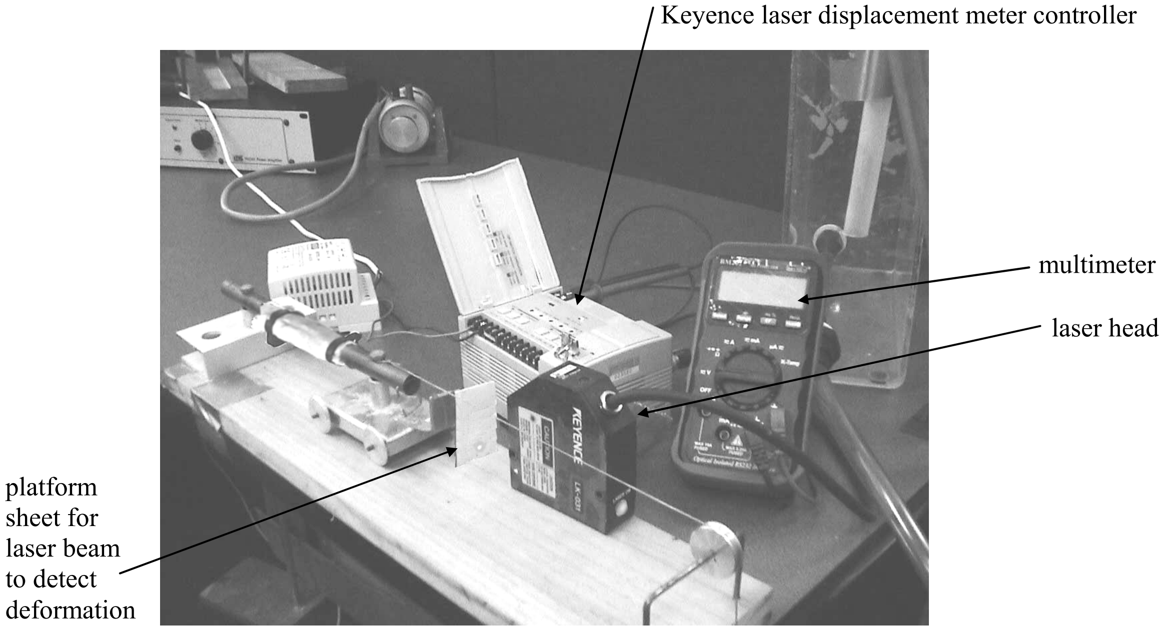

(b) Setup with laser displacement meter shown

Figure 3.7 Photographs of the conventional tension method setup for the axial deformation (continued)

3.4 Pressure Difference Method

This method is developed based on simulating the trachea as a pressurised vessel and deducing a special relationship between the pressure and the radial deformation. The tissues are placed under fluid pressure and by changing the pressure, the radial deformation is obtained [2]. Using the rate of change between pressure and radial deformation, the Young's Modulus of Elasticity can then be calculated using the principles explained in the chapter 2.

3.4.1 Apparatus

In this setup the measurement devices consist of Keyence laser displacement meter model LK-031 and a multimeter. The main parts of the rig are the tank, connecting pipes, two reservoirs and two poles with a height-adjustable holder for the reservoirs. Details of the rig components are shown in Table 3.2and Figure 3.8.

Table 3.2 Details of the rig component for the pressure difference method

Quantity	Components	Dimension	Description
1	Clear acrylic tank	250×300× 100 mm^3	On the 100 mm sides of the tank, two 15 mm holes diameter are made where one facing the opposite each other. Due to the operating distance of the laser displacement meter, the centre of the holes are positioned about 15 mm from the side and bottom edges. Custom made by Modern Plastics, Glenfield, Auckland.
2	Plastic hose clamps with adjustable closing grids	15 mm diameter	More often used in this method than the 20 mm clamps.
4	Plastic hose clamps with adjustable closing grids	20 mm diameter	One pair of the clamps can have slight cut at the end of grid lengths to achieve firm mounting of a tissue whenever 15 mm clamps are too small and 20 mm are too large.
2	Connecting pipes	15 mm with adaptive joint to 20 mm diameter	Attached to the tanks' holes where 20 mm parts are on the outside of tank. Small washer rings can be placed to prevent leaks at joints. Brand by Hansen.
2	Plastic container jars (reservoirs)	About 1.5 litre in volume.	15 mm diameter holes are made on the bottom for connecting pipes and hose
2	Connecting pipes	15 mm diameter	To be attached each to reservoir Brand by Hansen
2	Metal poles	1 metre	Mounted and restrained
2	Reservoir holder		Can be custom made to fit the metal pole or any common laboratory holders or clamp system used so heights on the pole can be adjusted.
2	Clear plastic hose	15 mm inner diameter, 2 metre in length	Each to be connected between a reservoir and a tank's washer.
1	Extra plastic hose	15 mm inner diameter, 1 metre in length	When the trachea's length is too short to reach between the two connecting pipes inside the tank, the trachea can be clamped on extra hose which is cut into appropriate short lengths to extend and link to the connecting pipes.
8 litres minimum	0.9 percent concentrated saline water	-	9g of sodium chloride (NaCl) for every litre of distilled water. Stored in clean bottles.

3.4.2 Procedure

By using the laser displacement meter, measurements are made without any direct physical contact that can disturb the structural properties of the trachea. Once the trachea is mounted and pressurised, using a contact measurement device like a vernier caliper does not give consistent and accurate readings. Manual hand operation may distort the structure while taking the measurements. Figure 3.8 shows how the experimental rig is laid out.

With this set up, input applied pressure is expressed as $q = \rho g h_w$ as described in chapter 2. The net internal pressure of the trachea is controlled by adjusting the heights of the reservoir. To remove any air bubbles, reservoir 1 was first dragged up above the pole and wait for the bubble to move up and the fluid to settle, then it was brought down again and aligned at the 'zero' pressure no-flow position. Reservoir 2 was positioned at the highest position possible to collect any out-flow fluid from reservoir 1.

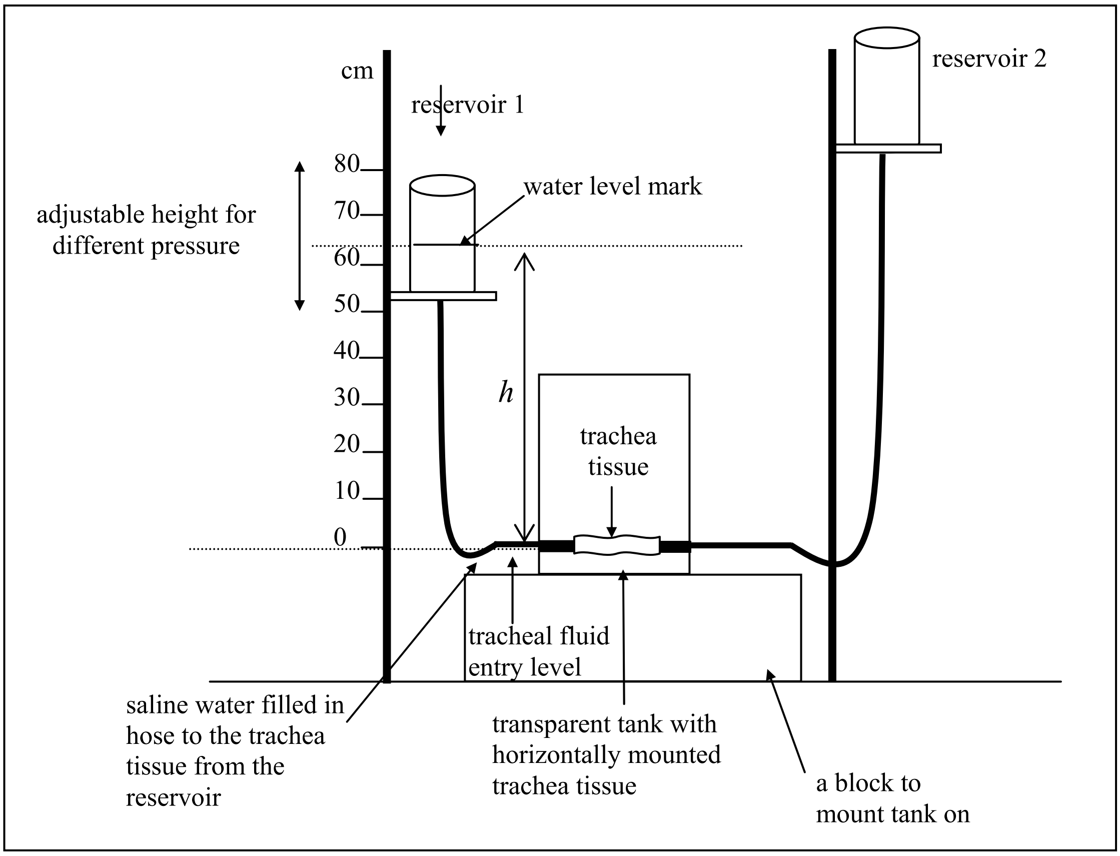

(a) The overall reservoir and tank setup

Figure 3.8 Experimental rig setup for the pressure difference method

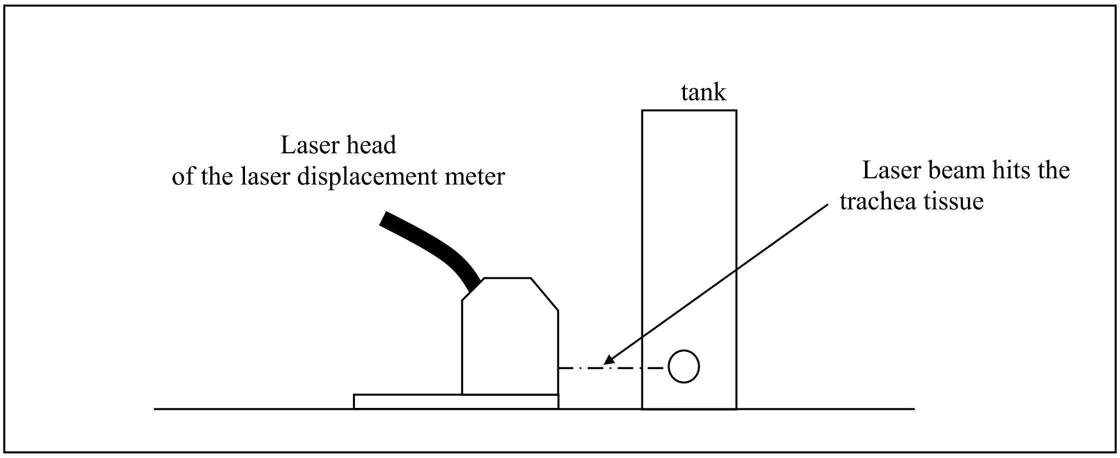

(b) Side view of the tank setup with laser displacement meter

Figure 3.8 Experimental rig setup for the pressure difference method (continued)

Due to the fact that the tissues are slippery and fragile, mounting the trachea between the two washers inside the tank needs special care and effort. See Table 3.2 for tips when trachea length is too short to be mounted between the two ends of the washer inside the tank. Simple plastic hose clamps with closing grips are sufficient to hold the tracheas securely in place to avoid tissue damage and leaks. The right size hose clamps are therefore essential for this function. A hose clamp that is too small requires much effort to close. A hose clamp that is too large will just not securely mount the trachea.

The pole is calibrated for different pressure levels (0 to 80 cm) that can be applied to the trachea. Marks are made on the pole for 1 cmWg to 20 cmWg with increments of 1 cmWg intervals and from 20 cmWg to 80 cmWg mark with increments of 10 cmWg intervals.

The Keyence Laser Displacement Meter is used to measure the radial deformation of the trachea under different internal fluid pressures. Figure 3.9 shows the picture of the trial measurements taken by the laser displacement meter with the trachea being submerged in the saline bath. In the later experiments, no saline solution was poured into the tank to give external fluid pressure but was left to have external atmospheric pressure. Although it is desirable to preserve the trachea freshly submerged in saline water, it is felt this is not practical as the water distorts the laser signal. The experiment is only carried out in a short period and no significant changes should occur to the tissue.

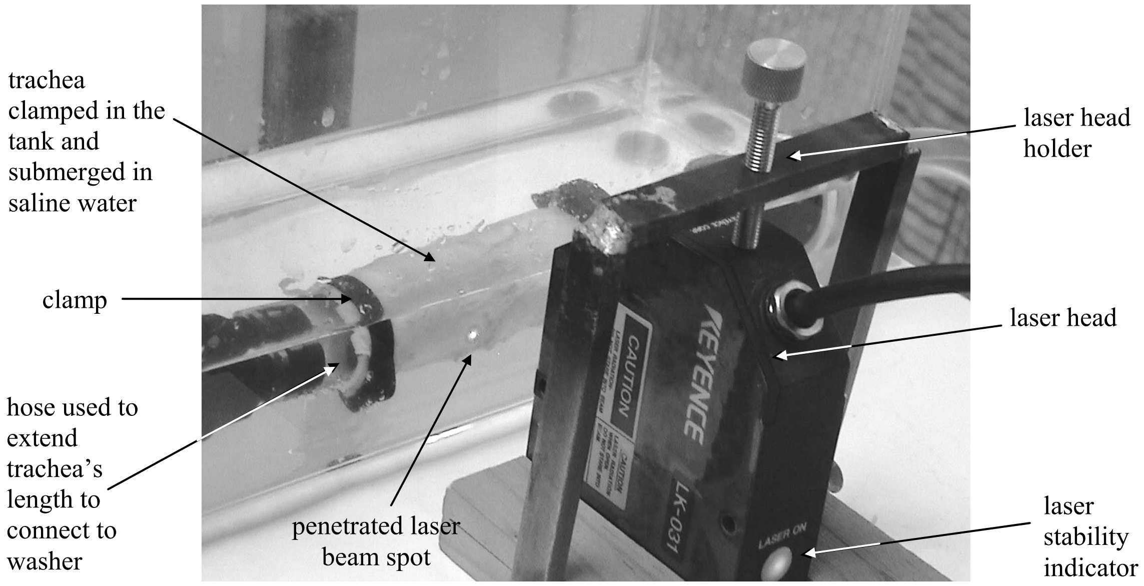

Figure 3.9 Laser beam detecting the radial strain of the trachea in the saline bath

The diagram of laser displacement meter used for this research is shown in the Figure 3.10.

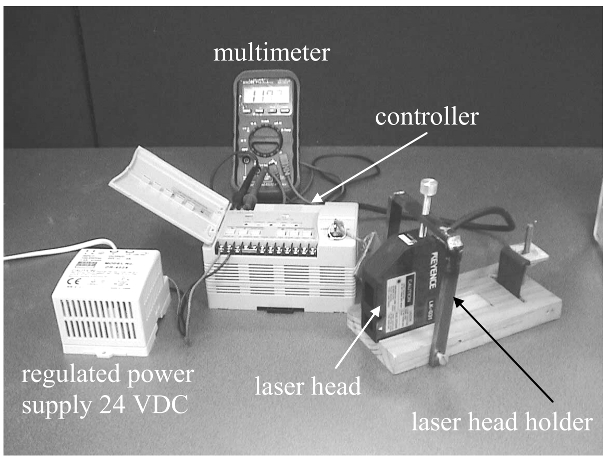

Figure 3.10 Keyence laser displacement meter LK-031

The Keyence laser displacement meter LK-031 comes with a laser head and a controller. The laser head is the device that emits laser beams which are aimed at the object. The direct distance between the object to be measured and the laser head must be within 25-35 mm. The green light indicates the stable or mid point distance of 30 mm between the device and the object. The orange light means the object is still within the range of measurement and a blinking orange light indicates the object is out of range from its measuring distance from the laser head. This laser stability indicator is shown in Figure 3.9. The sensitivity of this device is 1 mm/V. Hence, when the laser head is placed 35 mm from the trachea tissue, the maximum limit that can be detected is radial deformation of 10 mm. This is indicated by –10V on the multimeter readings and is large enough to cover any possible maximum deformation occurred by this type of viscoelastic tissues. Transmitting the laser beam through the transparent tank causes light dispersion. This may cause the stable measuring distance between laser head and object to be not exactly within the 25 – 35 mm range. This is acceptable as the deformations detected are relative and independent of this dispersion.

The laser beam is aimed at the middle point of the trachea away from the clamping effect. This position gives appropriate readings for maximum deformations, which subsequently are used to calculate the mean deformation value.

To achieve a stable measuring distance between the trachea and the laser head, the laser head is moved backwards and forwards slowly to obtain appropriate voltage readings on the multimeter. When the furthest stable position is reached, the controller mode is set to zero or cleared, ready to detect increases in radial deformation when change in pressure is applied. It is also helpful to mount the laser head on a secured holder (shown in Figure 3.9) as once a measuring distance position is achieved, the laser head and tank must not be moved at all.

By shifting and securing the reservoir holder from 'zero' level to the next pressure level, readings of deformation are recorded 2 minutes after the shifting in order to allow any fluctuations in the fluid level to settle. Figure 3.11 shows a photograph of the reservoirs and tank set up.

Results are tabulated in the next chapter. Calculations are made to obtain the mean value of the radial deformation using equation 2.17 from chapter 2. To compare with the standard tension test method, graphs of pressure applied q (Pa) against the instantaneous $\Delta R_m / R_i$ and engineering strain $\Delta R_m / R_{out}$ of tracheal deformation are also plotted. R_{out} is the engineering strain or initial outer radius of the trachea where it is calculated by adding inner radius R with thickness h and R_i is the instantaneous outer radius of the trachea.

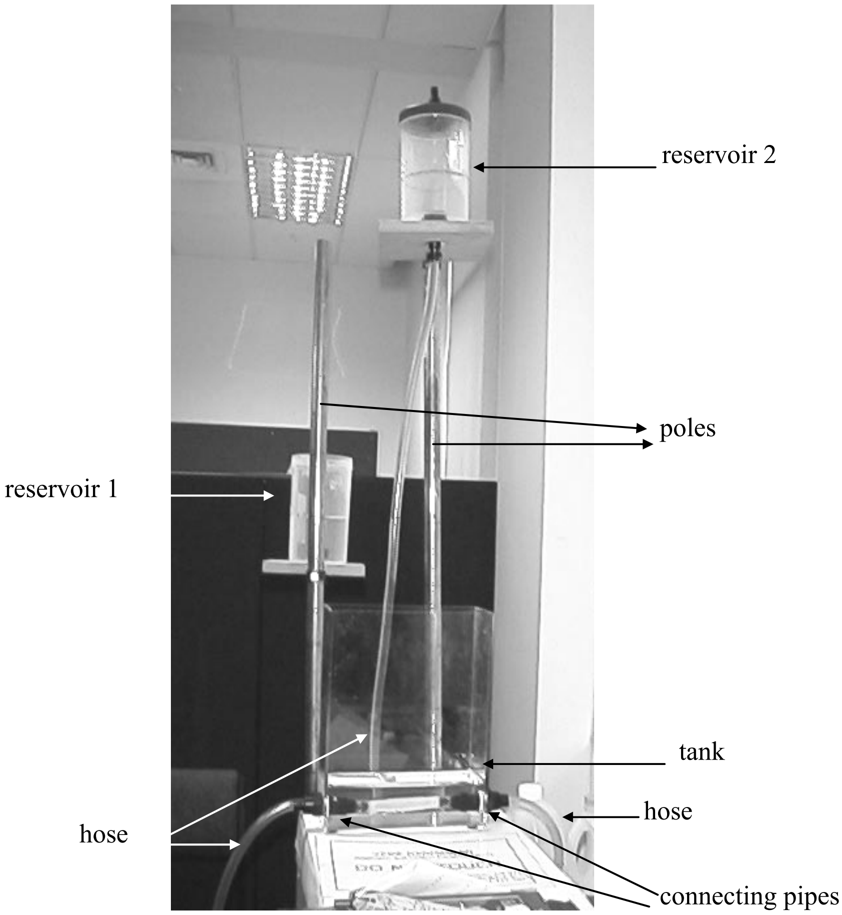

(a) Full view of reservoir and tank system

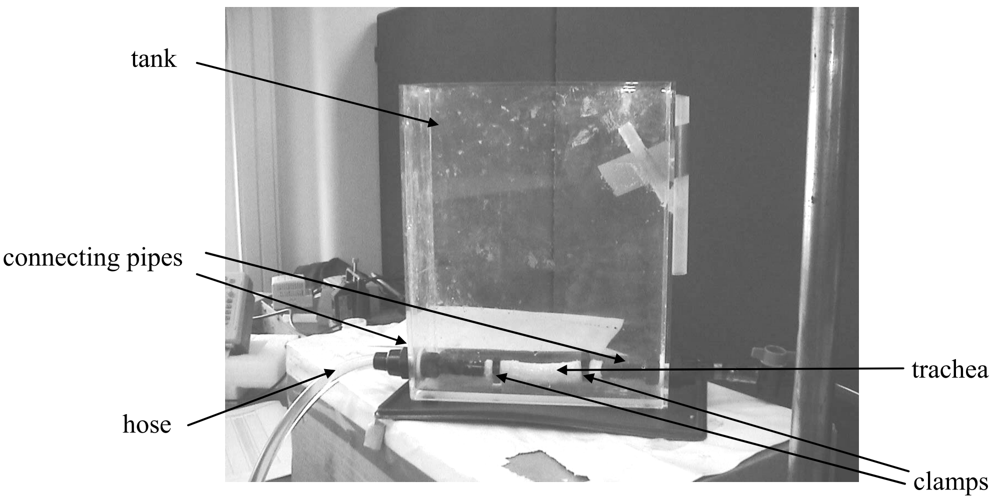

(b) Closer view of the tank system

Figure 3.11 Photographs of the reservoirs and tank set up

3.5 Two-hydrophones Method

This method is based on using two hydrophones and studying the variation in acoustic transmittance caused by the presence of the trachea in a water-bath. By comparing the transmitted signals under two different setups, the bulk and Young's modulus can be obtained by applying the acoustic theory of transmission.

3.5.1 Apparatus

The measurement devices consist of two Reson hydrophones model TC4013 which comes with their own manufactured voltage preamplifier model VP1000, Tektronix oscilloscope and two multimeters.

The rig consists of a tank system similar to the one used in the pressure difference method. An AC Signal Generator (15 Hz – 50 kHz) with input voltage capacity up to 40 Vrms and connecting wires are used to connect between devices.

3.5.2 Procedure

Two hydrophones, one as a transmitter and the other as a receiver, are used in two different setups for comparative means as shown on Figure 3.12 and 3.13. For Setup 1 the two hydrophones are in the saline bath with distance of l_h between them and for Setup 2, the transmitter hydrophone is placed inside the trachea where the receiver remains in the bath outside the trachea at the same distance l_h from the transmitter.

The transmitter hydrophone is connected to an AC generator that can transmit 15 Hz – 50 kHz sinusoidal signal. The maximum driving voltage of the generator is 20 Vrms which is used to obtain maximum amplification on the oscilloscope. A cable from the generator is connected to channel 2 of the oscilloscope in order to show the input signal. With an adaptor, a multimeter is also connected to channel 2.

The receiver hydrophone is connected to a manufacturer's matched voltage preamplifier VP1000 with its mode set to the highest amplification gain. The voltage preamplifier has a built-in high pass filter which is set to filter out 0.1 Hz of below frequency signals so that it would take account for 1 Hz frequency waves and onwards. From the voltage preamplifier, the connections lead to channel 1 of the oscilloscope. Another multimeter is also attached with an adaptor to channel 1 of the oscilloscope. Readings from the oscilloscope itself fluctuate due to the noises caused by the surrounding vibrational motion such as waves or motion of the water-bath, outside traffic and the room's air conditioner airflow. Multimeters are used because they give more stable readings. Voltage readings indicate how much pressure wave is received or transmitted by hydrophones. The sensitivity of the transmitter is at 1μPa/V and of the receiver is at 1V/μPa.

The tank is filled with saline water up to 10 cm depth from the trachea's centre and reservoir's height adjusted to 10 cmWg level of pressure. This way the hydrophones are fully submerged and under similar pressure to meet the boundary conditions of transmission principles mentioned in chapter 2. They are kept 5 cm apart in the two setups shown in Figures 3.12 and 3.13.

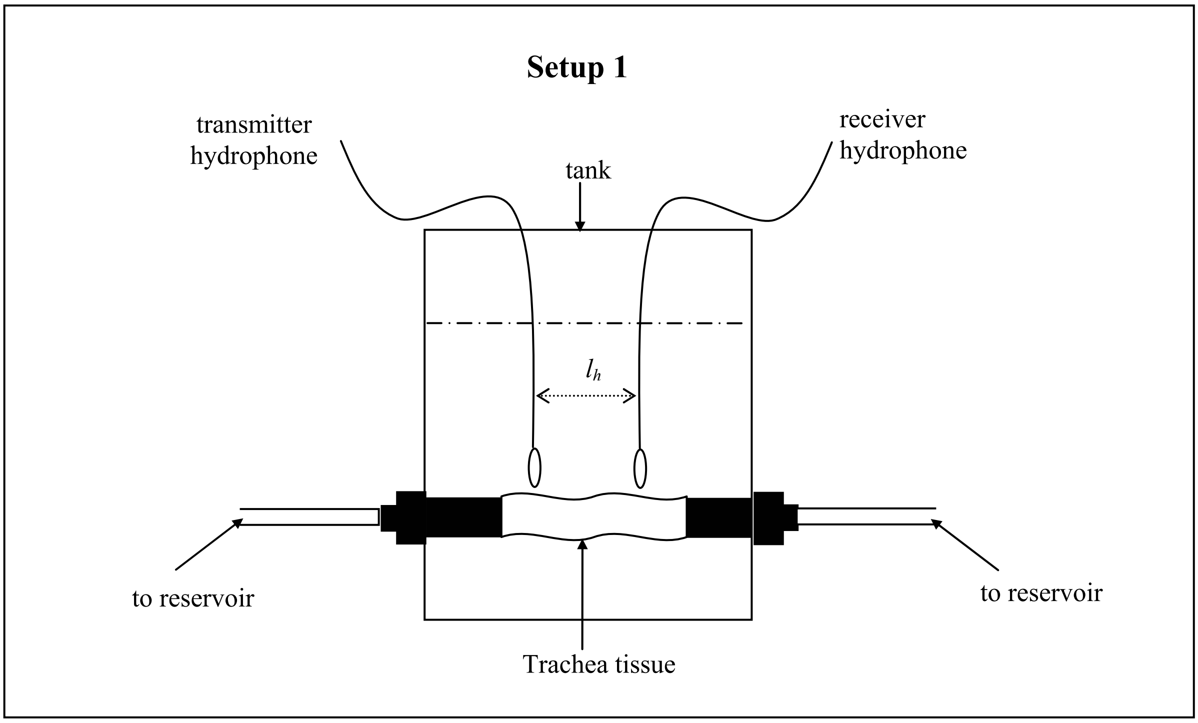

Figure 3.12 Setup 1, two hydrophones in the saline bath

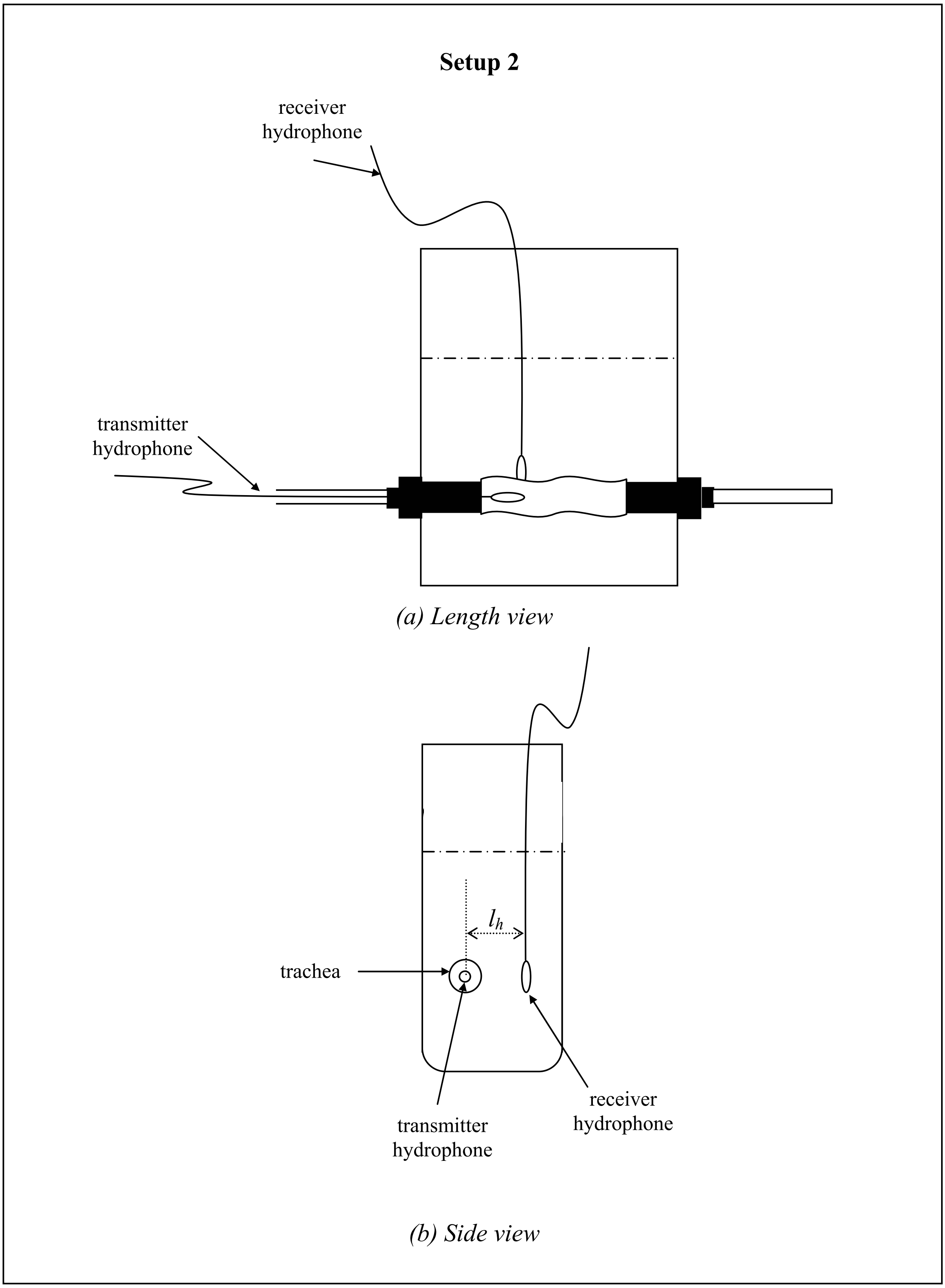

Figure 3.13 Setup 2, transmitter is inside the trachea

Signals are fed to the transmitter starting from 15 Hz up to 50 kHz. The input and output voltages from the multimeters are recorded. Frequency responses are then plotted for the two methods. The differences in results indicate the impedance imposed by the trachea tissue.

Figure 3.14 shows the set up of the tank with the generator and other devices, Figure 3.15 shows the schematic diagram of the set up and Figure 3.16 illustrates the layout of Setup 1 taken from one of the trial experiments.

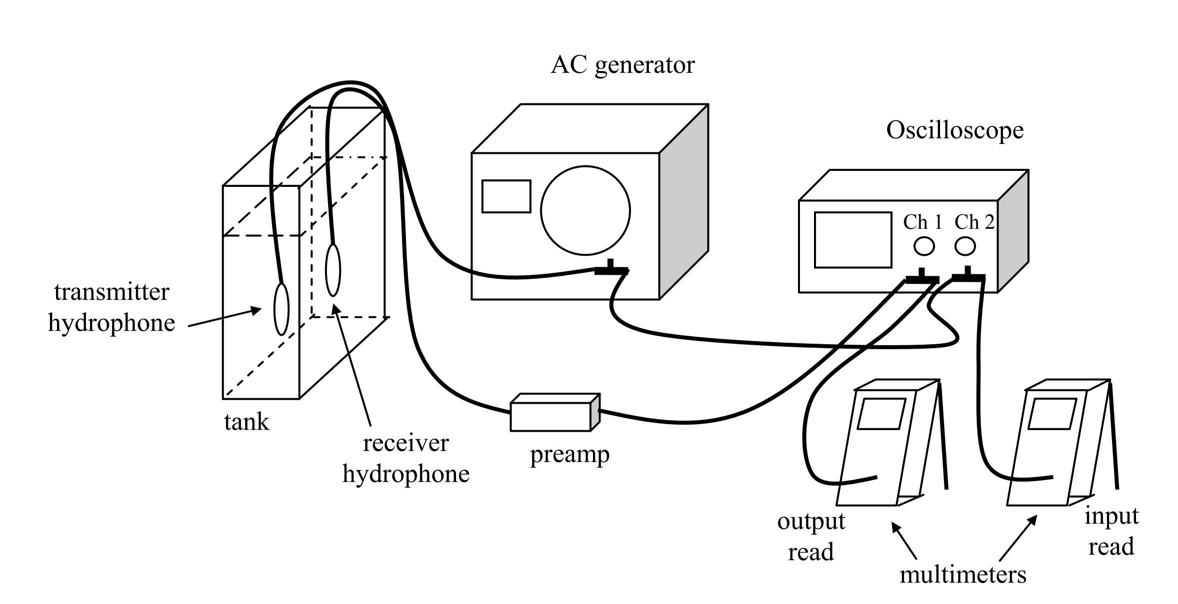

Figure 3.14 Experimental rig of the two-hydrophones method

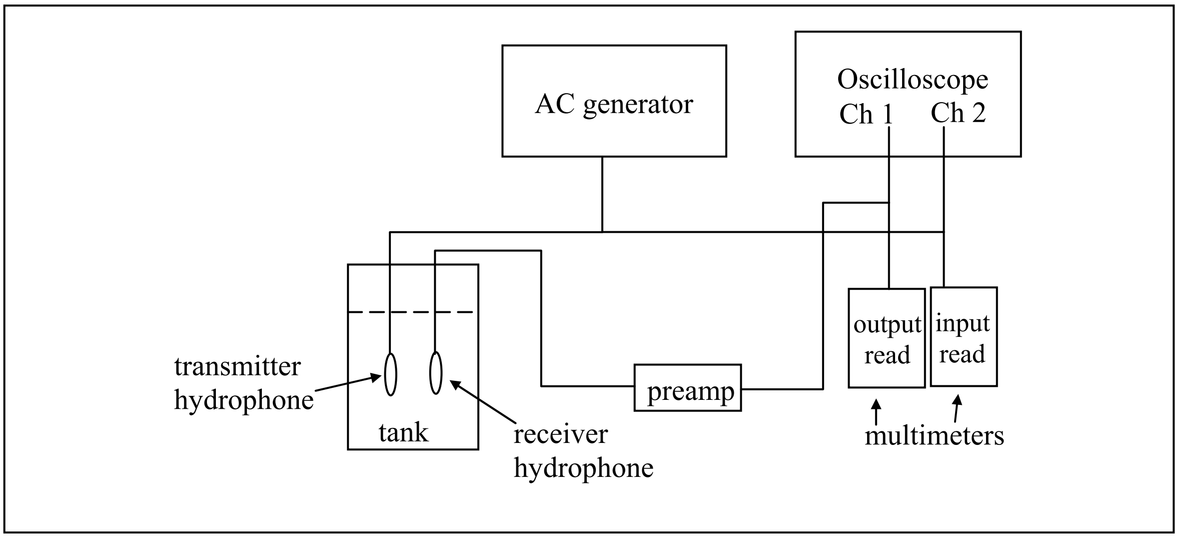

Figure 3.15 Schematic diagram of experimental rig of the two-hydrophones method

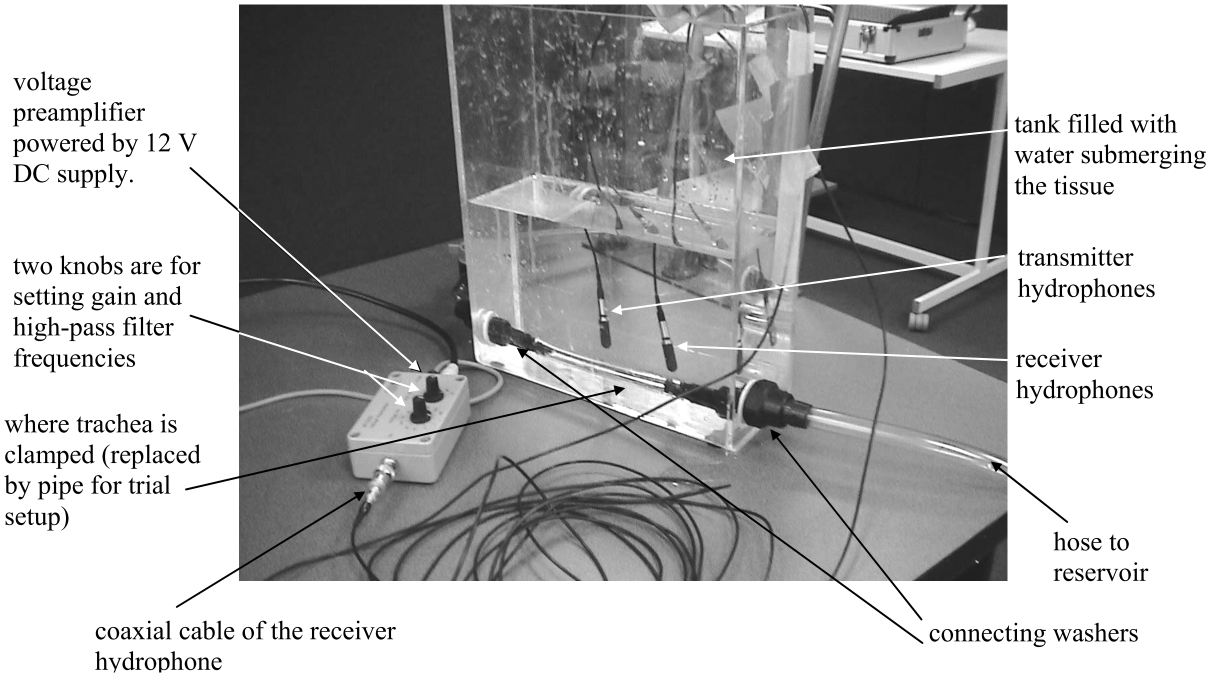

Figure 3.16 Picture of Setup 1 of the two-hydrophones method

3.6 Vibration Method

This method is based on considering the trachea as a thin cylindrical shell and obtaining the resonance vibration response. The Young's modulus can be determined by applying the formula developed in chapter 2. The natural frequencies are obtained by using a dynamic system which vibrates the tissue with various frequencies.

3.6.1 Apparatus

The measurement device consists of Polytec laser vibrometer which comes with a controller model OFV-5000 and sensor head model OFV-505, Tektronix oscilloscope and a tripod. The laser vibrometer needs to be mounted on a stable tripod.

The rig components are similar setup to the conventional tension method system apparatus, a shaker and a common AC generator.

3.6.2 Procedure

This method uses the basic experimental set up of the tension test system with additional devices such as a shaker for vibrating the tissue and laser vibrometer for detecting vibratory motion. A coaxial connection is made from the controller to the oscilloscope for displaying the vibrational waves. The shaker is then connected to a signal generator and its own manufactured amplifier.

Both ends of the trachea are clamped similarly in the axial direction as shown in Figure 3.7 and 3.17. Tension loads of 30 g are applied to prevent sagging of the tissue and to achieve steady vibration without distorting noises. The shaker is positioned along the axial side of the trachea where it is just touching the trachea walls without bending it. The laser sensing beam from the laser head is projected on the opposite side of the tissue. Figure 3.17 illustrates the layout of this method.

Vibrations are generated by the signal generator where the driving frequencies are varied by changing the knob setting of the generator. Starting from the lowest frequency of 1 Hz to about 5 kHz, the first resonance that corresponds to the first peak growth of waves amplitude is found. This first natural frequency is recorded.

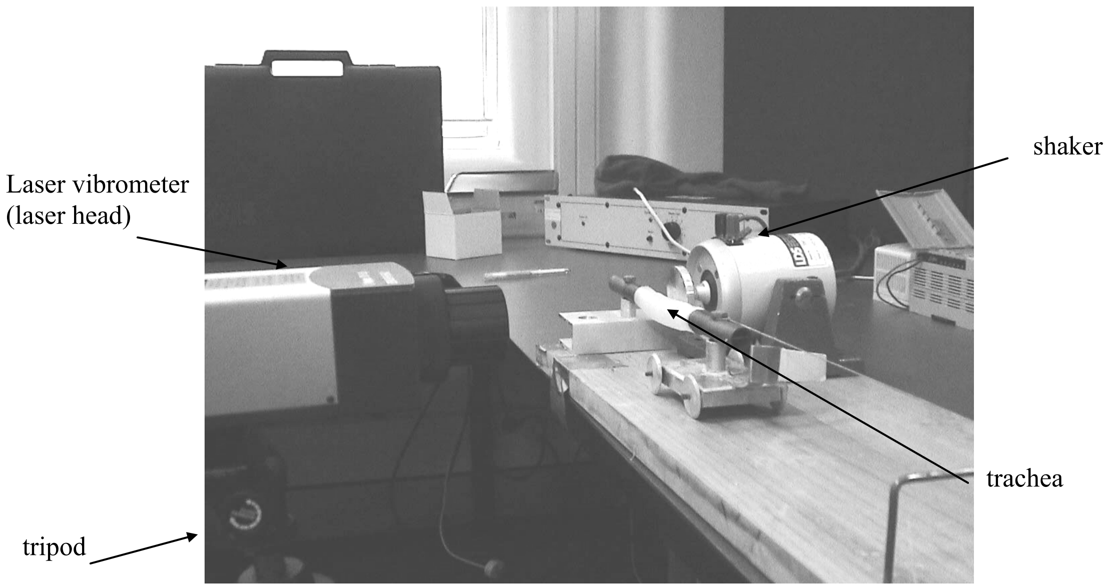

Figure 3.17 Experimental set up of the vibration method

The natural frequencies obtained are then substituted in to the formula of the vibrated thin cylindrical shell as expressed in equation 2.55 in chapter 2 where the unknown Young's modulus can be determined.

Chapter 4
Experimental Results

4.1 Introduction

This chapter presents the results of the experiments described in chapter 3. One trachea is selected as a sample showing the detailed measurements and calculations carried out. The results of the remaining tracheas are summarised and tabulated in terms of their 'equivalent' or average measured values. It is felt that an average range of the Young's modulus for each method described in chapter 3 would give more comparative meanings to this application in order to make recommendations for future use.

4.2 Tracheal Dimensions

For the tracheal radius and thickness, a number of measurements are taken at different sites of the trachea due to its shape irregularity consisting of muscles and cartilage grooves. Table 4.1 shows the measurement of ten readings and calculations for the mean radius of a sample pig's trachea.

Table 4.1 Measurements for the inner radius and thickness of the trachea

Measurements No.	Inner diameter d (mm)	Inner radius $R = d/2$ (mm)	Thickness h (mm)
1	16.00	8.00	2.10
2	16.70	8.35	2.20
3	17.40	8.70	2.20
4	17.60	8.80	2.20
5	17.10	8.55	3.50
6	15.60	7.80	2.20
7	16.90	8.45	2.90
8	15.60	7.80	2.60
9	15.90	7.95	2.90
10	17.10	8.55	2.80
Mean or Average	16.59	8.30	2.56
Standard deviation or error	0.75	0.38	0.46

The first column of Table 4.1 lists each reading taken and is called as the 'Measurement number one, two and so on. The second column presents the readings of inner tracheal diameter obtained using a vernier calliper in millimetres. The third column shows the inner radius in millimetres. The fourth column shows the thickness of the trachea in millimetres. The mean value of the ten readings and the standard deviation are given in the last two rows of the table respectively. The mean inner radius of the pig's trachea is 8.30 ± 0.40 mm, which gives a percentage error of 4.8%.

Rounding the value to one decimal place is usually a common practice to produce a meaningful average, particularly in treating a nonhomogenous object where obtaining accuracy to two decimal values is impractical and meaningless. The thickness of the pig's trachea is 2.60 ± 0.50 mm, which gives a percentage error of 19.2%.

Table 4.2 shows the measurements of the tracheal density. The trachea weight being 30.41 g and its displaced volume 30 ml gives the density of 1.014 g/ml which is 1014 kg/m^3 in SI unit. This value is close to the density of fresh water which is 998 kg/m^3 and sea water, 1026 kg/m^3. The density of water is usually rounded up to 1000 kgm^{-3} and with this reason, by rounding down the tracheal density to 1000 kgm^{-3}, its density is thus known to be the same as the density of water. The measurement errors included in Table 4.2 for the mass and volume are taken from the smallest increment unit displayed by the instruments used, whereas the error for tracheal density is produced by a common error calculation procedure.

Table 4.2 Measurements of the tracheal density

Parameters	Measurements	Percentage error (%)
Tracheal Mass	30.41 ± 0.01g	0.04
Volume displaced	30.0 ± 0.2ml	0.7
Tracheal density ρ	1.014 g/ml = 1014 ± 7 kg/m^3 ≈ 1000 kg/m^3	0.7

The measurement summary for this trachea is tabulated in Table 4.3.

Table 4.3 Summary measurement of the tracheal dimensions

Parameters	Measurement	Percentage error (%)
Inner radius R	8.3 ± 0.4 mm	4.8
Thickness h	2.6 ± 0.5 mm	19.2
Density ρ	1000 ± 7 kg/m^3	0.7

The inner radius of 8.3 mm, thickness of 2.6 mm and density 1000 kg/m^3 are the common parameters used for the calculation purposes in the four testing methods proposed by this research to determine the Young's modulus. The lengths of trachea are measured separately for each testing method as they change with clamping conditions of each test.

4.3 Conventional Tension Method

This section is divided into two parts where the first presents the results of testing the trachea in the circumferential direction, and the second presents the results in the axial direction. As described in chapter 3, the first part involves two ways of cutting the trachea and the results are presented in the following section accordingly.

4.3.1 Circumferential Testing – Cutting the Trachea Along the Connective Tissue and Muscle

As the trachea is cut and mounted in such a way as described in chapter 3, the following are the measurements taken for the purpose of calculating the strain and stress involved in this test. The initial length L_0 is the clamped length of the trachea between the two clamps mounted without any loads applied. The cross sectional area A is the thickness h times the cut-length of the trachea l_w and under tensile force $F=Mg$. Figure 4.1 depicts the configuration and cartilage direction for this test.

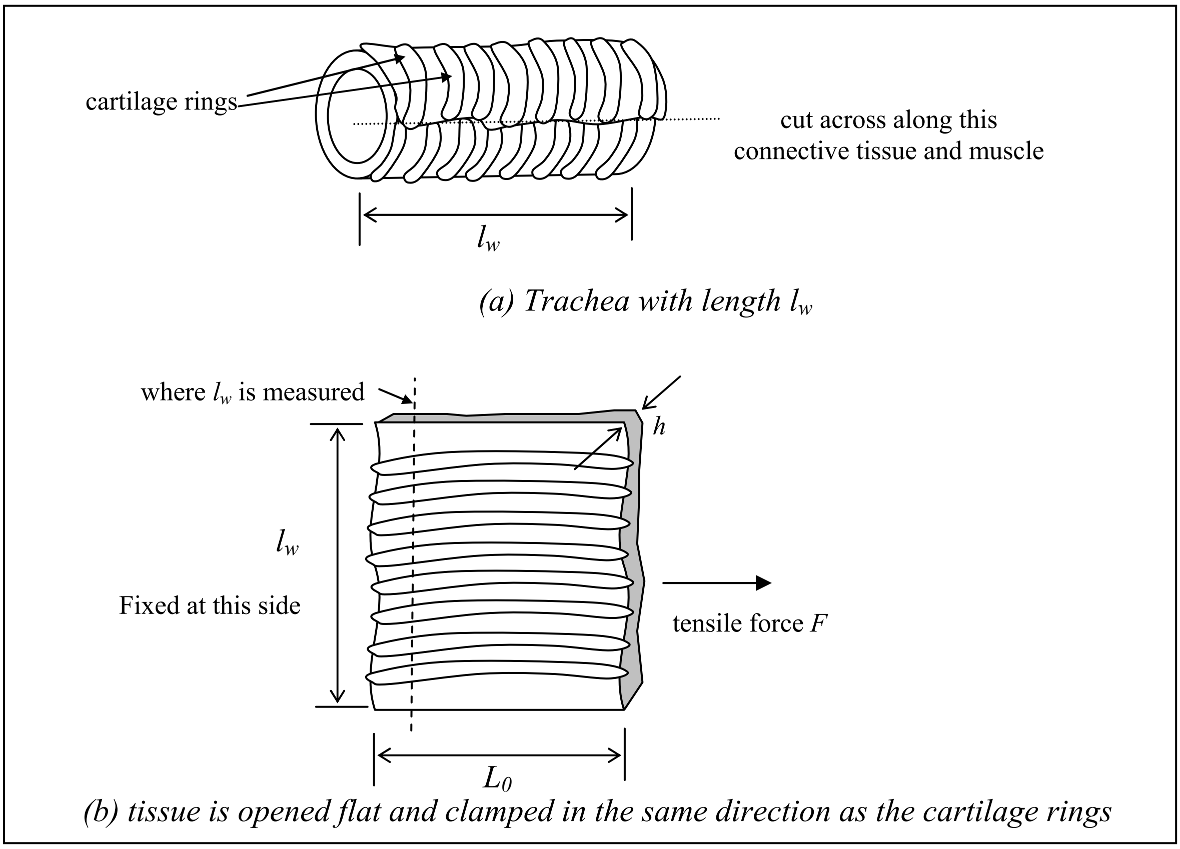

Figure 4.1 Configurations for the cutting of the trachea without the connective tissue and muscle

Table 4.4 shows the measurements of parameters L_0 and l_w and other related parameters h, g and cross-sectional area A which are used to determine the circumferential Young's modulus E without the connective tissue and muscle. Due to the non-uniform shape of the edges, the measured length is taken between the clamped ends. The error for l_w is considered to be 1 mm since the non-uniformity does not justify for 0.2 mm error from the vernier calliper accuracy. The error of 1 mm which is usually found on an ordinary ruler is more reasonable to use in this application.

The results of the tension test with loads up to 120 g are tabulated in Table 4.5. The first column lists the mass of loads used, the second column calculates for tensile force in Newton which is the mass times the acceleration due to gravity g = 9.8 m/s^2. The third column is the tensile stress F/A. The fourth column is the deformation length ΔL in millimetre detected by the laser displacement meter. The fifth column presents the instantaneous or true strain $\Delta L/L$ and the sixth column presents the engineering strain $\Delta L/L_0$.

Table 4.4 Related parameters for determining the circumferential Young's modulus (without the connective tissue and muscle)

Parameters	Symbols	Measurements and other related values	Percentage Measurement Error
Original length	L_0	42.6 ± 0.2 mm	0.5
Thickness	h	2.6 ± 0.5 mm	19.2
Cut length	l_w	35.0 ± 1 mm	2.9
Cross sectional area	$A = h \times l_w$	91 ± 22 mm^2	19.4
Gravitational acceleration	g	9.8 ms^{-2}	-

Table 4.5 Results of the circumferential testing without the connective tissue and muscle

Mass M (g)	Force F (N)	Tensile stress F/A (N/m^2)	Length of deformation ΔL (mm)	Instantaneous strain $\Delta L/L$	Engineering strain $\Delta L/L_0$
0	0.000	0.0	0	0.0	0.0
5	0.049	538.5	0.03	0.0007	0.0007
10	0.098	1076.9	0.12	0.0028	0.0028
15	0.147	1615.4	0.17	0.0040	0.0040
20	0.196	2153.8	0.23	0.0054	0.0054
25	0.245	2692.3	0.37	0.0086	0.0087
28.56	0.2799	3075.7	0.59	0.0138	0.0138
33.56	0.3289	3614.2	0.64	0.0148	0.0150
38.56	0.3779	4152.6	0.68	0.0157	0.0160
43.56	0.4269	4691.1	0.72	0.0166	0.0169
48.56	0.4759	5229.5	0.72	0.0166	0.0169
53.56	0.5249	5768.0	0.79	0.0182	0.0185
58.56	0.5739	6306.5	0.79	0.0182	0.0185
63.56	0.6229	6844.9	0.82	0.0189	0.0192
68.56	0.6719	7383.4	0.87	0.0200	0.0204
78.56	0.7699	8460.3	0.94	0.0216	0.0221
98.56	0.9659	10614.2	1.13	0.0260	0.0265
118.56	1.1619	12768.0	1.27	0.0290	0.0298

The plot of stress and strain combined from the results of Table 4.5 are depicted in Figure 4.2. This figure gives the stress and strain plot of a trachea in circumferential direction without the connective tissue and muscle by the conventional tension method based on both instantaneous and engineering strain. The plot configures × as instantaneous strain and ○ as engineering strain. It shows that both instantaneous and engineering strains fall within the same range, however, the latter tends to be slightly larger than the former. The two curves show linearity up to 30 g loads, where from then on non-linear behaviour is observed.

Table 4.6 tabulates the Young's modulus *E* determined by best-fit slopes from the plot of Figure 4.2. The first column gives the strain based on the 0-30 g load range while the second column is based on the 30-120 g load range.

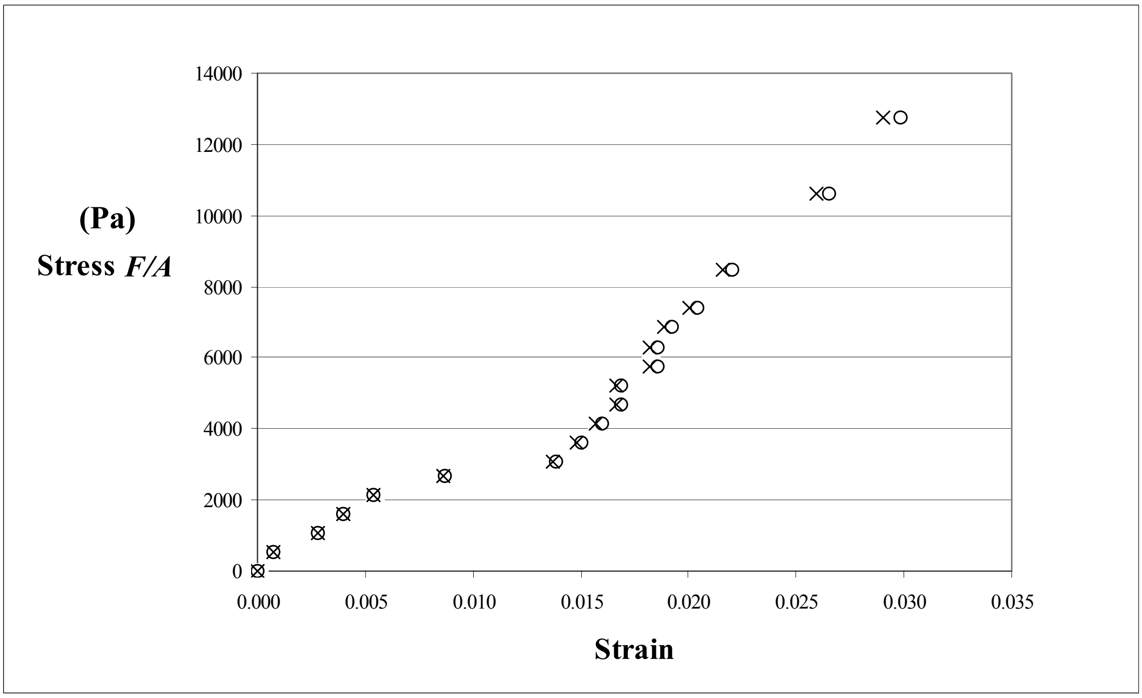

Figure 4.2 Stress and strain relationship in circumferential testing without the connective tissue and muscle. The plot configures × - instantaneous strain and ○ - engineering strain.

Table 4.6 Results of the circumferential Young's modulus without the connective tissue and muscle

Strain types	First modulus (0-30 g load) E_1 (MPa)	Second modulus (30-118.6 g load) E_2 (MPa)
Instantaneous	0.31	0.64
Engineering	0.31	0.61

4.3.2 Circumferential Testing – Cutting the Trachea Along the Cartilage

With the trachea being cut along the cartilage as shown in Figure 4.3, the connective tissue and muscle remains and gives more flexibility for the whole tissue deformation. Similarly, Table 4.7 shows the measurements of related parameters which are used to determine the circumferential Young's modulus E with the connective tissue and muscle.

The results of the conventional tension method with loads up to 120 g are tabulated in Table 4.8. In this table, the first column gives the mass of loads, the second column the tensile force in Newton which is mass times the acceleration due to gravity g = 9.8 m/s^2, the third column the tensile F/A, the fourth column the deformation length ΔL in millimetre detected by the laser displacement meter, the fifth column the instantaneous strain $\Delta L/L$ and the sixth column presents the engineering strain $\Delta L/L_0$. The plot from the results of Table 4.8 are depicted in Figure 4.4. This figure gives the stress and strain relationship of a trachea in circumferential direction with the connective tissue and muscle by the conventional tension method based on both instantaneous and engineering strain. The plot configures × as instantaneous strain and ○ as engineering strain.

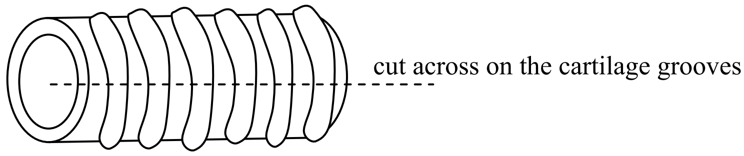

(a) Trachea being with length l_w

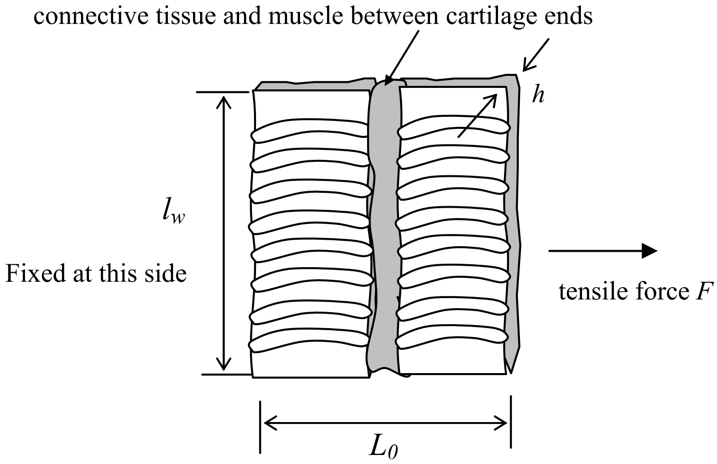

(b) tissue is opened flat and clamped in the same direction as the cartilage rings

Figure 4.3 Configurations for the cutting of the trachea with the connective tissue and muscle

Table 4.7 Related parameters for determining circumferential Young's modulus (with the connective tissue and muscle)

Parameters	Symbols	Measurements and other related values
Original length	L_0	37 ± 0.2 mm
Thickness	h	2.6 ± 0.5 mm
Cut length	l_w	45.5 ± 1 mm
Cross sectional area	$A = h \times l_w$	118.3 ± 22 mm^2
Gravitational acceleration	g	9.8 ms^{-2}

Table 4.8 Results of the circumferential testing with the connective tissue and muscle

Mass M (g)	Force F (N)	Tensile stress F/A (N/m^2)	Length of deformation ΔL (mm)	Instantaneous strain $\Delta L/L$	Engineering strain $\Delta L/L_0$
0	0.000	0.0	0	0.000	0.000
5	0.049	420.7	0.2	0.005	0.005
10	0.098	841.3	0.42	0.011	0.011
15	0.147	1262.0	0.9	0.024	0.024
20	0.196	1682.7	1.7	0.045	0.046
25	0.245	2103.4	2.3	0.059	0.062
30	0.294	2524.0	2.8	0.071	0.076
35	0.343	2944.7	3.1	0.078	0.084
40	0.392	3365.4	3.9	0.097	0.105
45	0.441	3786.1	4.1	0.100	0.111
50	0.490	4206.7	4.3	0.105	0.116
68.6	0.672	5768.3	5.8	0.157	0.140
78.6	0.770	6609.6	6.2	0.168	0.145
88.6	0.868	7451.0	6.4	0.173	0.148
98.6	0.966	8292.3	6.4	0.173	0.147
108.6	1.064	9133.7	6.5	0.176	0.150
118.6	1.162	9975.0	6.7	0.181	0.154

Obviously the curves indicate linearity up to 50 g loads then non-linear behaviour is observed. Table 4.9 tabulates the Young's modulus E which are determined by best-fit slopes from the plot of Figure 4.4. The first column gives the strain type they are based on, the second column is the first linear slope taken from the plot by best-fit line between 10-50 g loads and the third column is the second linear slope line between 50-120 g loads which is obtained after a non-linear change of slope. Loads between 0-10 g are disregarded since they are the lightweight load that removes the initial sagging of the tissue. The first linear deformation is thus set from 10 g loads and onwards.

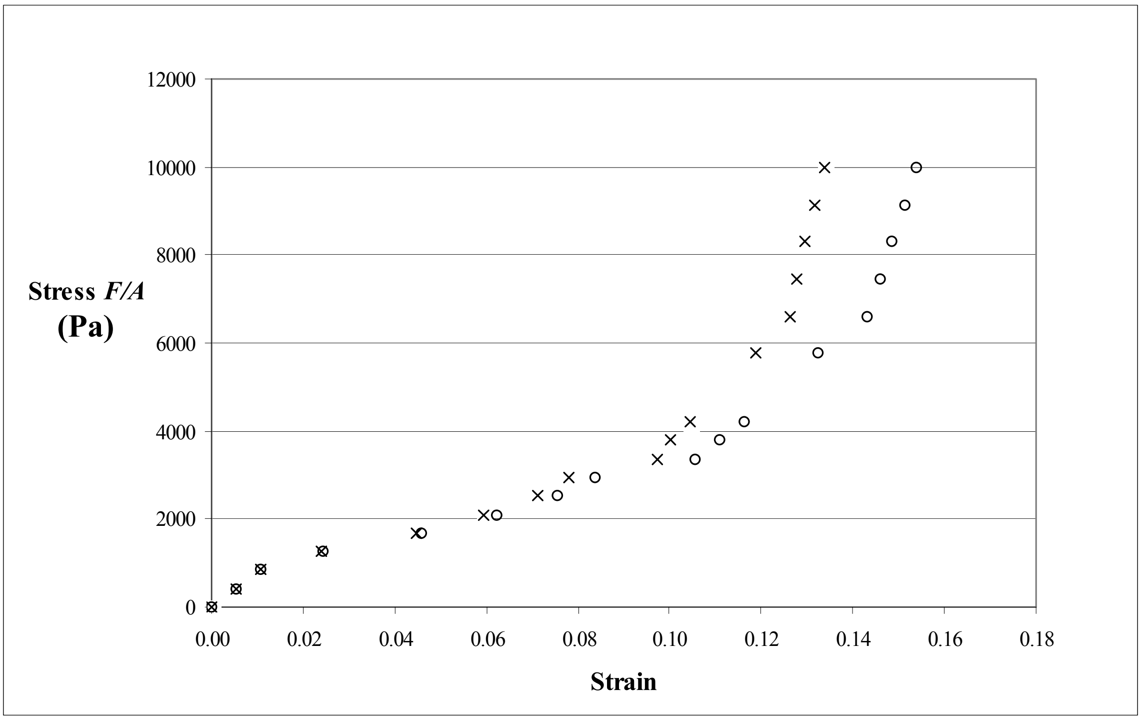

Figure 4.4 Stress and strain relationship in circumferential testing with the connective tissue and muscle. The plot configures × - instantaneous strain and ○ - engineering strain

Table 4.9 Results of the circumferential Young's modulus with the connective tissue and muscle

Strain types	First modulus (10-50 g load) E_1 (MPa)	Second modulus (50-118.6 g load) E_2 (MPa)
Instantaneous	0.031	0.110
Engineering	0.028	0.089

4.3.3 Axial Testing

To determine the axial Young's modulus, Table 4.10 shows the related measured parameters that are involved in the tension test. The cross-sectional area A subjected to tension load is the area of a ring which can be calculated by $A = \pi(h+R)^2 - \pi R^2$.

The results of the axial tension test with loads up to 30 g are tabulated in Table 4.11. In this table, both of the instantaneous and engineering strains are given in the last two columns respectively. These values are depicted in Figure 4.5.

Table 4.10 Related parameters for determining the axial Young's modulus

Parameters	Symbols	Measurements and other related values
Original length	L_0	100.7 ± 0.2 mm
Thickness	h	2.6 ± 0.5 mm
Inner radius	R	8.3 ± 0.4 mm
Outer radius	$R_{out} = R + h$	10.9 ± 0.6 mm
Cross sectional area	A	156.8 ± 11.9 mm^2
Gravitational acceleration	g	9.8 ms^{-2}

Table 4.11 Results of the conventional tension method for the axial testing

Mass M (g)	Force F (N)	Tensile stress F/A (N/m^2)	Length of deformation ΔL (mm)	Instantaneous strain $\Delta L/L$	Engineering strain $\Delta L/L_0$
0	0	0.0	0	0.0000	0.0000
5	0.049	312.5	0.11	0.0011	0.0011
10	0.098	625.0	0.28	0.0028	0.0028
15	0.147	937.5	0.40	0.0040	0.0040
20	0.196	1250.0	0.64	0.0063	0.0064
25	0.245	1562.5	1.96	0.0193	0.0195
30	0.294	1875.0	2.60	0.0253	0.0258

Figure 4.5 gives the stress and strain plot of a trachea in axial direction by the conventional tension method based on both instantaneous and engineering strain. The plot configures × as-instantaneous strain and ○ as engineering strain. Obviously in Figure 4.5, the stress-strain relationship is linear for the loads below 20 g. Changes in the modulus of elasticity occur as more loads are applied from 20 g onwards as slopes show non-linear behaviour. The slopes which indicates the Young's modulus of elasticity E are tabulated in the Table 4.12. The first

column lists the strain type they are based on. The second column is the first linear slope taken from the plot by best-fit line between 0-20 g loads and the third column is the second linear slope between 20-30 g loads after the non-linear behaviour.

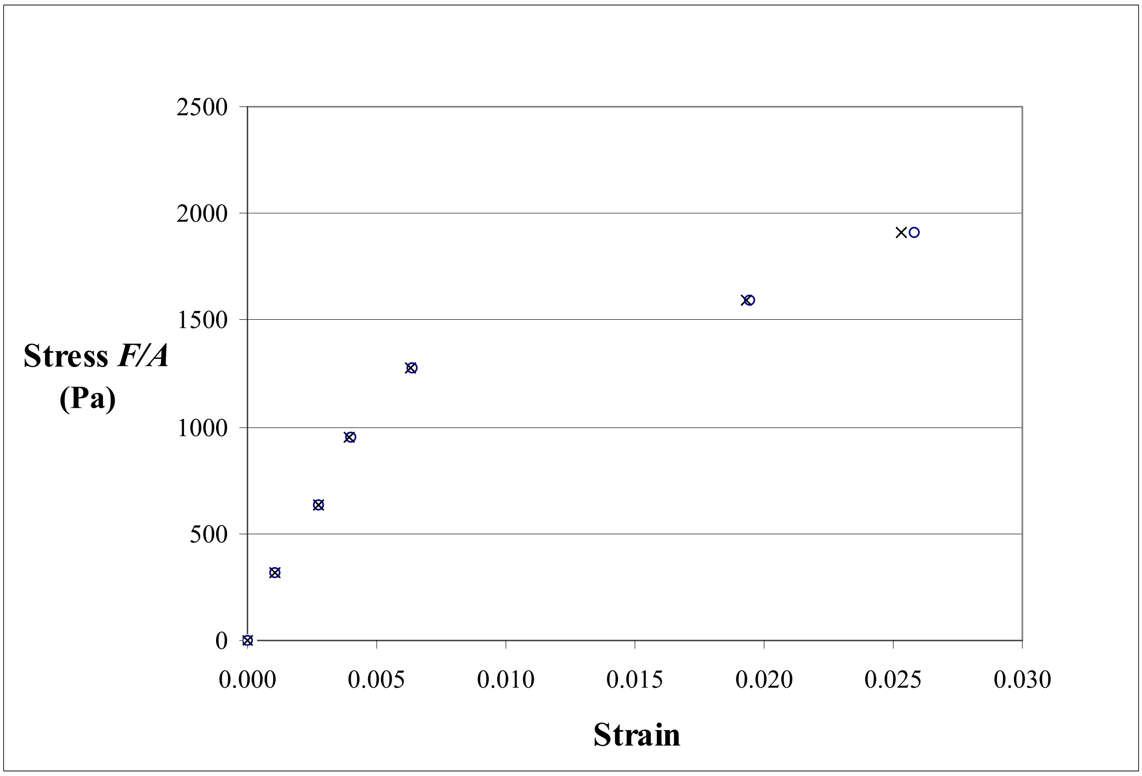

Figure 4.5 Stress and strain relationship in axial testing.
The plot configures × - instantaneous strain and ○ - engineering strain.

Table 4.12 Results of the axial Young's modulus by the conventional tension method

Strain types	First modulus (0-20 g load) E_1 (MPa)	Second modulus (20-30 g load) E_2 (MPa)
Instantaneous	0.201	0.032
Engineering	0.200	0.031

4.4 Pressure Difference Method

Table 4.13 presents the readings taken by the pressure difference method for the maximum deformation ΔR_{max} along with the calculations for the mean radial deformation ΔR_m as described in chapter 2. The first column lists the internal pressure applied by adjusting the height of the reservoir. The second column presents the maximum deformation detected by the laser displacement meter. The third, fourth and fifth column, respectively, show the calculated values of arc radius, arc angle and the mean radial deformation based on the theory described in chapter 2. For this calculation the clamped length measured is l = 94.5 mm.

Table 4.14 tabulates the calculations carried out to plot Figure 4.3 for pressure versus deformation. Again the first column lists the internal pressure and the second column presents the calculated value for pressure q applied in Pascal. For the applied pressure q, the density of water ρ_w=1000 kgm^{-3} and g = 9.8 ms^{-2}. The mean radial deformation ΔR_m from Table 4.8 is presented in the third column. The fourth and fifth column, respectively, record the instantaneous strain $\Delta R_m/R_i$ and the engineering strains $\Delta R_m/R_{out}$ where R_{out} is the engineering or initial outer radius of the trachea where it is calculated by adding inner radius R with thickness h and R_i is the instantaneous outer radius of the trachea.

Since the inner radius R to thickness h ratio is around 3.2, which is less than 10, the trachea is assumed to be a thick-walled cylindrical vessel. Therefore, to determine the Young's modulus E, the slope of the graph is used based on equation (2.14).

Figure 4.6 illustrates the applied pressure versus radial strain by the pressure difference method based on both instantaneous and engineering strain. The plot configures ♦ as instantaneous strain and ● as engineering strain. To determine the modulus of elasticity, E, the slope of the curve in Figure 4.6 must be multiplied by $\frac{2R^2}{R_{out}^2 - R^2}$, see equation (2.17). Figure 4.6 indicates four ranges of linearity, which are 0-4 cmWg, 10-20 cmWg and 20-60 cmWg. Thus four values of modulus of elasticity are determined and summarised in Table 4.15.

Table 4.13 Readings of the maximum deformation of trachea with calculations for the mean radial deformation

Pressure level h_w (cmWg)	Maximum deformation ΔR_{max} (mm)	Arc radius R_{arc} (m)	Arc angle β (rad)	Mean radial deformation ΔR_m (m)
0	0.0	0.00	0.000	0.00000
1	0.28	3.99	0.012	0.00017
2	0.60	1.86	0.025	0.00036
3	0.86	1.30	0.036	0.00052
4	1.01	1.11	0.043	0.00061
5	1.10	1.02	0.047	0.00066
6	1.20	0.93	0.051	0.00072
7	1.27	0.88	0.054	0.00076
8	1.30	0.86	0.055	0.00078
9	1.36	0.82	0.058	0.00082
10	1.43	0.78	0.061	0.00086
11	1.47	0.76	0.062	0.00088
12	1.51	0.74	0.064	0.00091
13	1.55	0.72	0.066	0.00093
14	1.59	0.70	0.067	0.00095
15	1.66	0.67	0.070	0.00100
16	1.70	0.66	0.072	0.00102
17	1.74	0.64	0.074	0.00104
18	1.75	0.64	0.074	0.00105
19	1.81	0.62	0.077	0.00109
20	1.86	0.60	0.079	0.00112
25	2.06	0.54	0.087	0.00124
30	2.16	0.52	0.091	0.00130
35	2.30	0.49	0.097	0.00138
40	2.43	0.46	0.103	0.00146
45	2.53	0.44	0.107	0.00152
50	2.63	0.43	0.111	0.00158
55	2.71	0.41	0.115	0.00163
60	2.83	0.40	0.120	0.00170
65	2.92	0.38	0.123	0.00175
70	2.97	0.38	0.126	0.00178
75	2.97	0.38	0.126	0.00178
80	2.98	0.38	0.126	0.00179

Table 4.14 Calculation table for radial deformation, instantaneous and engineering strain

Pressure level h_w (cmWg)	Pressure applied $q = \rho_w g h_w$ (Pa)	Mean radial deformation ΔR_m (m)	Instantaneous strain $\Delta R_m/R_i$	Engineering Strain $\Delta R_m/R_{out}$
0	0	0.00000	0.000	0.000
1	98	0.00017	0.015	0.015
2	196	0.00036	0.033	0.033
3	294	0.00052	0.046	0.048
4	392	0.00061	0.053	0.056
5	490	0.00066	0.058	0.061
6	588	0.00072	0.063	0.066
7	686	0.00076	0.066	0.070
8	784	0.00078	0.067	0.072
9	882	0.00082	0.070	0.075
10	980	0.00086	0.074	0.079
11	1078	0.00088	0.075	0.081
12	1176	0.00091	0.077	0.083
13	1274	0.00093	0.079	0.086
14	1372	0.00095	0.081	0.088
15	1470	0.00100	0.084	0.092
16	1568	0.00102	0.086	0.094
17	1666	0.00104	0.088	0.096
18	1764	0.00105	0.088	0.097
19	1862	0.00109	0.091	0.100
20	1960	0.00112	0.093	0.103
25	2450	0.00124	0.103	0.114
30	2940	0.00130	0.107	0.119
35	3430	0.00138	0.114	0.127
40	3920	0.00146	0.119	0.134
45	4410	0.00152	0.123	0.140
50	4900	0.00158	0.128	0.145
55	5390	0.00163	0.131	0.150
60	5880	0.00170	0.136	0.156
65	6370	0.00175	0.140	0.161
70	6860	0.00178	0.141	0.164
75	7350	0.00178	0.141	0.164
80	7840	0.00179	0.141	0.165

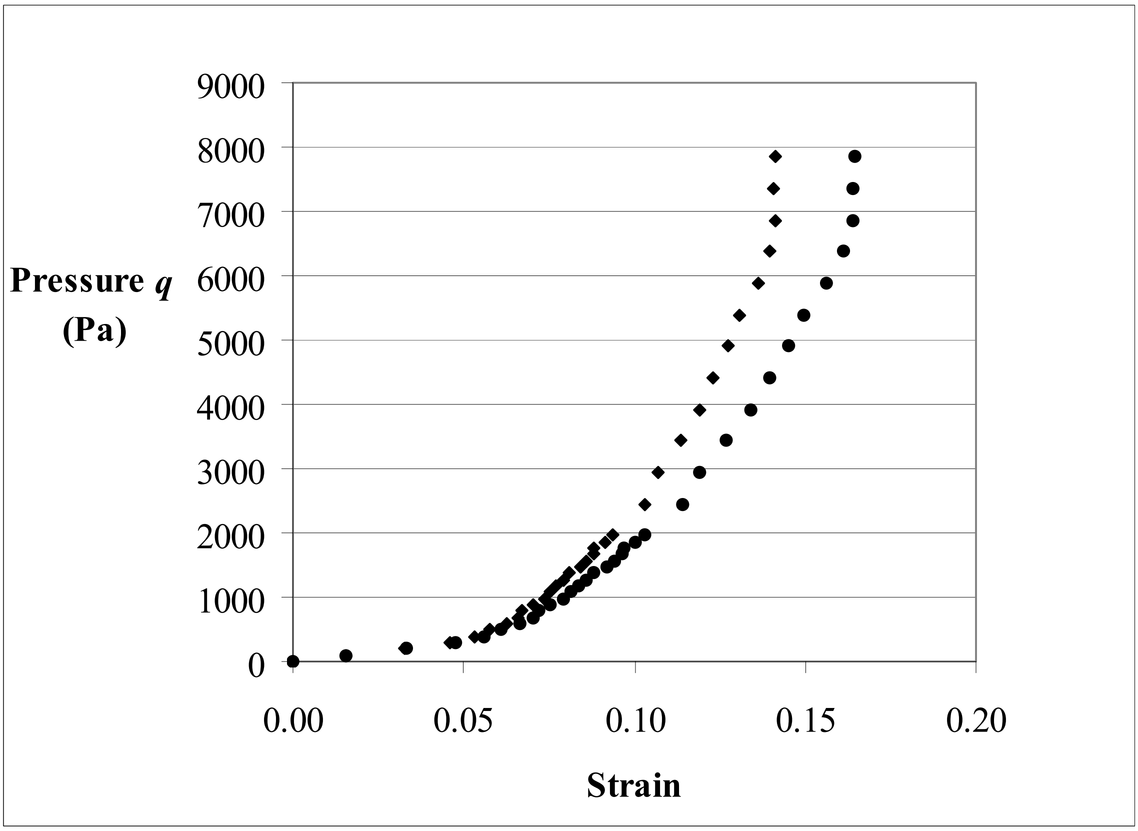

Figure 4.6 Graph of pressure versus radial strain.
The plot configures ♦ - instantaneous strain and ● - engineering strain.

Since the modulus for very small deformation is normally considered, discussions will concentrate on the first modulus with values between 0-4 cmWg. Values higher than 4 cmWg are disregarded in the discussion. At the higher end of the scales, above the pressure of 60 cmWg, tissue tends to have a slight bending effect as it reaches the maximum radial deformation. So values above 60 cmWg pressure are not recorded.

Table 4.15 Results of the Young's modulus by the pressure difference method

Strain types	First modulus (0-4 cmWg) E_1 (MPa)	Second modulus (4-10 cmWg) E_2 (MPa)	Third modulus (10-20 cmWg) E_3 (MPa)	Fourth modulus (20-60 cmWg) E_4 (MPa)
Instantaneous strain	0.020	0.083	0.14	0.26
Engineering strain	0.019	0.072	0.12	0.21

4.5 Two-hydrophones Method

The raw results data of this method is tabulated in Table A1 in the Appendix A where the frequency response from those results is plotted in this section. There are two types of frequency response which are considered useful for describing conditions that affect the results for comparing the difference in transmission coefficients. For both Setups 1 and 2 described in chapter 3, the first graph, as shown in Figure 4.7, shows the range in terms of gain in decibels where data are taken from Table A1. The second graph shown in Figure 4.8 shows the range in transmission coefficients **T** which are calculated and taken from data of Table A2 in the Appendix A.

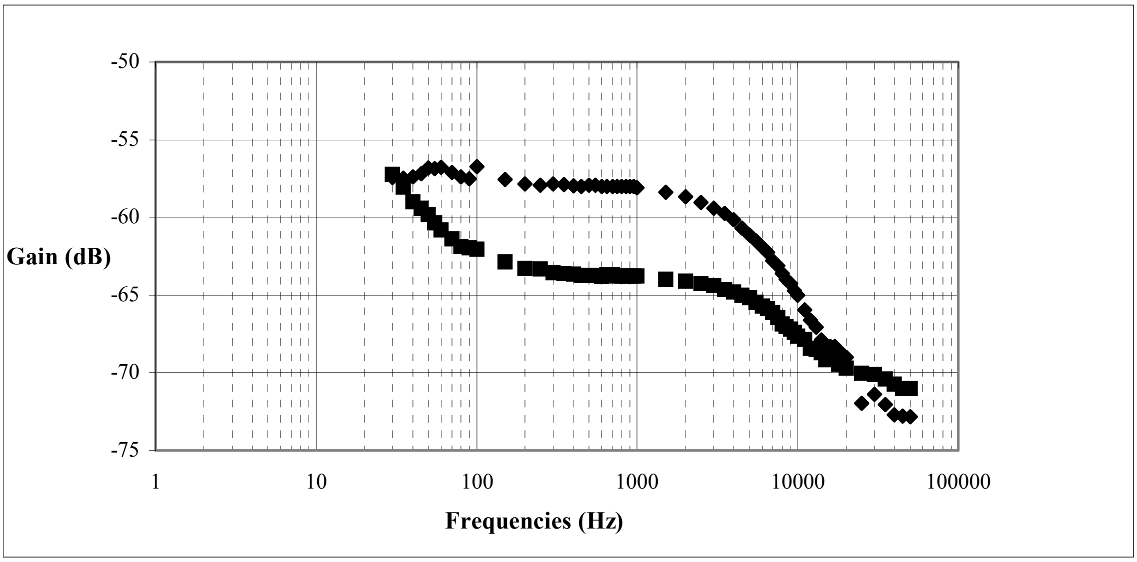

Figure 4.7 Frequency response of two-hydrophones method in decibels. The plot configures ■ - Setup 1 and ♦ - Setup 2.

The frequency response shows attenuation in the overall power of the transmitted pressure coefficients as it shows negative values in gain. This indicates that the incident pressures from the transmitter hydrophone experience loss by various aspects of the surrounding medium such as the water itself, the loss characteristics of the hydrophones and some reflected pressures when the trachea tissue is present in the Setup 2. The differences in attenuation value or transmission coefficients over the range of frequencies are due to the characteristics of the hydrophones. The shapes of the plot indicate that the hydrophones are of second-order system devices.

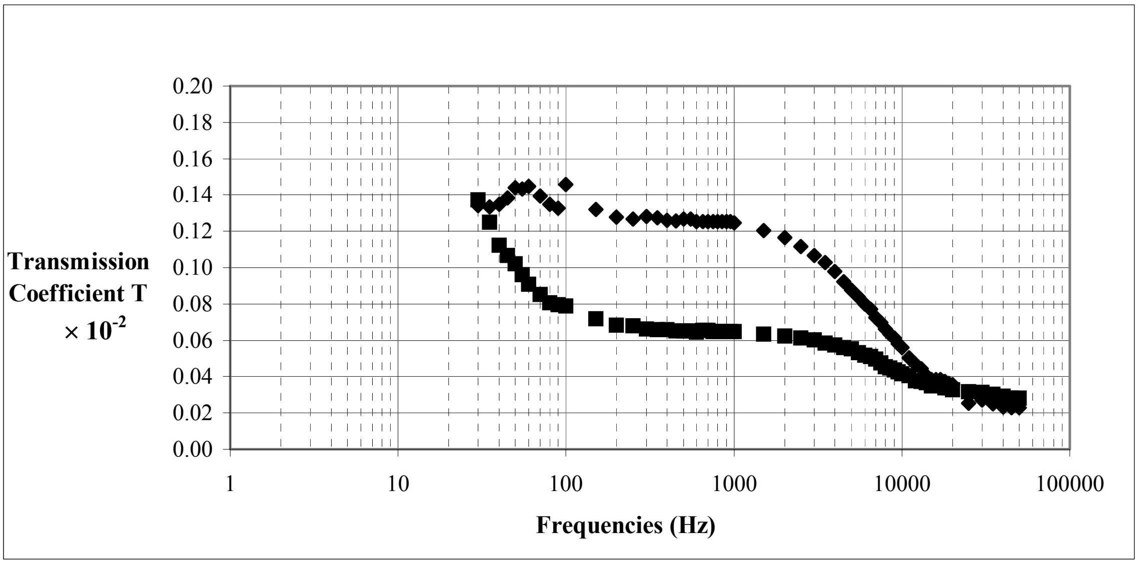

Figure 4.8 Frequency response of transmission coefficients by two-hydrophones method. The plot configures ■ - Setup 1 and ♦ - Setup 2.

The usable frequencies which give a steady state output are between the range of 750 to 950 Hz. This range has been highlighted in grey in Table A1 and A2 in Appendix A. Hence for further calculation, to determine the bulk and Young's modulus, only the coefficients that fall within the latter range are taken into account. Table 4.16 summarises these highlighted values. The first column lists the parameters involved in the two-hydrophones method, the second column presents the Setup 1 results data and the third column presents the Setup 2 results data. The first row shows the incident pressure generated by the transmitter hydrophone. The second row shows the transmitted pressure picked up by the receiver hydrophone. The third row presents the transmission coefficients for both setups.

Table 4.16 Results summary within the steady state of the two-hydrophones method

Parameters	Setup 1	Setup 2
Incident pressure	$\mathbf{P}_i$ = 10.5 μPa	$\mathbf{P}_i$ = 10.2 μPa
Transmitted pressure	$\mathbf{P}_{t1}$ = 0.00682 μPa	$\mathbf{P}_{t2}$ = 0.0128 μPa
Transmission coefficients	$\mathbf{T}_1$ = 0.000648	$\mathbf{T}_2$ = 0.001255

Using the difference in transmission coefficients of equation (2.57) where z_w = 1.48 × 10^6 Pas/m gives a solution for the tracheal characteristic impedance to be

$$z_t = 0.0484 \times 10^6 \text{ Pas/m}$$

With the density of trachea ρ_t = 1000 kgm^{-3}, equation (2.38) is used to determine the bulk modulus as

$$M_B = 2.3 \times 10^6 \text{ Pa}$$

and thus using equation (2.39)

$$\boxed{E = 0.70 \times 10^6 \text{ Pa}}$$

The characteristic impedance of the trachea is several hundreds times smaller than water which makes waves travel faster in the trachea tissue than the water. Thus, having the transmission coefficient $\mathbf{T}_2$ larger than $\mathbf{T}_1$ conforms to the acoustical principle.

4.6 Vibration Method

Based on equation (2.74), the measured parameters involved are listed in Table 4.17. The first column lists the related parameters and the second column presents their symbolic representations. The third column shows the obtained values where most of the dimensional values are measured previously. The fourth column shows the units of the corresponding parameters.

Table 4.17 Obtained values of related parameters for the vibration method

Parameters	Symbols	Obtained values	Unit
First resonance	f	20 ± 0.5	Hz
First resonance	$\omega = 2\pi f$	125.66 ± 3.14	rad
Inner radius	R	8.3 ± 0.4	mm
Thickness	h	2.6 ± 0.5	mm
Mean radius	$r = R+h/2$	9.6 ± 0.6	mm
Density	ρ	1000 ± 7.0	kgm^{-3}
Poisson's ratio	v	0.45	-
Clamped length	l	103.3 ± 0.2	mm

The results of other related constant parameters described in chapter 2 are calculated by the software program Matlab and tabulated in Table 4.18. The written Matlab codes are presented in the Appendix B. In Table 4.18, the first column lists the related parameters, the second column presents their symbolic representations and the third column shows the calculated values where its final value for the Young's modulus of elasticity is 0.31 MPa.

Table 4.18 Calculated values of related parameters for the vibration method

Parameters	Symbols	Calculated values
Constant	$\frac{1}{\xi}$	0.0059
Constant	k	0.1327
Constant	$\frac{\mu l}{r}$	1.506π
Constant	μ	0.4397
Constant	θ_1	1.0176
Constant	θ_2	0.5597
Arbitrary constant	R_0	0.0047
Arbitrary constant	R_1	1.2353
Arbitrary constant	R_2	2.6631
Constant	α	0.2308
Angle	θ	0.8428 rad
Non-dimensional natural frequencies (root 1)	Δ_1	2.0664
Non-dimensional natural frequencies (root 2)	Δ_2	0.0038
Non-dimensional natural frequencies (root 3)	Δ_3	0.5929
Young's modulus	E_1	0.31×10^6 Pa

4.7 Summary of Results

The summary of Young's modulus obtained by the four different methods for a trachea sample tested in the previous sections 4.1 to 4.6 are tabulated in Table 4.19. The first column lists the four methods used and the second column shows the category of strain types used particularly for the conventional tension method and pressure difference method. The third, fourth and fifth column respectively list the values obtained for the first, second and third modulus as they change when loads or pressure are increased.

Table 4.19 Summary of a trachea's Young's modulus measured by four different methods

Methods	**Strain Types**	**First modulus E_1 (MPa)**	**Second modulus E_2 (MPa)**	**Third modulus E_3 (MPa)**
Conventional Tension – without the tracheal connective tissue and muscle	Instantaneous	0.31	0.64	-
	Engineering	0.31	0.61	-
Conventional Tension – with the tracheal connective tissue and muscle	Instantaneous	0.031	0.110	-
	Engineering	0.028	0.089	-
Conventional Tension – axial deformation	Instantaneous	0.201	0.032	-
	Engineering	0.200	0.031	-
Pressure Difference	Instantaneous	0.020	0.083	0.13
	Engineering	0.019	0.072	0.11
Two-hydrophones	-	0.68	-	-
Vibration	-	0.31	-	-

It is not sufficient to make an analysis and interpretation for the recommendation from Table 4.19 as it only represents the results for one trachea sample. Although one trachea sample can be taken as a representation of the whole, due to the trachea's nonhomogeneity it is still more appropriate to consider a range of values. The purpose of this exercise in presenting results for one trachea with four different methods is to show the steps and calculation procedures taken to measure further number of tracheas. To obtain a range of values of Young's modulus, a total number of 12 tracheas are tested. The results of these tracheas tested are shown in Table 4.20 where they are summarised and tabulated in terms of their 'equivalent' or average range rather than their measured values. Since there is no major difference in the Young's modulus between the instantaneous and engineering strain, only the instantaneous strain is included in Table 4.20. In this table, the second, third and fourth columns, respectively, lists the values obtained for the first, second and third modulus.

At a glance, the overall results show a wide range of values which are from 0.01 to 1 Megapascals. More analysis is focused on the first Young's modulus as it involves a smaller range of applied loads or pressures which are more in place within the natural environment or biological application. More discussions, detailed analysis and comparative interpretations for each method are presented in chapter 5.

Table 4.20 Results summary of ten trachea tested by four different methods

Methods	**First modulus E_1 (MPa)**	**Second modulus E_2 (MPa)**	**Third modulus E_3 (MPa)**
Conventional Tension – without the tracheal connective tissue and muscle	0.14– 0.91	0.1 – 1.0	0.23 – 1.0
Conventional Tension – with the tracheal connective tissue and muscle	0.03 – 0.21	0.1 – 0.32	0.15 – 0.32
Conventional Tension - Axial Deformation	0.019-0.201	0.011-0.046	0.016 – 0.028
Pressure Difference	0.019 – 0.11	0.051 – 0.23	0.11 – 0.3
Two-hydrophones	0.28 – 0.68	-	-
Vibration	0.011- 0.31	-	-

Chapter 5
Discussion and Conclusions

5.1 Introduction

This chapter presents the analysis and interpretation of the results from chapter 4 and some comparative discussion on results and methods from other literature. More analysis is focused on the first Young's modulus which is the first linear element from the related stress-strain plot that involves a smaller range of applied loads or pressures. The smaller range of loads or pressure are more in place within the natural physiological application.

For each of the methods, the analysis includes discussion of the results and the conditional aspects of the experimental setups which affect those results. Discussion is also presented for each method and comparison is made with related literature. The overall comparative analysis is then written for the results of the four methods, taking the conventional tension method as reference value. Pros and cons of the setups, the expected results and the procedural activities are also presented for each testing method. A recommendation is then made for the method that gives the most suitable outcome.

As there are three different mounting orientations involved in the conventional tension method, comparisons are made within these three types of results. The methods that excluded the connective tissue and muscle, contained mostly cartilage and produced results in the higher range of modulus between 0.14 and 0.91 MPa. The absence of connective tissue and muscle caused less deformation as it was more difficult to stretch the tissue. On the other hand, tests with the connective tissue and muscle produced results in the lower range between 0.03 – 0.21 MPa. The presence of the connective tissue and muscle gave more flexibility for the trachea to deform with less force applied. This was shown by the results of the axial Young's modulus which were almost within similar range with the conventional tension method that included the connective tissue and muscle. These were expected as both types of tissue orientations consisted of various flexible connecting tissue and muscle between the cartilage.

The pressure difference method presented a similar range of results with the conventional tension method that included the connective tissue and muscle. The radial deformation by the pressure difference method also included the connective tissue and muscle that bulged out under the applied pressure. This produced a similar range of modulus.

The two-hydrophones method generated a narrower range of results which were closer to the results of the conventional tension method that excluded the connective tissue and muscle. The acoustical effect influenced the initial results since transmission was through a bulk modulus of a medium rather than its Young's modulus [26]. Although the results were modified into Young's modulus based on the triaxial stresses formula described in chapter 2, the overall transmitted waves went through a nature of the medium's bulk modulus rather than the change of shape or deformation of the tissue. In the two-hydrophones method, the connective tissue and muscle did not have a direct contact nor was it directly affected by the transmitted waves and thus the results were produced in the higher and narrower range.

The vibration method, on the other hand, included the trachea as a whole during the vibratory motion, where its results ranged from 0.011 to 0.31 MPa. The direct presence and effect of connective tissue and muscle during vibration produced the results in the similar range to those of the conventional tension method that included the connective tissue and muscle.

The first Young's modulus, particularly by the conventional tension and the pressure difference methods, tended to be in the lower range as a smaller range of loads or pressures was applied. The second and third modulus tended to be in the higher range than the first modulus as a result of applying increasing loads or pressure.

5.2 Tracheal Dimensions

Due to the nonhomogeneity and non-isotropic shape of the tissue, the measurement procedure was not as straight forward as hoped for. Extra care was needed to avoid distorting the trachea's initial shape while measuring it. An average of ten measurements were taken for its thickness and inner radius. The latter was obtained by measuring the inner diameters then dividing them by two. The shape of the vernier calliper itself limited the amount of depth that could be measured inside the tracheal shell. Although it is ideal to take measurements around the middle part of the trachea, most measurements could only be taken around the edges of both tracheal ends. Also, while the outer diameter of the trachea could be measured at the middle part, the tendency to squeeze the tissue could deform its initial shape and reduce its actual value, hence this exercise was avoided.

The cross-sectional tube shell of the trachea did not have a symmetrical round circle shape were but rather irregular. Some looked like loose triangular shapes or ellipses, and they varied along the length of the tissue. Measurements for the inner diameter of the tracheal end were thus taken in several dimensions, not just the largest diameter possible but also the smallest possible, with care taken to not stretch the tissue, which could be done easily by hand movement upon using the vernier. The range of inner radius obtained were between 8.2 to 9.5 mm and the range of thickness measured were between 2.1 to 3.1 mm. Their averages were 8.7 mm for the inner radius and 2.5 mm for the thickness.

5.3 Conventional Tension Method

The conventional tension is a standard method based on uniaxial state of stress which is commonly used by other research in this area [1, 3]. This method puts the tissue under extreme conditions and is a destructive approach. As previously mentioned in the procedure section in chapter 3, the three types of cutting and mounting of the tissue should produce the minimum and maximum value of Young's modulus. The results from this method are treated as reference values for comparison with other methods. Obviously this method is never accurate for tissue material and is affected by a number of variants such as cutting, loading, clamping, tracheas age and so on.

The conventional tension method is a destructive approach, particularly for the radial testing because the tissues were cut across its axial shell as explained in chapter 3. Although the cut without the connective tissue and muscle did not give more flexibility than its uncut initial state, the results of this test are useful for comparison purposes where maximum modulus is expected. In addition to the fact that this test is destructive, clamping of the boundaries affected the results significantly. As the tissue was slippery and fragile to some degree, handling them for clamping may have changed its initial property. Tensile stress was kept to a maximum of 120 g loads to avoid damage and change to the tissue's mechanical properties.

Readings could also be affected by the way the loads are applied. Placing the loads gently avoided sudden stretch on the tissues causing a forced non-linearity curve in the deformation plot. However, the circumferential testing without the connective tissue and muscle needed a larger load of more than 30 g to start with, in order to initially remove the sagging and to obtain first linear results. Other conditions that may have affected the readings involved the quality of the tension system. As it was man-made with simple materials such as woods, metals and screws, its rugged form may have contributed a degree of inconsistency in achieving accurate deformation effects. For example, wobbly wheels may have not moved the trolley in a straight line towards the tensile direction when little increments of loads were applied.

The plots in chapter 4 showed both instantaneous and engineering strains where the latter tended to be slightly larger than the instantaneous strain but was close and still within a similar range. The overall results from this test with three different cutting types showed a wide range of values which were from 0.03 to 1 MPa. Comparisons were made within these three types of results for the first Young's modulus.

The curves in the figure for test without the connective tissue and muscle showed more consistent linearity. This test mostly included cartilage which produced results in the higher range of modulus between 0.14 and 0.91 MPa. The absence of the connective tissue and muscles caused less deformation as tissue was harder to be stretched. A source of literature [1] studying articular cartilage, used a typical mechanical property of 0.36 MPa for the solid extracellular matrix of articular cartilage's Young's modulus, which falls within the range of values obtained by this research.

From other literature, the Young's modulus for rabbit's tracheal cartilage was 10 MPa from research by Holzhäuser and Lambert [22], and 5.8 ±2.9 MPa for a pig's tracheal cartilage rings from research by Sera [2]. Suki et al [21] gives results of 0.25 MPa for the soft tissue and 1.96 MPa for the cartilage of calf trachea. These values from other literature for cartilage are in the higher range than the results obtained by this research, which may be attributed to the different measuring methods, the freshness and the types of tissue specimen used. However, some of the outlier values obtained by the conventional tension method still fell within the values by these literatures.

On the other hand, tests with the connective tissue and muscle produced results in the lower range between 0.03 – 0.21 MPa. This was expected as cutting that included the connective tissue and muscle gave more viscoelastic properties to the tissue. With the presence of the connective tissue and muscle, the tissue deformed more easily with more flexibility. The results of this test were almost within a similar range with the tests for axial Young's modulus which were 0.019-0.201 MPa. These were expected as both types of tissue orientations consisted of various flexible connective tissue and muscle between the closing of the arc-shaped cartilage.

As loads were increased, the stress-strain curves were non-linear which indicated changes in the modulus of elasticity. The modulus increased with larger loads as shown in the second and third modulus. This was particularly shown in the results for the circumferential Young's modulus with both cutting types. The tissue was more flexible and softer initially or with smaller loads. As it was stretched further and nearer to its maximum deformation, the tissue got harder or stiffer and thus produced larger Young's modulus. The difference between the circumferential and axial modulus was that the axial modulus did not have any significant changes in the second and third Young's modulus with increasing loads. This may have been due to the structural form of cartilage grooves being joined together by the connecting cartilage, tissues and other muscles in the axial direction that gave a more spring-like effect to it.

In summary, the results from this method could be treated as reference values for other methods to be compared with in this research. The reason was that tissues were being subjected to extreme conditions in order to obtain a minimum and maximum modulus; the value from a source of literature [1] is comparably within the range obtained by this research; and the differences in results within the three types of cutting are within explainable reasons.

5.4 Pressure Difference Method

The range of results obtained by this method for the first Young's modulus were between 0.019 – 0.11 MPa, the second were between 0.051 – 0.23 MPa and the third were between 0.11 – 0.3 MPa. These results presented a similar range with results of the conventional tension method with the connective tissue and muscle which were between 0.03 – 0.21 MPa for the first modulus, 0.051 – 0.23 MPa for the second and 0.11 – 0.3 for the third. These similarities in range may have been due to the presence of the connective tissue and muscle where radial deformation by the applied pressure gave a bulging effect on the tissue.

The bulges tended to be irregular around the circumference. One side or point could bulge more than the other. Sometimes bulges or deformation could be absent and not detected by the laser displacement meter. Factors that may have affected this absence included if the trachea was cut too short in length. Then clamping required more stretch on its axial length so the initial property of radial elasticity was changed as it was already stretched to its maximum radial deformation. In this condition, no more deformation could be detected when pressure was increased. Cutting and mounting the trachea into a suitable length played a critical role in obtaining useful or informative results. A trachea which was cut too long would bend and twist when pressure was increased and thus readings became inaccurate. With every trachea being different in dimensions and with their degree of elastance, axially or radially, it was difficult to decide for an exact length to test for all tracheas.

This method took numerous trials and initial testing in order to observe the changes in deformation. Often no informative results were produced due to the clamping techniques described in the last paragraph or for other reasons such as the freshness of the tissues and its natural elastance. Some trachea came with a smaller radius and were larger in thickness compared with the others. These were harder to stretch radially by the pressure difference method.

Compared with the results obtained by the literature for a pig's trachea [2], the smooth muscle has E = 0.65±0.32 MPa and the cartilage rings, E=5.8±2.9 MPa. Both are results using under 3 cmWg applied internal pressure. Under similar pressure, the results from this research lies in the lower range which are between 0.019 – 0.11 MPa. These values are comparably similar to the circumferential testing of the conventional tension method with the connective tissue and muscle.

The difference between the literature [2] and the results of this research could be due to the formula or equation used to describe the relationship between pressure and the radial deformation. Apart from that, other experimental aspects such as the set up of the rig, the measurement devices used, the measurement procedures taken and the nature of the pigs such as species, weight, age and sex may also have affected the results. Although this research used the assumption of a thick-walled homogenous cylindrical shell and other geometrical approximations as described in chapter 2, the results of the pressure difference method by its adopted theoretical principle were sufficiently comparable with the ones of the conventional tension method. The overall theoretical approach used in this method is thus appropriate for such application in measuring the Young's modulus of elasticity of nonhomogeneous material. The drawback from this method concerns the practicality and consistency of the experimental rig and the clamping technique as they can greatly affect the data measurement accuracy. In order to minimise reading inconsistencies, further improvements could be made for the design of the tank, clamping conditions and measuring setup of the laser displacement meter.

5.5 Two-hydrophones Method

The range of results obtained for the Young's modulus by the two-hydrophones method were between 0.28 – 0.68 MPa. This method generated a narrower range of results which were closer to the results of circumferential testing of the conventional tension method without the connective tissue and muscle, which were between 0.14– 0.91 MPa. The narrow range may have been due to the acoustical principle that governed and influenced the initial results of transmission to be in bulk modulus rather than Young's modulus [26]. Although the results were modified into Young's modulus based on triaxial stresses, the overall transmitted waves went through a nature of medium's bulk modulus rather than change of shape or deformation of tissues. According to the deformation characteristics, the modulus of elasticity changed with the increasing force applied which was absent in the results of this method. The presence of the connective tissue and muscle in the pressure difference method and the conventional tension method produced lower modulus of elasticity than that produced by the two-hydrophones method. In the two-hydrophones method, the connective tissue and muscle was not directly deformed nor affected by the low pressure acoustical transmitted wave, which therefore produced results in the higher range.

In carrying out this test method, the hydrophones were found to be extremely sensitive devices. They picked up noises from the surroundings such as the air conditioner and outdoor traffic. Particularly with the noise from the air conditioner, the incident and transmitted signal waves shown by oscilloscope fluctuated significantly and was difficult to obtain a meaningful set of data. Hence, experiments could only be carried out with the air conditioner being off and minimal presence of other noises.

Other than the noise factor, the two-hydrophones method had other conditional factors that could affect the results and should be considered. Most of these were due to the electronic characteristics of the hydrophone itself and its surrounding medium. The results from the frequency response plot in Figure 4.8 showed attenuation in the overall power of the transmitted pressure coefficients as it shows negative values in gain. This indicated that the incident pressures from the transmitter hydrophone experienced loss by various aspects of the surrounding medium such as the water itself, the loss characteristics of the hydrophones and some reflected pressures when trachea tissue is present in the Setup 2.

The hydrophone was also voltage dependent. With a fixed initial power voltage set in the AC generator, the output and input signals voltage amplitude varied when frequencies from the AC generator were changed. Hence this produced different transmission coefficients over the varying range of frequencies. The shapes of the plot indicated that the hydrophones were of second-order system devices. The usable frequencies which gave steady state output were between the range of 750 to 950 Hz. This range has been highlighted in grey in the Table A1 and A2 in the Appendix A.

To the best of our knowledge this method has not been used for applications to find Young's modulus of elasticity for biomaterial tissue measurement. It is crucial to be familiar with the electronic characteristics of the hydrophones before proceeding to the actual tissue test.

This method can be a potentially powerful measuring technique when further tests are carried out with hydrophones made by other manufacturers. The end aim of this two-hydrophones method would be a recommendation that includes the most suitable brand for this application. For high sensitivity hydrophone devices, a way of isolating the tank from surrounding noises could be to cover it with polystyrene boards. With Reson hydrophones, the AC generator required high input voltage power and its characteristics of being voltage dependent gave an inconsistency for the transmission coefficients. Although the results are within the reference range from the tension test, this method is still felt insufficiently explored due to the use of one brand of hydrophone with its own unique characteristics. Further investigations with other brands of hydrophones should confirm the validity of this method using Reson hydrophones.

5.6 Vibration Method

With the trachea being mounted on its axial direction with loads up to only 30 g, this method was considered non-destructive. The vibration method presented results that ranged from 0.011 to 0.31 MPa which covered the reference range by three types of the conventional tension method. This method included the trachea as a whole during the vibratory motion. The direct presence and effect of connective tissue and muscle during vibration produced results to close to the results of the conventional tension method with the connective tissue and muscle.

Below 10 Hz, vibration signals were not smoothly picked up by the vibrometer as noises from unsteady vibration were present. The first natural frequency was taken when the first peak growth of voltage amplitude was shown on the oscilloscope. Often this was unclearly shown as it was usually the first peak amplitude just before steady vibration signals were formed on the scope screen.

The advantages of this method was the setup which involved a simple tension system and could be carried out with any simple designed clamping system, any brand of shaker, AC generator and laser vibrometer. A firm base for the clamping or tension system was crucial for the shaker to give steady vibration and its signals to be shown on the oscilloscope.

To the best of our knowledge, this also was the first time this method was used for such an application. The drawback of this method was that although the results are within the range of reference, they were within a wide range of values. The literature shows higher range values such as 0.36 MPa for articular cartilage [1] and 0.5 MPa for trachea [2]. Another drawback involved with this test was that when vibrating the object, the first resonance might not have been purely the resonance from the tissue alone but also included the clamping system attached to the tissue such as from the clamping pole, trolley and loads.

The load of 30 g was used to remove the sagging of the tissue without stretching it so far where it could change its properties. Although an ordinary clamping pole on both ends of the tissue seemed preferable instead of 30 g loads, deciding on the length where it could be clamped securely without stretching it too far could have created an inconsistency for every different trachea tested.

The formula used from thin cylindrical shells included very involved expressions for the related arbitrary constants so it was difficult to visualise and relate directly with the relatively simple experimental setup.

Overall, the results by this method gave more consistency than the other non-destructive methods investigated in this research. Out of the total trachea tested, this method gave the least outliers and produced more calculation results that were meaningful and within the range of reference by the tension test.

Thus a strong recommendation is given for the vibration method at this stage where a potentially stronger technique by the two-hydrophones method can be further investigated.

5.7 Conclusions

Three non-invasive and non-destructive experimental techniques were proposed and developed in this research to determine the trachea wall's Young's modulus of elasticity in the radial direction. The results from these three proposed techniques were then compared with reference values obtained by the standard uniaxial state of stress, which in this research is referred to as the conventional tension method.

In this thesis, literature reviews related in this area of research were presented along with brief information about characterisation of biomaterials and viscoelasticity. Appropriate theoretical principles which governed each of the experimental methods have been described and elaborated with detailed apparatus and setups. The experimental investigations were carried out to obtain the results by the three proposed methods and the conventional tension method that includes three ways of mounting. The results were compared with the reference values and analysed. In the end a recommendation was made for the most suitable method for such an application.

The result from the reference values concludes that the presence of the tracheal connective tissue and muscle at the closing of the arc-shaped cartilage mainly gives the viscoelastic characteristics of the tissue and the lower range of modulus than the ones without. The conventional tension method put the tissue under the most extreme conditions where the three ways of cutting and mounting gives the minimum and maximum reference values for the modulus of elasticity.

The results from the three proposed measuring techniques compared with the reference values lead to the following conclusions:

1. The pressure difference method adopts appropriate theoretical principles as results fell within the range of the reference values. However, the experimental technique of this method gives a degree of inconsistency which mainly due to the clamping conditions of the tissue. Further improvement of the tank design, clamping and measuring set up with the laser displacement could minimise reading inconsistencies.

2. The two-hydrophones method may potentially provide a powerful measuring technique as results fell within a narrower range than any other methods proposed and still lie within the reference values. Improvement is expected if the test is conducted in an acoustically isolated medium.

3. The vibration method with its selected theoretical principles gives more consistency in results than any other methods, which means less outliers are produced in the results. The results lie within the reference values but fell in a wider range. The simple setup provides practical advantages in carrying out experiments. The first resonant frequencies obtained may have not been purely from the tracheal tissue, but instead may have come from the whole clamping and setup system. However, the results' average range, consistency and conformity to the reference values provides assurance in recommending this method to be the most suitable at this stage.

5.8 Recommendations

1. The vibration method is the most recommended approach concluded in this research. More vibration experiments can be carried out on a large number of tracheas in order to achieve a population or statistical average of the modulus of elasticity.

2. The two-hydrophones methods should be carried out with other brands of hydrophones and in an acoustically isolated medium.

3. An experimental investigation to determine the Young's modulus of elasticity by the means of ultrasound devices should be conducted for comparison with this research.

Appendix A

Table A1 Results of the two-hydrophones method

Input frequency (Hz)	Setup 1			Setup 2		
	Incident pressure $\mathbf{P}_i$ (μPa)	Transmitted pressure $\mathbf{P}_{t1}$ (μPa)	Amplitude Ratio (dB)	Incident pressure $\mathbf{P}_i$ (μPa)	Transmitted pressure $\mathbf{P}_{t2}$ (μPa)	Amplitude Ratio (dB)
30	3.2	0.0044	-57.23	3.5	0.0047	-57.44
35	3.6	0.0045	-58.06	3.9	0.0052	-57.50
40	4.1	0.0046	-59.00	4.3	0.0058	-57.40
45	4.4	0.0047	-59.43	4.7	0.0065	-57.18
50	4.8	0.0049	-59.82	5.0	0.0072	-56.83
55	5.1	0.0049	-60.35	5.3	0.0076	-56.87
60	5.5	0.005	-60.83	5.6	0.0081	-56.79
70	6.1	0.0052	-61.39	6.1	0.0085	-57.12
80	6.7	0.0054	-61.87	6.6	0.0089	-57.40
90	6.9	0.0055	-61.97	7.0	0.0093	-57.53
100	7.1	0.0056	-62.06	7.2	0.0105	-56.72
150	8.5	0.0061	-62.88	8.4	0.0111	-57.58
200	9.2	0.0063	-63.29	9.0	0.0115	-57.87
250	9.4	0.0064	-63.34	9.3	0.0118	-57.93
300	9.8	0.0065	-63.57	9.6	0.0123	-57.85
350	10.0	0.0066	-63.61	9.8	0.0125	-57.89
400	10.2	0.0067	-63.65	10.0	0.0126	-57.99
450	10.3	0.0067	-63.74	10.1	0.0127	-58.01
500	10.3	0.0067	-63.74	10.1	0.0128	-57.94
550	10.3	0.0067	-63.74	10.1	0.0128	-57.94
600	10.4	0.0067	-63.82	10.2	0.0128	-58.03
650	10.4	0.0068	-63.69	10.2	0.0128	-58.03
700	10.4	0.0068	-63.69	10.2	0.0128	-58.03
750	10.5	0.0068	-63.77	10.2	0.0128	-58.03
800	10.5	0.0068	-63.77	10.2	0.0128	-58.03
850	10.5	0.0068	-63.77	10.2	0.0128	-58.03
900	10.5	0.0068	-63.77	10.2	0.0128	-58.03
950	10.5	0.0068	-63.77	10.2	0.0128	-58.03
1000	10.5	0.0068	-63.77	10.2	0.0127	-58.10
1500	10.6	0.0067	-63.98	10.3	0.0124	-58.39
2000	10.6	0.0066	-64.12	10.3	0.012	-58.67
2500	10.6	0.0065	-64.25	10.3	0.0115	-59.04
3000	10.6	0.0064	-64.38	10.3	0.0110	-59.43

Table A1 Results of two-hydrophones method (continued)

3500	10.6	0.0062	-64.66	10.3	0.0106	-59.75
4000	10.6	0.0061	-64.80	10.3	0.0101	-60.17
4500	10.7	0.006	-65.02	10.5	0.0097	-60.69
5000	10.7	0.0059	-65.17	10.5	0.0092	-61.15
5500	10.7	0.0057	-65.47	10.6	0.0089	-61.52
6000	10.8	0.0056	-65.70	10.5	0.0084	-61.94
6500	10.8	0.0055	-65.86	10.5	0.0081	-62.25
7000	10.9	0.0054	-66.10	10.6	0.0077	-62.78
7500	10.9	0.0052	-66.43	10.6	0.0074	-63.12
8000	11.0	0.005	-66.85	10.6	0.007	-63.60
8500	11.0	0.0049	-67.02	10.6	0.0067	-63.98
9000	11.0	0.0048	-67.20	10.6	0.0065	-64.25
9500	11.0	0.0047	-67.39	10.7	0.0062	-64.74
10000	11.1	0.0046	-67.65	10.7	0.006	-65.02
11000	11.1	0.0045	-67.84	10.7	0.0054	-65.94
12000	11.1	0.0042	-68.44	10.7	0.005	-66.61
13000	11.2	0.0042	-68.52	10.8	0.0048	-67.04
14000	11.2	0.0041	-68.73	10.9	0.0044	-67.88
15000	11.2	0.0039	-69.16	10.9	0.0042	-68.28
16000	11.2	0.0042	-68.52	10.9	0.0042	-68.28
17000	11.3	0.004	-69.02	10.9	0.0042	-68.28
18000	11.3	0.0038	-69.47	11.0	0.0041	-68.57
19000	11.3	0.0038	-69.47	11.0	0.004	-68.79
20000	11.3	0.0037	-69.70	11.0	0.0039	-69.01
25000	11.4	0.0036	-70.01	11.1	0.0028	-71.96
30000	11.5	0.0036	-70.09	11.1	0.003	-71.36
35000	11.6	0.0035	-70.41	11.2	0.0028	-72.04
40000	11.7	0.0034	-70.73	11.2	0.0026	-72.68
45000	11.7	0.0033	-70.99	11.3	0.0026	-72.76
50000	11.7	0.0033	-70.99	11.4	0.0026	-72.84

Table A2 Results of the two-hydrophones method in terms of transmission coefficients

Input frequency (Hz)	Transmission coefficient $\mathbf{T}_1$ of Setup 1 $\times 10^{-2}$	Transmission coefficient $\mathbf{T}_2$ of Setup 2 $\times 10^{-2}$
30	0.1375	0.1343
35	0.1250	0.1333
40	0.1122	0.1349
45	0.1068	0.1383
50	0.1021	0.1440
55	0.0961	0.1434
60	0.0909	0.1446
70	0.0852	0.1393
80	0.0806	0.1348
90	0.0797	0.1329
100	0.0789	0.1458
150	0.0718	0.1321
200	0.0685	0.1278
250	0.0681	0.1269
300	0.0663	0.1281
350	0.0660	0.1276
400	0.0657	0.1260
450	0.0650	0.1257
500	0.0650	0.1267
550	0.0650	0.1267
600	0.0644	0.1255
650	0.0654	0.1255
700	0.0654	0.1255
750	0.0648	0.1255
800	0.0648	0.1255
850	0.0648	0.1255
900	0.0648	0.1255
950	0.0648	0.1255
1000	0.0648	0.1245
1500	0.0632	0.1204
2000	0.0623	0.1165
2500	0.0613	0.1117
3000	0.0604	0.1068
3500	0.0585	0.1029
4000	0.0575	0.0981
4500	0.0561	0.0924

Table A2 Results of two-hydrophones method in terms of their transmission coefficients (continued)

5000	0.0551	0.0876
5500	0.0533	0.0840
6000	0.0519	0.0800
6500	0.0509	0.0771
7000	0.0495	0.0726
7500	0.0477	0.0698
8000	0.0455	0.0660
8500	0.0445	0.0632
9000	0.0436	0.0613
9500	0.0427	0.0579
10000	0.0414	0.0561
11000	0.0405	0.0505
12000	0.0378	0.0467
13000	0.0375	0.0444
14000	0.0366	0.0404
15000	0.0348	0.0385
16000	0.0375	0.0385
17000	0.0354	0.0385
18000	0.0336	0.0373
19000	0.0336	0.0364
20000	0.0327	0.0355
25000	0.0316	0.0252
30000	0.0313	0.0270
35000	0.0302	0.0250
40000	0.0291	0.0232
45000	0.0282	0.0230
50000	0.0282	0.0228

Appendix B
Matlab Program for the Vibration Method Calculation for the Young's Modulus of Elasticity

```
R=[0.01087,0.00961,0.00985,0.0096,0.0099]
% inner radius of five measured trachea tissues

h=[0.00274,0.0023,0.0021,0.00256,0.00257]
% thickness of five measured trachea tissues

Lo=[0.05224,0.0961,0.0306,0.1007,0.0736]
% initial length of five measured trachea tissues

dl=[0.0026,0.0063,0.00086,0.0026,0.0005]
% change in length or deformation of five measured trachea tissues with
loads

f =[50,80,20,20,11.8]
% first natural frequencies noted for five trachea tissues

L=Lo+dl                 % total length of trachea subjected to vibration
rho=1000                % density of trachea
v=0.45                  % Poisson's ratio

mew=1.506.*pi.*R./L
% first root as in equation (2.64)

k=sin(mew.*L./(2.*R))./sinh(mew.*L./(2.*R))
% constant as expressed in equation (2.62)

omega=2.*pi.*f          % angular frequencies
El=h.^2./(12.*R.^2)     % coefficient as expressed in equation (2.58)

theta1=1+k.^2           % coefficient as expressed in equation (2.56)

% the following lines are part of constant as expressed in equation (2.57)
theta21=1-k.^2
theta22=2./(1.506.*pi)
theta23=sin(1.506.*pi)
theta2=theta21+theta22.*theta23
% coefficient as expressed in equation (2.57)

% with n=1 the following lines are part of constant as expressed in
equation (2.59)
b1R2=(mew.^2).*((theta1./theta2)+(0.275.*theta2./theta1))
b2R2=2.275
b3R2=El.*(mew.^4+1+(2.*mew.^2.*theta2./theta1))
R2=b1R2+b2R2+b3R2       % constant as expressed in equation (2.59)

% with n=1, the following lines are part of coefficient as expressed in
equation (2.60)
b1R1=0.275.*(mew.^4+1)
b2R1=mew.^2.*((theta1./theta2)-(0.45.*theta2./theta1))
b3R1=0.275
```

```
b4R1=mew.^2.*((theta1/theta2)+((theta2/theta1).*0.0725))
b51=0.275.*(1+mew.^2.*theta2./theta1)
b52=El.*(b51+1+mew.^2.*(theta1./theta2))
b53=mew.^4+1+(2.*mew.^2.*theta2./theta1)
b5R1=b52.*b53
R1=b1R1+b2R1+b3R1+b4R1+b5R1   % constant as expressed in equation (2.60)

% with n=1 the following lines are part of coefficient as expressed in
equation (2.61)
b1R0=mew.^4.*0.275.*(1-v.*theta2.^2./theta1.^2)
b21=mew.^2.*((0.725.*theta2./theta1)-(theta1./theta2)-
(0.075625.*theta2./theta1))
b22=0.275.*(mew.^4+1)
b2R0=El.*(b21-b22)
b3R0=mew.^4+1+(2.*mew.^2.*theta2./theta1)
R0=b1R0+b2R0.*b3R0            % coefficient as expressed in equation (2.61)

alpha1=-1./27.*((R1-(R2.^2./3)).^3)       % part of equation (2.68)
alpha=sqrt(alpha1)            % coefficient as expressed in equation (2.68)

% the following lines are part of equation (2.69)
b1theta=R0-(R1.*R2./3)+((2.*R2.^3)./27)
b2theta=1./(2.*alpha).*b1theta
theta=acos(b2theta)           % coefficient as expressed in equation (2.69)

% the following lines are part of equation (2.65), (2.66) and (2.67)
respectively
delcos1=cos(theta./3)
delcos2=cos((theta+2.*pi)./3)
delcos3=cos((theta+4.*pi)./3)

% the following lines are coefficients expressed as in equation (2.65),
(2.66) and (2.67) respectively for the non-dimensional first natural
frequencies of the trachea
delta1=(2.*(alpha.^0.3333).*delcos1)+(R2./3)
delta2=(2.*(alpha.^0.3333).*delcos2)+(R2./3)
delta3=(2.*(alpha.^0.3333).*delcos3)+(R2./3)

% the following lines are the Young’s Modulus expressed by in equation
(2.55 for the three roots of the non-dimensional first natural frequencies
of the trachea
E1=rho.*R.^2.*0.7975.*omega.^2./delta1          % for first root
E2=rho.*R.^2.*0.7975.*omega.^2./delta2          % for second root
E3=rho.*R.^2.*0.7975.*omega.^2./delta3          % for third root
```

```
Matlab processed values


n =

     1


R =

    0.0109    0.0096    0.0098    0.0096    0.0099


h =
```

```
    0.0027    0.0023    0.0021    0.0026    0.0026

Lo =

    0.0522    0.0961    0.0306    0.1007    0.0736

dl =

    0.0026    0.0063    0.0009    0.0026    0.0005

L =

    0.0548    0.1024    0.0315    0.1033    0.0741

v =

    0.4500

f =

   50.0000   80.0000   20.0000   20.0000   11.8000

f2 =

   146   377   123    44    16

f3 =

   330   700   470    66    24

rho =

        1000

mew =

    0.9378    0.4440    1.4813    0.4397    0.6321


k =

    0.1327    0.1327    0.1327    0.1327    0.1327

omega =

  314.1593  502.6548  125.6637  125.6637   74.1416

El =
```

```
    0.0053    0.0048    0.0038    0.0059    0.0056

theta1 =

    1.0176    1.0176    1.0176    1.0176    1.0176

theta21 =

    0.9824    0.9824    0.9824    0.9824    0.9824

theta22 =

    0.4227

theta23 =

   -0.9998

theta2 =

    0.5597    0.5597    0.5597    0.5597    0.5597

b1R2 =

    1.7319    0.3882    4.3212    0.3807    0.7868


b2R2 =

    2.2750

b3R2 =

    0.0145    0.0060    0.0312    0.0074    0.0090

R2 =

    4.0214    2.6692    6.6274    2.6631    3.0708

b1R1 =

    0.4877    0.2857    1.5992    0.2853    0.3189

b2R1 =

    1.3811    0.3096    3.4461    0.3036    0.6275
```

```
b3R1 =

    0.2750

b4R1 =

    1.6339    0.3663    4.0768    0.3592    0.7423

b51 =

    0.4080    0.3048    0.6069    0.3042    0.3354

b52 =

    0.0159    0.0079    0.0212    0.0098    0.0116



b53 =

    2.7409    1.2558    8.2292    1.2501    1.5992

b5R1 =

    0.0436    0.0100    0.1744    0.0123    0.0185

R1 =

    3.8214    1.2466    9.5715    1.2353    1.9822

b1R0 =

    0.1837    0.0092    1.1439    0.0089    0.0379

b21 =

   -1.2847   -0.2880   -3.2055   -0.2824   -0.5837

b22 =

    0.4877    0.2857    1.5992    0.2853    0.3189

b2R0 =

   -0.0094   -0.0027   -0.0182   -0.0034   -0.0051

b3R0 =

    2.7409    1.2558    8.2292    1.2501    1.5992
```

```
R0 =

    0.1580    0.0058    0.9941    0.0047    0.0298



EM =

    1.0000    4.0214    3.8214    0.1580


EG =

    1.0000    2.6692    1.2466    0.0058


EH =

    1.0000    6.6274    9.5715    0.9941


EI =

    1.0000    2.6631    1.2353    0.0047


TE =

   -2.5432
   -1.4348
   -0.0433


TG =

   -2.0677
   -0.5968
   -0.0047


TH =

   -4.5887
   -1.9262
   -0.1125


TI =

   -2.0664
   -0.5929
   -0.0038


alpha1 =

    0.1431    0.0532    4.8246    0.0533    0.0580
```

```
alpha =

    0.3783    0.2307    2.1965    0.2308    0.2408

b1theta =

   -0.1472    0.3054    1.4116    0.3071    0.1458

b2theta =

   -0.1946    0.6620    0.3213    0.6654    0.3028

theta =

    1.7667    0.8473    1.2437    0.8428    1.2632

delcos1 =

    0.8316    0.9604    0.9153    0.9608    0.9127

delcos2 =

   -0.8968   -0.7216   -0.8065   -0.7205   -0.8103

delcos3 =

    0.0652   -0.2388   -0.1088   -0.2403   -0.1023

delta1 =

    2.5433    2.0678    4.5887    2.0664    2.1592

delta2 =

    0.0433    0.0047    0.1125    0.0038    0.0154

delta3 =

    1.4348    0.5968    1.9262    0.5929    0.8963

E1 =

  1.0e+003 *

    3.6567    8.9994    0.2663    0.5617    0.1990

E2 =

  1.0e+006 *
```

```
    0.2150    3.9998    0.0109    0.3078    0.0280

E3 =

  1.0e+004 *

    0.6482    3.1181    0.0634    0.1958    0.0479
```

Appendix C
Extended Theoretical Principle of the Free Vibration of Cylindrical Shells

With the assumption that the effect of the transverse shearing stress resultant on the equilibrium of forces in the circumferential direction is negligible, the following equations are developed for axial, circumferential and radial equilibrium [27]

$$\frac{\partial^2 u_x}{\partial x^2}+\frac{1-v}{2r^2}\frac{\partial^2 u_x}{\partial\theta^2}+\frac{1+v}{2r}\frac{\partial^2 u_\theta}{\partial x\partial\theta}+\frac{v}{r}\frac{\partial w}{\partial x}-\frac{1-v^2}{E}\rho\frac{\partial^2 u_x}{\partial t^2}=0 \tag{C.1}$$

$$\frac{1+v}{2r}\frac{\partial^2 u_x}{\partial x\partial\theta}+\frac{1-v}{2}\frac{\partial^2 u_\theta}{\partial x^2}+\frac{1}{r^2}\frac{\partial^2 u_\theta}{\partial\theta^2}+\frac{1}{r^2}\frac{\partial w}{\partial\theta}-\frac{1-v^2}{E}\rho\frac{\partial^2 u_\theta}{\partial t^2}=0 \tag{C.2}$$

$$\frac{v}{r}\frac{\partial u_x}{\partial x}+\frac{1}{r^2}\frac{\partial u_\theta}{\partial\theta}+\frac{w}{r^2}+\frac{h^2}{12}\nabla^4 w+\frac{1-v^2}{E}\rho\frac{\partial^2 w}{\partial t^2}=0 \tag{C.3}$$

where

u_x = axial displacement [m]

x = *s*patial distance in vibration forms [m]

v = Poisson's ratio

r = mean radius [m]

θ = Spatial angle in vibration forms [rad]

u_θ = circumferential displacement [m]

w = radial displacement [m]

E = Young's modulus of elasticity [Pa]

t = time [s]

h = thickness of a cylinder [m]

Figure C1 shows the configuration of the above equations [27].

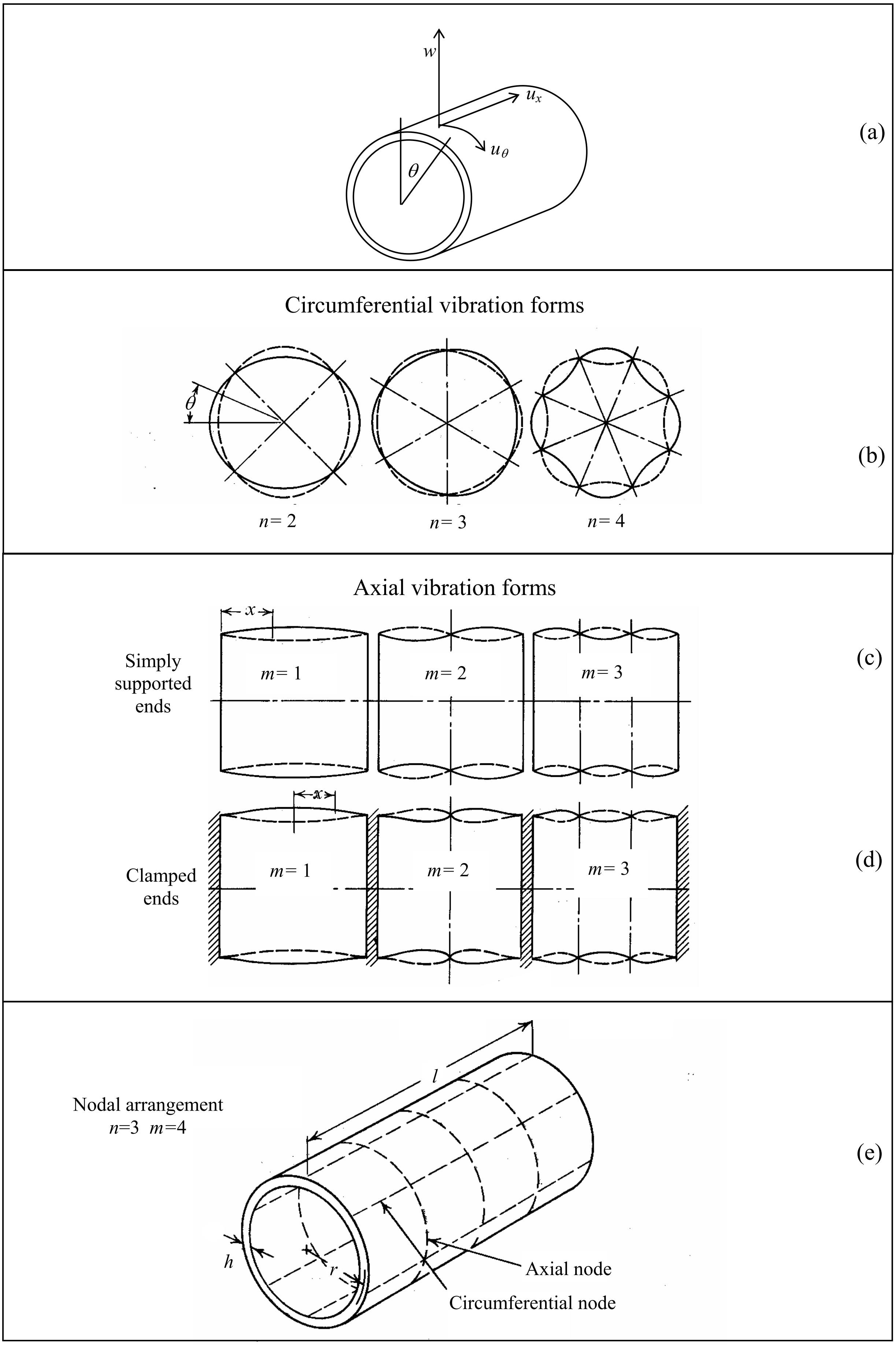

Figure C1 Vibration forms for cylindrical shells

Figure C1 (a) configures the direction of the displacements where u_x is axial, u_θ is circumferential and w is radial displacement. Figure C1 (b) shows from end viewing where vibration of cylinders may consist of any number of waves n distributed around the circumference which in this diagram shown for n = 2, 3 and 4, forming circumferential nodes shown in Figure C1 (e).

Figure C1 (c) and C1 (d) shows side viewing where the deformation of the cylinder consists of a number of waves m distributed along the length of the shell. In this diagram denoted by number of axial half waves m=1, 2 and 3. The appearance of the axial wave form depends on the end condition of the shell, whether it is simply supported as shown in Figure C1 (c) or clamped as shown in Figure C1 (d). When the ends of the cylinder are completely free, the motion of all points along the length is similar. For any end conditions, Figure C1 (b) will always present the circumferential wave form. In fact, for each different end support, the deformation of the cylindrical shell resembles that of a beam which has the same end conditions as the shell. Figure C1 (e) shows an example of constant nodal line pattern of a shell with n=3 and m=4.

With the configuration in Figure C1 above, solving for solutions to equations (C.1) to (C.3) are approached by analysing typical free-vibration problems of the circular cylindrical shell. Arnold and Warburton carried out this problem solving by not using Donnell's assumptions and produced 'variational' solutions that were theoretically comparable to Donnell's 'exact' solution [27]. Instead they selected Rayleigh's method which clamped at both ends. The solutions must satisfy the boundary conditions

$$u_x = u_\theta = w = \frac{dw}{dx} = 0 \tag{C.4}$$

at the end x=0,l of the cylinder.

Further assumptions are postulated that the displacement functions that satisfy the boundary conditions are given by

$$u_x = A_i\left[-sin\frac{\mu}{r}\left(\frac{1}{2}-x\right)+k\,sinh\frac{\mu}{r}\left(\frac{1}{2}-x\right)\right]cos\,n\theta\,cos\,\omega\,t \tag{C.5}$$

$$u_\theta = B_i\left[cos\frac{\mu}{r}\left(\frac{1}{2}-x\right)+k\,cosh\frac{\mu}{r}\left(\frac{1}{2}-x\right)\right]sin\,n\theta\,cos\,\omega\,t \tag{C.6}$$

$$w = C_i\left[cos\frac{\mu}{r}\left(\frac{1}{2}-x\right)+k\,cosh\frac{\mu}{r}\left(\frac{1}{2}-x\right)\right]cos\,n\theta\,cos\,\omega\,t \tag{C.7}$$

where A, B, and C are arbitrary coefficients and

$$k = \frac{sin\left(\mu\,l/2r\right)}{sinh\left(\mu\,l/2r\right)} \tag{C.8}$$

The quantity μ insures that the end conditions will be met and satisfies the equation

$$tan\frac{\mu\,l}{2r}+tanh\frac{\mu\,l}{2r}=0 \tag{C.9}$$

whose roots are

$$\frac{\mu l}{r}=1.506\pi, 3.5\pi, 5.5\pi, 7.5\pi,... \tag{C.10}$$

These values correspond to 1, 3, 5, 7, ...axial waves respectively. For an even number of half waves, a different but similar form of solution would have to be assumed.

The variational equation of the problem is

$$\int_{t_0}^{t_1}\int_0^{2\pi}\int_0^{l}\left\{\left[\frac{\partial^2 u_x}{\partial x^2}+\frac{1-v}{2r^2}\frac{\partial^2 u_x}{\partial\theta^2}+\frac{1+v}{2r}\frac{\partial^2 u_\theta}{\partial x\partial\theta}+\frac{v}{r}\frac{\partial w}{\partial x}-\frac{1-v^2}{E}\rho\frac{\partial^2 u_x}{\partial t^2}\right]\delta u_x+\right.$$

$$\left[\frac{1+v}{2r}\frac{\partial^2 u_x}{\partial x\partial\theta}+\frac{1-v}{2}\frac{\partial^2 u_\theta}{\partial x^2}+\frac{1}{r^2}\frac{\partial^2 u_\theta}{\partial\theta^2}+\frac{1}{r^2}\frac{\partial w}{\partial\theta}-\frac{1-v^2}{E}\rho\frac{\partial^2 u_\theta}{\partial t^2}\right]\delta u_\theta+$$

$$\left.\left[\frac{v}{r}\frac{\partial u_x}{\partial x}+\frac{1}{r^2}\frac{\partial u_\theta}{\partial\theta}+\frac{w}{r^2}+\frac{h^2}{12}\nabla^4 w+\frac{1-v^2}{E}\rho\frac{\partial^2 w}{\partial t^2}\right]\delta w\right\}dxd\theta dt=0 \tag{C.11}$$

The assumed displacement functions from equations (C.5) to (C.7) are substituted into the equation (C.11) followed by integration with respect to x and θ yields

$$\left\{\left[\mu^2\theta_1+\frac{1}{2}\left(1-v^2\right)n^2\theta_2-\Delta\theta_2\right]A-\frac{1}{2}(1+v)\mu n\theta_2 B_i-v\mu\theta_2 C_i\right\}\delta A_i$$

$$+\left\{\frac{-1+v}{2}\mu n\theta_2 A_i+\left[n^2\theta_1+\frac{1-v}{2}\mu^2\theta_2-\Delta\theta_1\right]B_i+n\theta_1 C_i\right\}\delta B_i$$

$$-\left\{v\mu\theta_2 A_i-n\theta_1 B_i-\left[\theta_1-\Delta\theta_1+\frac{1}{\xi}\left(\mu^4\theta_1+n^4\theta_1+2\mu^2 n^2\theta_2\right)C_i\right]\right\}\delta C_i=0 \tag{C.12}$$

where

$$\frac{1}{\xi}=\frac{h^2}{12r^2} \tag{C.13}$$

$$\Delta = \rho r^2 \left(1 - \nu^2\right) \frac{\omega^2}{E} \qquad \text{(C.14)}$$

$$\theta_1 = 1 + k^2 \qquad \text{(C.15)}$$

$$\theta_2 = 1 - k^2 + \frac{2r}{\mu l} sin \frac{\mu l}{r} \qquad \text{(C.16)}$$

Since the variations δA_i, δB_i and δC_i are arbitrary, the above equation can be satisfied only if the quantities in the brackets which multiply these variations each vanish individually. If these quantities are set to zero, three homogeneous and linear equations in the three unknowns A_i, B_i and C_i are obtained. These are the trivial solutions which are avoided by setting the determinant of the coefficients to zero. As a result, the following cubic equation for the natural frequencies is obtained:

$$\Delta^3 - R_2 \Delta^2 + R_1 \Delta - R_0 = 0 \qquad \text{(C.17)}$$

References

1. Likhitpanichkul, M., Sun. D. D., Guo, X. E., Lai, W. M., Mow, V. C. 2002. Influence of the Fixed Negative Charges on the Measured Poisson's Ratio, Young's Modulus and Electrical Response of Articular Cartilage in *Proceedings of IMECE2002 ASME International Mechanical Engineering Congress & Exposition*. New Orleans, Louisiana, USA.

2. Sera, T., Satoh, S., Horinouchi, H., Kobayashi, K., Tanishita, K. 2000. The Inspiratory and Expiratory Flow in Distensible Tracheostenosis Model. *Proceedings of ASME International Mechanical Engineering Congress and Exposition*. Orlando, Florida, USA.

3. Hoppin, F. G. J., Lee, G.C., Dawson, S. V. 1975. Properties of Lung Parenchyma in Distortion. *Journal of Applied Physiology*, **39**(5), p. 742-751.

4. Sarma, P. A., Pidaparti, R. M., Meiss, R.A. 2001. A Material Model for Shortening-Dependent Stiffness of Tracheal Smooth Muscle in *Proceedings of 2001 ASME International Mechanical Engineering Congress and Exposition*. New York, USA.

5. Wiebe, C. 2003. Tester to Measure the Tensile Properties of Embryonic Epithelia in *Proceedings of IMECE 2003 ASME International Mechanical Engineering Congress*. Washington D.C., USA.

6. Vincent, J. F. V. (ed). 1992. *Biomechanics Materials - A Practical Approach*. Oxford University Press, Oxford. p. 133-164.

7. Tomlinson, S. P., Tilley, D. G., Burrows, C. R. 1994. Computer Simulation of the Human Breathing Process. *IEEE Engineering in Medicine and Biology*, February/March 1994, p. 115-124.

8. Tomlinson, S.P., Lo, J. K. W., Tilley, D. G. 1993. Time Transient Gas Exchange in the Respiratory System. *IEEE Engineering in Medicine and Biology*, September 1993, p. 64-70.

9. Hayashi, K., Ishikawa, H., (eds). 1996. *Computational Biomechanics*. Springer, Tokyo. p. 247-268.

10. Al-Jumaily, A. M., Du, Y. 2001. Obstruction Detection in the Upper Airways Using Input Impedance in the Frequency Domain in *Proceedings of 2001 ASME International Mechanical Engineering Congress and Exposition*. New York, USA.

11. Al-Jumaily, A. M., Y. Du. 2001. Simulation of the Central Airways for Identifying Airway Partial Obstruction in *Proceedings of 2001 ASME International Mechanical Engineering Congress and Exposition*. New York, USA.

12. Al-Jumaily, A. M., Mithraratne, P. 2000. Simulation of Respiratory System for Identifying Airway Occlusion. *Journal of Nonlinear Sciences and Numerical Simulations*, **2**(1), p. 21-28.

13. Reisch, S., Steltner, H., Timmer, J., Renotte, C., Guttmann, J. 1999. Early Detection of Upper Airway Obstructions by Analysis of Acoustical Respiratory Input Impedance. *Biological Cybernetics*, **81**, p. 25-37.

14. Desager, K. N., Cauberghs, M., Naudts, J., Van De Woestijne, K. P. 1999. Influence of Upper Airway Shunt on Total Respiratory Impedance in Infants. *Journal of Applied Physiology*, **87**, p. 902-909.

15. Fredberg, J. J., Sidell, R. S., Wohl, M. E., DeJong, R. G. 1978. Canine Pulmonary Input Impedance Measured by Transient Forced Oscillations. *Journal of Biomechanical Engineering*, **100**, p. 67-71.

16. Louis, B., Glass, G. M., Kresen, B., Fredberg, J. J. 1993. Airway Area by Acoustic Reflection: The Two-Microphone Method. *Journal of Biomechanical Engineering*, **115**, p. 278-285.

17. Leondes, C. (ed). 2001. *Biofluid Methods in Vascular and Pulmonary Systems*. CRC Press, Boca Raton. p. 12.1-12.29.

18. Poort, K. L., Fredberg, J. J. 1999. Airway Area by Acoustic Reflection: A Corrected Derivation for the Two-Microphone Method. *Journal of Biomechanical Engineering*, **121**, p. 663-665.

19. Al-Jumaily, A. M., Al-Fakhiri., Y. 2002. Significance of Elastance Variation on Respiratory System Dynamics in *Proceedings of IMECE2002 ASME International Mechanical Engineering Congress & Exposition*. New Orleans, Louisiana, USA.

20. Tai, R. C., Lee, G. C. 1981. Isotropy and Homogeneity of Lung Tissue Deformation. *Journal of Biomechanics*, **14**(4), p. 243-252.

21. Suki, B., Habib, R. H., Jackson, A C. 1993. Wave Propagation, Input Impedance, and Wall Mechanics of the Calf Trachea from 16 to 1,600 Hz. *Journal of Applied Physiology*, p. 2755-2766.

22. Holzhauser, U., Lambert, R. K. 2001. Analysis of Tracheal Mechanics and Applications. *Journal of Applied Physiology*, **91**, p. 290-297.

23. Rains, J. K., Bert, J. L., Roberts, C. R., Pare, P. D. 1992. Mechanical Properties of Human Tracheal Cartilage. *Journal of Applied Physiology*, **72**, p. 219-225.

24. Fung, Y. C. 1993. *Biomechanics Mechanical Properties of Living Tissues*. Springer, New York.

25. Young, W. C., Budynas, R. G. 2002. *Roark's Formula for Stress and Strain*. McGraw-Hill, Boston. p. 122,553-688,808.

26. Kinsler, L.E., Frey, A. R., Coppens, A. B., Sanders, J. V. 1982. *Fundamentals of Acoustics*. John Wiley & Sons, New York. p. 59-131.

27. Kraus, H. 1967. *Thin Elastic Shells*. John Wiley & Sons, New York. p. 297-314.

28. *Medical Dictionary Search Engine*. 2002-2004. Retrieved from the World Wide Web on 7 January 2004: http://cancerweb.ncl.ac.uk/cgi-bin/omd?query=Tyrode%27s+Solution&action=Search+OMD.